Numerical Analysis of the Time-Dependent Partial Differential Equations Motivated by the Biological Processes

A Thesis

submitted in partial fulfillment of the requirements for the award of the degree of

Doctor of Philosophy

in

School of Mathematics

by

Dipty Sharma
(Reg. No. 951411005)

under the guidance of

Dr. Paramjeet Singh

Thapar Institute of Engineering & Technology
Patiala-147004, Punjab, India
April 02, 2021.

Candidate Declaration

I hereby declare that this Ph.D. thesis, entitled **"Numerical Analysis of the Time-Dependent Partial Differential Equations Motivated by the Biological Processes"** in partial fulfillment of the requirement for the award of degree of "Doctor of Philosophy" submitted in the School of Mathematics of Thapar Institute of Engineering and Techonology, Patiala, is an authentic record of my own research work carried out under the guidance and supervision of Dr. Paramjeet Singh. The websites, books, and articles which I have made use of are acknowledged at the respective place in the text. The matter presented in this thesis has not been submitted elsewhere for the award of any other degree or diploma from any institution.

Date: April 02, 2021

Dipty Sharma

Dipty Sharma
Candidate

This is to certify that the above statement made by the candidate is correct to the best of our knowledge.

Date:

Dr. Paramjeet Singh
Supervisor

The Ph.D. Viva-Voce examination of **Dipty Sharma**, Research Scholar has been held on _____.

(Supervisor)	(External Examiner)	(Chairperson of Doctoral Committee)

To my parents, husband, brother, sister, nephew who are the pride and joy of life

Abstract

Mathematical models based on partial differential equations have become the vital components of quantitative analysis in many areas of biological science, finance, engineering, image processing, and many other fields. Moreover, the time-dependent partial differential equations play a preeminent role in many fields of science and engineering. In this dissertation, we have studied partial differential models for biological science and designed the appropriate numerical schemes to find the approximate solutions.

Chapter 1 starts with the introduction, motivation, and literature review for the research work. A brief overview of the governing equations related to computational neuroscience and population dynamics are presented. Further, a short introduction of the numerical techniques related to this study is given. Moreover, the structure of the thesis is presented at the end of this chapter.
Chapter 2 begins with a brief background of the nervous system and its related model [1]. Further, it presents the proposed numerical scheme based on the finite element method, which is used to find the approximate solution of the governing model equation. The chapter concludes with a performance evaluation of the proposed work using some numerical experiments.
Chapter 3 presents the excitatory and inhibitory population density model based on leaky-integrate-and-fire neurons with the effect of the refractory period and transmission delays. The chapter starts with the overview of the integrate-and-fire neuron model for deriving of governing equation with the help of the population density approach. Further, it presents a discontinuous Galerkin numerical scheme to find the approximate solution of the model equation. This chapter also discusses the stability of the proposed framework. To evaluate the performance of the proposed scheme, some numerical experiments present in this chapter.
Chapter 4 deals with the non-linear age-structured population model. The model consists of tumor cells population dynamics based on an age-structured approach where each cell has a finite maximum age. The model comprises the fertility and mortality factors, which depend on age. This chapter presents a high-order accurate numerical scheme to approximate the solution of the governing equation. Finally, test examples are taken to demonstrate both the effectiveness and efficiency of the proposed method.

Chapter 5 concludes the dissertation and also shed light on some future direction of the present work.

Keywords: Partial differential equation, Noisy leaky integrate-and-fire neuron, Population density approach, Finite element method, Discontinuous Galerkin method, Age-structured models, Population dynamics.

Acknowledgements

It has been a most wonderful and overwhelming experience for completing this doctoral work. I am grateful for the advice, support, encouragement, and friendship of many individuals who contributed to this dissertation. First and above all, I praise Lord (Shiva), the Almighty for providing me this opportunity and granting me the capability to proceed successfully.

I have been very privileged to have undoubtedly the most intuitive, smart and supportive advisor anyone could ask for, namely Paramjeet Singh. Ever since I learned from him what an avoided crossing was, I have been stimulated and excited by his constant flow of good ideas. All the discussions and freedom has really shaped my carrier. He has also known when (and how) to give me a little push in the forward direction when I needed it. His constructive criticism and valuable suggestions at every step of my work has not only shaped the present version but also broadened my perspective during the entire course of my study

I am also grateful to Dr. Satish Kumar Sharma, Head, School of Mathematics, for providing me a great environment to work in throughout this period. I am thankful to my wonderful teachers for their constant support and encouragement. I am also thankful to all the concerned people in the School for providing the necessary facilities and help during my research work. I would like to express my gratitude to Professor Rafat Siddique (Dean, Research and Sponsored Projects) for his invaluable support.

I would like to thanks my friends and colleagues for providing a friendly and entertaining environment and for the enjoyable tea breaks. A very special thanks to Mrs. Sonia Bhalla for her psychological support, many personal discussions, and for sharing her own experiences with me.

My sincere appreciation goes to my superb parents for showing faith in me and giving me the liberty to choose what I desired. Without the substantial help and support from my parents, I would not have been able to shape up this work. I warmly thank you all for the selfless love, care, pain, and sacrifice you did to shape my life. I would also like to thanks my brother, sister, brother-in-law, and nephew for all their love, support, and encouragement. My special thanks go to my elder sister for her selfless love, care, and dedicated efforts that contributed a lot for the compilation of this dissertation.

I express my deepest gratitude to my husband for his affection, encouragement, patience, and unconditional support. I greatly value his contribution and extremely appreciate his belief in me. Also, I express to thank my parents-in-law for supporting me during my

research work.

Finally, yet importantly, I am thankful to all my relatives, friends, and well-wishers whoever helped me in many ways so that I could complete my research work successfully.

Dipty Sharma

Table of Contests

List of Figures

List of Tables

List of Abbreviations

FDM	Finite Difference Method
FVM	Finite Volume Method
FEM	Finite Element Method
DGM	Discountinuous Galerkin Method
WENO	Weighted Essentially Non-Oscillatory
RK	Runge-Kutta
SSP	Strong Stability Preserving
FPE	Fokker-Planck Equation
LIF	Leaky Integrate-and-Fire

Chapter 1

Introduction and Related Work

Mathematical modeling is an art to convert problems originating from applications into a mathematical representation. The theoretical and numerical analysis of mathematical models provides answers and insights and can be very useful for further investigation. The experts from different backgrounds come with their ideas to improve existing results to develop better mathematical models and use their skills to estimate the behavior of certain situations. These models are omnipresent as they depend upon ordinary differential equations (ODEs) and partial differential equations (PDEs) and these are emerging in different areas like engineering, physics, biology, and many other areas. Further, the applications of these models include option pricing, neuronal networks, population dynamics, age-structured, tumor growth, fluid mechanics, etc. Due to the complexity of these models, it becomes too difficult to find the exact solution even for a simple problem. Therefore, the numerical methods play an incredibly important role to discover the approximate solution of the governed PDE equations.

Numerical solution of differential equations particularly non-linear PDEs, is the only way to get the solution to problems that are not analytically solvable. The numerical solution of PDEs has been a subject of intense activity for the last 60 years or so, primarily due to advances in computer technology and the introduction of numerical computing applications like Maple, Fortran, Mathematica, Python, Matlab, PETSc (Portable Extensible Toolkit for Scientific Computation) and MOOSE (Multiphysics Object-Oriented Simulation Environment), which in turn has led advancement in numerical methods that are being used. As a result, many unsolved problems related to ODEs and PDEs are solved by appropriate numerical methods such as the finite difference method (FDM), finite element method (FEM), finite volume method (FVM), discontinuous Galerkin method (DG), spectral method, boundary element, meshless or meshfree methods.

1 Research Motivation

Mathematical and Computational modeling is the most popular approach for exploring the functionality of the biological system. Therefore, the purpose of this dissertation is to understand the behaviors of the nervous system and population dynamics, which

inspires mathematical analysis and study of the computer simulation and this can be done by computational biology. The biological systems are explicitly processors of information as compared to the other physical systems. In this way, computational models are not only used for forecasting or count but are mainly explained the functionality of the living system. In today's scenario, computing technology and numerical techniques are extending their scope by doing more development in the research activity. Due to these advancements, the researchers are mostly involved in knowing the functionality of various parts of the nervous system means what and how they do it.

Overview of the concept of neuroscience. The brain is like a computer that controls the nervous system as well as the functions of the body. It consists of a huge number of different cells that convey messages to other parts of the body. The neurons or the nerve cells among all these are the basic functional units, which are mainly known as electrically excitable cells. According to Kandel et al. [5], the human brain has approximately 10^{11} neurons and which are interconnected in a very complex manner. More precisely, each neuron is connected to tens of thousands of other neurons. Therefore, there are many connections during a single milliliter of brain tissue, it is like stars within the Milky Way Galaxy [6].

Computational neuroscience. Computational neuroscience is a part of computational biology and a scientific study of the neural system. From many decades, computational models, and especially quantitative models are emerging as a vital tool for research in the area of neuroscience. In fact, one of the key achievements in this area is the Hodgkin-Huxley model. This model defines the generation of action potentials which is based on a quantitative approach [5]. Besides, much of what is understood about the functionality of the nervous systems has been informed by mathematical and computational modeling.

In 1977, spanish histologist Santiago Ramón y Cajal specified the neuron as the fundamental functional unit of the nervous system. He proposed that all neurons are discrete cells, which communicate via circuits and junctions. Moreover, he was the first who gave the detailed account of the structure of the nerve cells, and revealed that all these share the same fundamental structure (see in [7]).

Structure of Neuron. The four major structural regions of a typical neuron are: dendrites, cell body (soma), axon, and axon terminals (presynaptic terminals). Each region has a different function (see Figure 1.1). The most vital component of the neuron is the cell body, which consists of the nucleus in it and is known as soma. Each cell is connected to other cells by dendrites and they are the one which brings information to other neurons. A long thin structure is used as a transformer to convey the information from one neuron to the other neurons and it is also known as the axon. The portion of

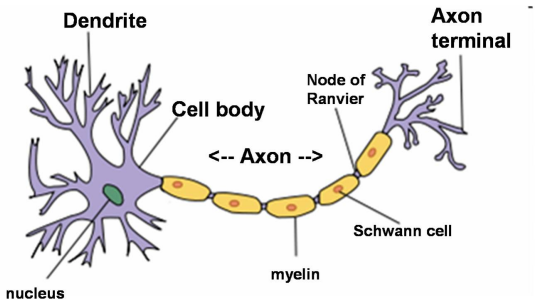

Figure 1.1: Structure of a typical neuron (this image is taken from Wikipedia, [2].)

the axon where it originates from the cell body is known as axon hillock, which is that a part of the neuron and it has the greatest density of voltage-dependent sodium channels. At the end of the axon, it is further divided into branches that are used to communicate with other neurons. It contains the synapse i.e. interaction among neurons and which is usually knows as axon terminal or presynaptic cell. Synapses are also divided into two categories: electrical synapses and chemical synapses. They can be differentiated based on how the one cell transmitted the signal to the next cell. The synapses where the signal is transmitted from one neuron to another by using gap junctions are known as electrical synapses and there is no need for any receptors of the postsynaptic cell (see Figure 1.2a). Consequently, signaling through the electrical synapses is much faster than that which comes through the chemical synapses. On the other side, a neurotransmitter is the one who transmits the signal from one neuron to another in chemical synapses by using the receptors of the postsynaptic cell (see Figure 1.2b). When the receptors receive neurotransmitter molecules, the ion channels begin to open. Consequently, the flow of ions comes in or out, and changing the local membrane potential of the cell and that change in voltage is called a postsynaptic potential. The outcome of this process varies means it can be excitatory or inhibitory. In the case of depolarizing currents, the result is excitatory and on the other side in the case of hyperpolarizing currents, the result is inhibitory. The excitatory or inhibitory nature of a synapse also relies on the varieties of ion channel carry the postsynaptic current displays, that is a function of both the type of receptors and the type of neurotransmitter occupied at the synapse. Whereas a signal is sent at an excitatory synapse, then the depolarization of the cell can be strong enough so that an action potential can be initiated in the postsynaptic cell. Since the depolarization triggered by the excitatory postsynaptic potential is not sufficient for an action potential initiation, then the effect of the depolarization will last for some time, and will be progressively attenuated. Therefore, if the neuron receives signals from the same or other neurons, the postsynaptic potentials they provoke will be added. This phenomenon is known as synaptic integration.

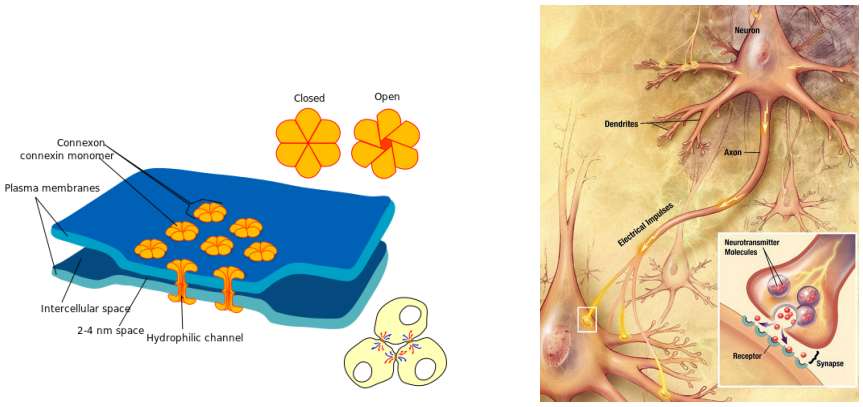

(a) Depiction of a electrical synapse

(b) Depiction of a chemical synapse

Figure 1.2: Structure of a synapse, (both images taken from Wikipedia, [2].)

Finally, we can conclude that neurons are like miniature self-contained information processors. It receives the information, processes that information, and then generates outputs based on that information. The dendrites are the one who receives the inputs and then cell body process that information and axon terminal is responsible to generate output based on the processed information (see Figure 1.3). The more detailed information about the modeling of neurons and neural networks can be found herein [8–12].

Population Dynamics is derived from mathematical biology and deals with population size and other biological factors that affect them. Besides this, it has a long history of more than 200 years or more. Previously such type of studies are limited to demography, but nowadays the mathematical theory is useful in epidemiology, the simulation of cancer, neurons and ecological systems, and numerous other areas, see herein [13–23].

2 Literature Review

The main component of the neural system is the integrate-and-fire (IF) neuron. It is used to depict the neuron's transmembrane potential in the form of the injected current and the synaptic inputs that it receives. Also, the membrane potential gets inputs in two ways (excitatory or inhibitory) from different neurons. More precisely, premised on these inputs there are two types of models, the current synapse model, and the conductance synapse models. It is called a current synapse model when the input is modeled as injected current and termed as a conductance synapse model when there is a change within the membrane conductance. Further, these models (conductance synapse models) depend on the difference between the transmembrane potential and therefore the reversal

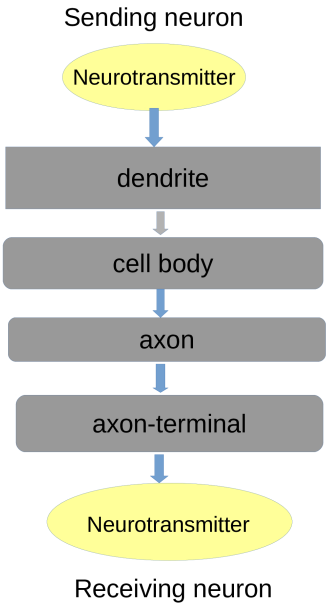

Figure 1.3: Neuron signal direction

potential, and it describes the amplitude of the excitatory and inhibitory inputs. Additionally, the IF neuron model is understood as a point neuron model during which the dendrite's spatial structure of the neuron is neglected.

Leaky integrate-and-fire (LIF) neuron. The neuron is said to be leaky as the participation of all synaptic inputs to the transmembrane potential of a neuron decay with a membrane time constant. Additionally, the model is called a perfect integrator as the decay in membrane potential over time is neglected. Furthermore, when the membrane potential of a neuron reaches a fixed level that is also known as a threshold level, it generates a spike or action potential that specifies the first passage time of the membrane potential across the threshold. Subsequently, the membrane potential is deactivated for a short time as it reaches back to its resting state.

Background of an integrate-and-fire neuron. The IF neuron encompasses a long-standing history. In 1907, Lapicque [14] presented a neuron model that depicts the subthreshold electrical potential of a single neuron, using its membrane voltage, i.e., the neuron's membrane voltage in the terms of an electric circuit comprising of a parallel capacitor and resistor that epitomize the capacitance and leakage resistance of the neuron membrane, respectively. The membrane potential is charged until it reaches a given threshold implies it is charged at a level where a spike appears. After reaching this level, the potential comes back at the resting state (see Figure 1.5). Thereby, the membrane

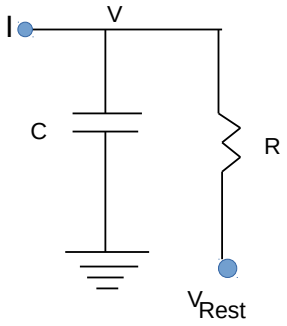

Figure 1.4: The equivalent circuit represents the membrane voltage of a neuron in subthreshold level, where V denotes the membrane potential, C is the membrane capacitance, R depicts the membrane resistance, V_{rest} is the resting membrane voltage, and I is an injected current.

potential dynamics is represented as

$$C\frac{dV(t)}{dt} = -V + V_{rest},$$

where C is the membrane capacitance, $V(t)$ is the membrane potential of a neuron at time t, and V_{rest} is the resting potential. With the aid of this model, Lapicque could easily evaluate the spiking (firing) rate of a neuron (Fig. 1.1). Further, this model is used for another neuron modeling for several decades.

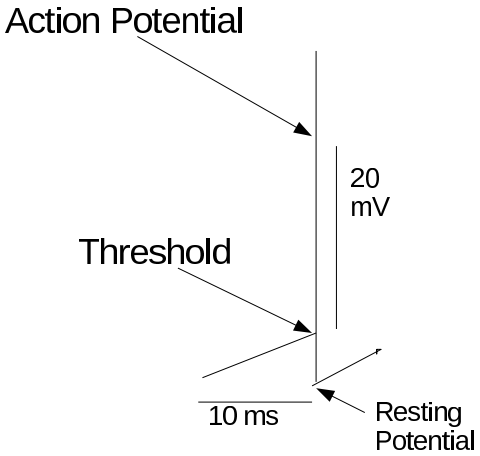

Figure 1.5: The dynamics of the membrane potential of a neuron.

In 1936, Lapicque's model is analyzed by Hill [24], with external injected current in the neuron

$$C\frac{dV(t)}{dt} = -V + V_{rest} + I_e(t).$$

Here, I_e denotes an external current that is directly injected into the neuron. The approach of the IF model is extremely useful to separate the time scale between the extremely rapid spike generation and the relatively slow subthreshold integration. It is one of the key points on which neuronal behaviors depend. More concentration upon the subthreshold mechanism proves that the properties of the subthreshold membrane are a powerful tool to analyze the information processing capabilities of neurons. In 1964, Mandelbrot and Gerstein proposed a neuron model known as the stochastic IF model [25]. Additionally, it is constructed as a random walk problem with a threshold barrier. Stein in 1965 and then in 1967, further modified this model that includes the decay of the membrane potential [26, 27]. Many authors uses stochastic differential equations (SDEs) with different numerical techniques for further developments in this model (Knight in 1972 [28], Kryukov in 1976 [29], Tuckwell in 1977 [30], Lánskỳ in 1984 [31], and Wilbur et al. in 1982 [32]). Furthermore, these above-mentioned approaches have been used for the examination of the effect of reversal potential and inhibition in the Stein's model (Tuckwell in 1978 [33] and then in 1979 [34], Cope et al. in 1979 [35], Hanson et al. in 1983 [36] and Musila et al. in 1994 [37]).

IF model equation. The general form of the membrane potential in the IF model is

$$C\frac{dV(t)}{dt} = I_l(V) + I_{syn}(V,t) + I_e(t),$$

where I_{syn} is the synaptic current and I_l is a leak current. There are many variants available for this model. Some of them are considered in the literature. For instance, the IF model has a leak current: $I_l(V) = -g\ (V - V_{rest})$, where g denotes the leak conductance. Dividing the above equation on both sides by g, and rewrite it as

$$\tau\frac{dV(t)}{dt} = f(V) + I_{syn}(V,t) + I_e(t),$$

where $\tau = \dfrac{C}{g}$, $f(V) = -(V - V_{rest})$ and g has been absorbed in the currents I_{syn} and I_e. The above form of the IF model is known as a leaky integrate-and-fire (LIF) neuron model.

The Linear IF neuron model is introduced by Mattia and Fusi in 1999, [38], for the examination of the collective behaviours of the neural networks. Further, in this model, the depolarization of the subthreshold membrane potential is constant that is

$$\frac{dV(t)}{dt} = -\beta + I(t),$$

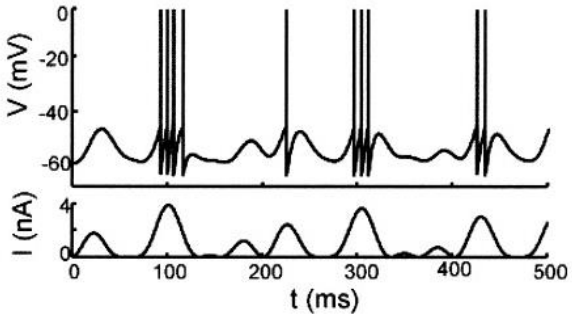

Figure 1.6: An IF model neuron driven by a time varying current. The upper trace is the membrane potential and the bottom trace is the input current. This image taken from [3].

where $\beta > 0$ is a constant decay.

Kopell and Ermentrout [39], proposed a *quadratic-integrate-and-fire (QIF) neuron model* in 1986 for the examination of neuron firing. In this model, neuron firing is determined by Type I bifurcation (Izhikevich in 1999 [40]) and neurons are described as the canonical form. This model is similar to the neuron model (Latham et al. in 2000 [41]), Gutkin et al. in 1998 [42], Ermentrout in 1996 [43]. QIF model is used by a couple of authors to describe the intrinsic properties of the neural system (Lindner et al. in 2003 [44], Brunel et al. in 2003 [45]). Moreover, Fourcaud-Trocmé et al. in 2005 presented the exponential IF neuron model to describe the time evolution of the firing rate [46, 47]. Later this model was used by Brette et al. to describe the neural activity [48].

Neuronal Noise. Nowadays, the fascinating field of research is the IF models with noise for a single neuron or network of neurons. Long decades ago (DeFelice in 1981 [49], Schmitt in 1967 [50], and Holden in 1976 [51]), introduced the word noise in neuroscience. The random fluctuation which occurs in the environment is known as neuronal noise. Moreover, this fluctuation can occur for a single neuron or as a firing activity of the neural network. Neurons always respond differently if the presentation of a specific input signal is repeated. The outcomes of the neural network function and the response variability have been under observation for many years. There are two different types of sources of noise, external and internal. Further, the external source of noise typically refers to the random fluctuation and the probabilistic nature of the chemical reactions, which provide the firing activity of neurons is known as an internal source of the noise [48, 52–55]. More precisely, noise is omnipresent in the nervous system since a single neuron is capable to get a huge number of synaptic inputs from other neurons, and due to the fact of randomness occurring in the opening and closing gates of the ion channels [56–58].

The noisy leaky-integrate-and-fire model (NLIF). NLIF is a mathematical model which describes the stochastic properties of neurons [53, 59–69]. The model equation is determined by a Langevin equation and a discontinuous reset mechanism which stimulates the generation of the action potential. Langevin equation may utilize to write the corresponding Fokker-Planck equation (FPE), which represents the time evolution of probability density to figure out the transmembrane potential of a neuron at a specific voltage level. Moreover, the NLIF model is also known as a simpler version of the Hodgkin-Huxley model [70], which allowed a detailed, qualitative comparison with physical data [9]. Later, many other authors have contributed in this field see herein [66, 68, 71–75].

The probability density function in computational neuroscience has a long-standing history [52, 76, 77]. This concept has been used in many contexts of neuronal modeling, but this approach is not appropriate for the simulation of large neural networks [63, 68, 78]. Knight introduced a population density approach in 1996, which deals with the simulation of neural networks in a more efficient way [79]. This approach is later reformed (see herein [80–82]) and used by many authors for analyzing the firing activity of the neural network [53, 62–69]. Nowadays, this approach is widely used for the derivation of model equations based on PDEs.

Mathematical population models. Mathematical models of population dynamics comprises a long standing history and include age structure and another structuring of the population with continuously changing properties. Aging is a vital and basic premise when forming the population because numerous internal aspects are determined by age as the variation in behaviors, the variation in reproduction, and the variation in the capacity of survival are due to the difference in ages. Thereby, the age-structure population model plays a prominent role in population dynamics. A foundation set up by McKendrick and Lotka et al. for the PDEs technique to the modeling of an age structure in an evolving population [83, 84]. The basic population dynamical model based on the age-structured approach

$$\begin{cases} \dfrac{\partial p}{\partial t} + \dfrac{\partial p}{\partial a} = -\mathbf{m}\left(a, \mathsf{P}(t)\right) p(a,t), \ a \geq 0, \ t \geq 0, \\ \mathsf{P}(t) = \int\limits_0^\infty p(a,t) da, \\ p(0,t) = \int\limits_0^\infty \mathbf{B}(a, \mathsf{P}(t)) p(a,t), \\ p(a,0) = p_0(a), \end{cases}$$

for the age density function $p(a,t)$ at a time t. The term $\mathsf{P}(t)$ denotes the size of the total population in the above equation. Further, $\mathbf{m}(a)$ denotes the age-specific mortality

rate of population having age duration $[a, a + da]$ for the one-time unit and $\mathbf{m}(a, \mathsf{P}(\mathsf{t}))$ represents the mortality rate at the time t. Further, $\mathbf{B}(a)$ indicate the age-dependent fertility rate implies number of newborn formed through the single individual whose age falls in $[a, a+da]$ and $\mathbf{B}(a, \mathsf{P}(\mathsf{t}))$ indicates the total reproduction rate. Lastly, $p_0(.)$ denotes the population size at the initial stage. The PDEs in the above model is commonly called the Lotka-McKendrick equation.

The stabilization of the age-structure model with linear fertility and mortality identified at the earlier stages and the study of these linear models was established later in [85, 86]. MacCamy and Gurtin in 1974 introduced a new technology based on a nonlinear Volterra integral equation approach then used this approach to confirm the existence, uniqueness, and convergence of equilibrium solution to the Sharpe-Lotka-McKendrick model [14]. During the last two decades, numerous authors developed various algorithms to solve these types of the modeled equation of population dynamics [87–89]. Further, Iannelli and Milner in 2001 concluded that the numerical methods where the standard order is lower could not be appropriate to solve the model equations of population dynamics [18]. Therefore, it would be ideal to choose suitable higher-order methods to find a long-term phenomenon of the model equations. The progressively complex mathematical problems included in the nonlinearities of the age-structured models addressed the advancement of new technology. Thereby, some other approaches are available in the literature that employed very efficiently to solve non-linear age-structured model equations [88, 90–95].

3 Research Gaps and Objectives

This section is devoted to the research gaps and the objectives for this research.

Research Gaps

- The absence of higher-order numerical techniques for the population density approach of an integrate-and-fire neuron.
- Discontinuous Galerkin method is not widely used to examine the behavior of neural population dynamics.
- The higher-order schemes need to be studied for the population model of an excitatory-inhibitory network of an integrate-and-fire neuron.
- The application of population density approach for an excitatory-inhibitory neuron population with delays and refractory periods.

- The application of population dynamics: an age-structured tumor growth population model with non-linear mortality rate and fertility rate need to be investigated.

Objectives

- Development of numerical approximation based on discontinuous Galerkin finite element method for the time-dependent partial differential equations arising in neuronal variability.
- Construction of stable and convergent discrete numerical approximation based on the finite element method for the biological process motivated by neuroscience.
- Usual extension of the numerical methods for the other realistic phenomena arising in related processes.

The remaining sections present an overview of some important mathematical concepts that are related to this study.

4 Numerical Methods

Numerical analysis is the branch of mathematics and also computer science that deals with the study of algorithms to determine the numerical solution of the problems of continuous mathematics. Due to the rapid advancements in computer technology, the uses of numerical techniques for solving realistic mathematical model problems whose analytical solution cannot be found, have been increased. There are several numerical methods such as FDM, FEM, FVM, spectral method, boundary element method, and many more, which provide the best approximate results for an appropriate system of PDEs (see herein [96–100]). Here, we present a brief introduction to some of the methods that are widely used to tackle non-linear PDEs.

The finite difference method is the easiest method to apply and to solve a differential equation. The basic idea of the finite difference method is to replace the derivative appearing in a differential equation with an approximate difference formula. The difference formula is derived from Taylor series expansion. In the consequence of the relative ease of implementation and flexibility, the difference method is the first choice method for the numerical solution of the differential equation. However, this method has some disadvantages: the method becomes intricate when solving the differential equation on an irregular domain, the PDEs are non-linear or based on the variable coefficient, it is not easy to prove the stability, consistency, and convergence for the difference method. However, this method serves as a basis for other numerical methods (see [101–104]).

The spectral method is another numerical technique to solve the differential equation. This method is only useful when the solution is smooth and the domain is simple. This method has some drawbacks: it is very complicated to implement, it cannot represent the physical processes in spectral space. Moreover, this method is very expansive at high resolution. The interested readers can find more details about these methods herein [105–110].

The boundary element method is a numerical technique, which is applied to solve those PDEs that may be converted into integral equations. This method tries to utilize the given boundary conditions (BCs) to fit boundary values into the integral equation, instead of the values throughout the space specified by the PDE. The interested readers can find more details about this method herein [111, 112].

The finite element method has a basic idea of a piece-wise representation of the solution in terms of specified basis functions, meshing the modeled domain into smaller elements, and solution in each element is constructed from the basis functions. Moreover, the FEM has the advantages of low sensitivity to a large gradient and high-order polynomial refinement. Additionally, FEM can be implemented for those situations where the other numerical techniques are bounded to the problems having only a finite regular space as in realistic situations, the irregular space is always determined. Thus, this method is suitable for the solution to the problems that depict real-life situations. Thereby, in this research work, the FEM approach is used for the simulation of the biological process arising from neuronal variability. The detailed study of these methods can be found in [113, 114].

Moreover, a wide range of FEM exists for the numerical analysis of PDEs with higher-order accuracy. Classic approaches include DG methods which combine the properties of the FEM and the FVM techniques and have been effectively implemented for hyperbolic, parabolic, elliptic, and mixed form problems resulting from a wide range of applications.

Discontinuous Galerkin method is a class of FEM using completely discontinuous basis functions generally chosen as piece-wise polynomials. This method provides local approximation flexibility by using discontinuous piecewise polynomials as a basis function and thus, can be designed for the higher order of accuracy that is determined locally by using a higher-order polynomial approximation within an element. Therefore, discontinuous Galerkin (DG) methods have the local approximation flexibility, along with good stability properties. These methods provide a range of appealing properties for the numerical approximations of various classes of PDE problems whereby standard methods underperform or even fail.

This thesis aims to understand the biological phenomena in terms of non-linear mathematical models that are very difficult to solve analytically. Hence, we need the appropri-

ate numerical methods to get the numerical solutions of such non-linear model equations. Because of the above-mentioned properties, the DG method is a decent choice among these types of non-linear PDEs. The detailed study of the DG method can be found herein [115]. Here, we provide a simple example to describe the implementation of the DG method for the first-order time-dependent PDE equation

$$\begin{cases} \partial_t u + \partial_x f = 0, \quad t \geq 0, \quad f(u) = u, \\ u(x,0) = u_0(x), \quad x \in \mathbb{R}. \end{cases} \tag{1.1}$$

We suppose that the domain Ω is well approximated by Ω_h that can be discretized into K non-overlapping sub-domains (or elements) D^k where $k \in [1, K]$. So we have

$$\Omega \approx \Omega_h = \bigcup_{k=1}^{K} D^k.$$

Here we represent the numerical approximation to the true solution of the problem with $u_h(x,t)$ and the local approximations (in each element) by $u_h^k(x,t)$. We wish to express the local solution in each element by a polynomial of order N using the shape functions $\varphi_i^k(x)$:

$$u_h^k(x,t) = \sum_{i=1}^{N+1} u_h^k(x_i^k, t)\varphi_i^k(x), \quad x_i^k \in D^k.$$

Defining the residual function $R_h(x,t)$ as below, we need to determine in which sense we want the residual to vanish and u_h to approach the true solution:

$$R_h(x,t) = \frac{\partial u}{\partial t} + \frac{\partial f}{\partial x}.$$

Now suppose that the solution u and the test function φ arise from a finite-dimensional approximation space V_h, that generally taken as the space of piecewise polynomials of degree up to N. To this end, we take the globally defined test space

$$V_h = \bigoplus_{k=1}^{K} V_h^k, \quad \text{where} \quad V_h^k = span\{\phi_i(D^k)\}_{i=1}^{N+1}.$$

Define the Legendre inner product on interval I in the following form:

$$(u,v)_I = \int_{-1}^{1} uv dx$$

resulting in the L^2 norm $||u||^2 = (u,u)_I$. Now we can desire the residual that is orthogonal to this test space; i.e. the inner product of the residual and all the test functions in V_h to vanish:

$$\int_{D^k} R_h(x,t)\phi_i(x) = 0 \quad 1 \leq i \leq N+1, \quad \forall\, k \in [1,K].$$

Now, if the space of the test functions ϕ_i is the same as the space of the shape functions φ_i, the method of approximation is called Galerkin method. In discontinuous Galerkin finite element methods, the shape functions only need to be smooth within each element D^k and are not continuous across element faces or otherwise constrained. This gives the advantage of these discontinuous Galerkin Methods over other methods. After multiply the equation (2.3) with the test function φ_j then taking the integration by parts over the cell D^k, we get as follows:

$$\int_{D^k} \frac{\partial u^k}{\partial t}\varphi_j^k dx - \int_{D^k} f^k \frac{\partial \varphi_j^k}{\partial x} dx + \left[(f^k)\varphi_j^k\right]_{x_l^k}^{x_r^k} = 0, \quad \text{where } 1 \leq j \leq N+1. \tag{1.2}$$

Now, it is considerable that because of the lack of continuity of the test functions at the element faces, the solution at these points is not unique. Let us assume for the moment that these values are given by $(f)^*$, representing the numerical flux at the element boundaries. Further, these values are reliable to get global solution to the problem from the local approximations and applying the BCs.

If we integrate the Eq.(1.2) by parts again to remove the smoothness constraint on the test function, we will achieve the strong form:

$$\int_{D^k} \frac{\partial u^k}{\partial t}\varphi_j^k dx + \int_{D^k} \frac{\partial f^k}{\partial x}\varphi_j^k dx = \left[\left(f^k - f^*\right)\varphi_j^k\right]_{x_l^k}^{x_r^k}. \tag{1.3}$$

As mentioned above the constraint on the test functions has been removed and they can even be non-smooth or essentially delta functions. Using local mass and stiffness matrix defined

$$M_{ij}^k = (\varphi_i, \varphi_j)_{D^k} \quad \text{and} \quad S_{ij}^k = (\varphi_i, \frac{\partial \varphi_j}{\partial x})_{D^k}, \tag{1.4}$$

we can rewrite the equation as the local semi-discrete equation

$$\int_{D^k} \left(M^k \frac{\partial}{\partial t} u^k + S^k(f^k) \right) dx = \left[\left(f^k - f^*\right)\varphi\right]_{x_l^k}^{x_r^k}. \tag{1.5}$$

This gives a system of $K \times (N+1)$ system of equations with the same number of unknowns. As a result, by defining the specific test functions that we want to use for our approximations and the appropriate flux functions, we can recover the local nodal values as well as the global solution.

However, the boundary terms are not well defined when u in this space, are discontinuous at the cell interfaces. As there is a lack of the continuity of test functions at element interfaces, the solution is not exactly unique at these boundary points. That is the stage where the traditional technique of the finite volume method is adopted by the discontinuous Galerkin method. These element interface values must be replaced by the numerical flux to guarantee stability and convergence. The critical ingredient for developing an accurate and stable scheme is the right design of these fluxes. Thus, replace the interface term $f(u)^*$ by a single-valued numerical fluxes

$$\hat{f}(u) = f(u^-, u^+), \tag{1.6}$$

which depends on both the values, the left limit, and the right limit. Additionally, the subscript "$-$" is used for the interior information within the element, and "$+$" is used for the exterior information within the neighboring element. Moreover, the properties of single-valued approximated flux are $\hat{f}(u,u) = f(u)$(consistency), monotonicity, and Lipschitz continuous concerning both arguments. Various numerical flux functions exist in the literature that satisfied the above-mentioned requirements such as Roe flux functions, Lax-Friedrichs flux, and many others. Furthermore, types of monotone fluxes that are appropriate for DG methods can be found herein [116].

5 Thesis Organization

The thesis is organized into five chapters. A brief outline is given below:

- **Chapter 1: Introduction and Summary**
  This chapter starts with the overview of mathematical modeling, some aspects of computational biology, and then discusses the structure of neurons and their behaviors. Further, it presents the literature survey on computational neuroscience and population dynamics and introduces some theories of the related model equations. Additionally, it summarizes the discontinuous Galerkin method that used in this study.

- **Chapter 2: Numerical Approximation for Nonlinear Noisy Leaky integrate-and-fire Neuronal Model**

This chapter begins with a brief background of the nervous system and its related model equation. Further, it presents the proposed numerical scheme based on the finite element approach, which is used to find the approximate solution of the governing equation. Finally, numerical experiments are taken to demonstrate both the effectiveness and efficiency of our proposed method.
The research work in this chapter has been appeared in " Mathematics", 2019 [117].

- **Chapter 3: Discontinuous Galerkin Approximation for the Excitatory and Inhibitory Population Density Model**
  This Chapter presents the excitatory and inhibitory neuron population model based on LIF neurons with the effect of the refractory period and transmission delays. Firstly, it starts with the overview of the IF neuron model for deriving of governing equation with the help of the population density approach. Further, it presents a discontinuous Galerkin numerical scheme to find the approximate solution of the model equation. This chapter also discusses the stability of the proposed framework. For the performance evaluation of the proposed technique, some numerical examples are present in this chapter.
  The research work in this chapter has appeared in the " International Journal of Modern Physics C", 2020 [118].

- **Chapter 4: Numerical Study of the Age-structured Tumor Cell Population Model**
  This chapter deals with the non-linear population dynamical model which is based on the age-structured approach. Particularly, this model consists of tumor cell population dynamics based on an age-structured approach where each cell has a finite maximum age. The model comprises the fertility and mortality factors, which depend on age. Further, it presents a high-order accurate numerical scheme to find the approximate solution of the model equation. The chapter concludes with a performance evaluation of the proposed work using some numerical experiments.
  The research work in this chapter has appeared in the " International Journal of Modern Physics C", 2021 [119].

- **Chapter 5: Conclusions and Future Scope**
  This chapter concludes the study and discusses some future directions of the present work.
  The relevant references are appended at the end of the thesis.

Chapter 2

Numerical Approximation for Nonlinear Noisy Leaky Integrate-and-Fire Neuronal Model [1]

In this chapter, the population density approach of integrate-and-fire neurons is being used to describe the neuronal variability. The resulting model is known as a noisy leaky-integrate-and-fire (NLIF) model which is governed by the nonlinear time-dependent partial differential equation (PDE). The derived PDE is termed as Fokker-Planck Equation (FPE) which depicts the dynamical behavior of the probability density. In this chapter, FEM is applied to determine the numerical solution of the governed equation. The importance of this scheme is that FEM can be implemented to tackle those situations whereas the other numerical techniques are restricted to the problems having only a finite regular space as in the realistic neural network, the irregular space is always determined. Due to these advantages, FEM is a preferable numerical technique for the simulation of these model equations. Further, some numerical examples are included to discuss the solution behavior graphically.

1 Introduction

The large-scale neural network models in computational neuroscience have become familiar. The classical description of these (excitatory-inhibitory) neural network models is based on the deterministic/stochastic system. The most popular one is the NLIF neuron model in which the biological phenomena of the whole population of neurons are modeled as an SDE equation for the time evolution of membrane potential of a single neuron representative of the network. Thereby, the dynamics of a single neuron is presented by ([9, 54, 80, 120])

$$\tau_m \frac{dV}{dt} = -V(t) + I(t), \tag{2.1}$$

[1] Dipty Sharma, Paramjeet Singh, Ravi P. Agarwal, Mehmet Emir Koksal. *"Numerical Approximation for Nonlinear Noisy Leaky Integrate-and-Fire Neuronal Model"*, Mathematics, **7 (4)**, 363, 2019.

where $V(t)$ represents the membrane potential of a single neuron and τ_m is the time relaxation of the membrane potential in the absence of any communication. The communication of a single neuron with the network is modeled by the synaptic input current, $I(t)$. The form of $I(t)$ is based on the stochastic approach as given in ([121])

$$I(t) = J_E \sum_{n=1}^{N_E} \sum_{m} \delta(t - t_{E_m}^n) - J_I \sum_{n=1}^{N_I} \sum_{m} \delta(t - t_{I_m}^n).$$

Here, each spike is treated as a delta function, and if a spike occurs at time $t = t_0$, it is denoted by $\delta(t - t_0)$. The terms $t_{E_m}^n$ and $t_{I_m}^n$ in above equation represent the time of mth-spike receiving from nth-presynaptic neuron for excitatory and inhibitory (EI) neurons, respectively. Moreover, the terms N_E and N_I are the total number of presynaptic neurons, where J_E and J_I are the strength of the synapses for EI neurons, respectively. Since the above form of the synaptic input current is the discrete Poisson process, it becomes very difficult for further investigation. In addition, the researchers have used the diffusion approximation in which the synaptic input current $I(t)$ is simulated stochastically by a continuous in time Ornstein-Uhlenbeck-type as given by

$$I(t)dt \approx \mu_c dt + \sigma_c d_{B_t}. \tag{2.2}$$

Initially, it is assumed that every neuron generates spikes according to a stationary Poisson process with constant probability of generating a spike per unit time r, and it is also assumed that all these processes are independent between neurons, because of these assumptions, the mean value of the current, indicated by μ_c, is given by $br = (N_E J_E - N_I J_I)r$ and its variance, $\sigma_c^2 = (N_E J_E^2 + N_I J_I^2)r$. Here, we have to depict the likelihood of firing per unit time of the Poissonian spike train r and it is thus recognized as the rate of firing, which should be computed as $r = I_{ext} + N(t)$, where $N(t)$ is the mean firing rate of the network. On the other side, B_t is the standard Brownian motion in above equation.
The next important factor in the modeling is that the neurons generate a spike only when its membrane potential $V(t)$ arrives at a certain voltage, known as threshold V_F, and instantly reset toward a resetting potential $V_R < V_F$ and sends a signal over the network. Comprising the continuous form of $I(t)$ in SDE model (3.1), we obtain

$$\tau_m dV = (-V + \mu_c)dt + \sigma_c dB_t,\ V \leq V_F,\ t \geq 0,$$

where $\tau_m = 1$. We suppose that the voltage of a neuron arrives at threshold level at time t_o^-, i.e., $V(t_o^-) = V_F$ and after that the voltage arrives suddenly at resting potential, i.e., $V(t_o^+) = V_R,\ V_R < V_F$. Furthermore, one can write the associated FPE with source

term by using Ito's rule [122], for the evolution of probability density function $p(v,t) \geq 0$ of finding neurons at a voltage $v \in (-\infty, V_F]$, with time $(t \geq 0)$

$$\frac{\partial}{\partial t}p(v,t) + \frac{\partial}{\partial v}[h(v,N)p(v,t)] - a(N(t))\frac{\partial^2}{\partial v^2}p(v,t) \;\; = \;\; N(t)\,\delta(v - V_R), \qquad (2.3)$$

where $h(v,N) = -v + \mu_c$, $a(N(t)) = \frac{\sigma_c^2}{2}$, and $N(t)$ is the mean firing rate of the network which is computed as the flux of neuron at the firing voltage. The source term of the Equation (2.3) comes from the fact that when the neurons generate spikes and send the signals over the network, their voltage immediately reset to the reset potential V_R. At the relaxation time, no neuron have the firing voltage, for this reason, the initial and boundary conditions are given by

$$p(v,0) = p^0(v) \geq 0,\;\; p(V_F,t) = 0,\;\; p(-\infty,t) = 0. \qquad (2.4)$$

We can easily verify the conservation of the total number of neurons in above equation. For this purpose, we need to describe the mean firing rate for the network. Since the mean firing rate is the flux of neurons at V_F, the value of $N(t)$ is given by $N(t) = -a(N(t))\frac{\partial p(V_F,t)}{\partial v}$. Integrating (2.4) across the voltage domain and using the above BCs, we obtain the required condition.
Equation (2.3) represents the probability density evolution and thereby

$$\int_{-\infty}^{V_F} p(v,t)dv = \int_{-\infty}^{V_F} p^0(v)dv = 1. \qquad (2.5)$$

If we translate the new voltage variable by considering $v = v + bI_{ext}$ then we have $h(v,N) = -v + \mu_c = -v + br = -v - bI_{ext} + br = -v - bI_{ext} + b(I_{ext} + N(t)) = -v + bN$, and diffusion coefficient is of the form $a(N) = a_0 + a_1 N, a_0 > 0, a_1 \geq 0$. The more detail information about mathematical aspects of nonlinear NLIF models, can be found herein [123–127]. We are concern about finding the value of the unknown $p(v,t)$ using an alternative approach. The problem (2.3)–(2.5) cannot be solved analytically, because of its complexity arising from nonlinearity and having a source term [128–135]. Therefore, numerical methods are generally used, for example, the finite difference method (FDM) is used to find the approximate solution of the governing equation [122]. However, FDM has some disadvantages, for instance, the singularity in the delta source term, as in the above-mentioned equation, makes the solution divergent. In order to use the FDM appropriately, the governing equation must be modified, due to the fact that the procedure becomes complicated. Hence, in the present work, we propose a formulation based on finite element approximation to find the solution of governing equation. FEM is one of

the powerful numerical methods for the solutions of problems that describe the real-life situations [136–142]. Moreover, the characteristics of FEM tackle the singularity problem in an effective manner [114, 143–153]. The applicability of FEM regarding this model problem is demonstrated in the final section. The description of the chapter is as follows: We consider the NLIF model described by Equations (2.3) and (2.4). In Section **??**, we develop the numerical approximation based on the finite element approach. We report some numerical examples from [122] and discuss the solution behavior graphically in Section **??**. In the last section, we conclude the work done in this chapter.

1.1 Preliminaries

Here, we state some basic definitions and auxiliary results, which will be used throughout the manuscript. As we are studying a nonlinear version of the FPE, we start with the notion of weak solution.

Definition 1.1. *We say that a pair of non-negative functions* (p, N) *with* $p \in L^\infty(\mathbb{R}^+; L^1_+(-\infty, V_F))$, $N \in L^1_{loc,+}(\mathbb{R}^+)$ *is a weak solution of (2.3) and (2.4) if for any test function* $\phi(v,t) \in C^\infty((-\infty, V_F) \times (0,T))$ *such that* $\frac{\partial^2 \phi}{\partial v^2}, v\frac{\partial \phi}{\partial v} \in L^\infty((-\infty, V_F) \times (0,T))$*, we have*

$$\begin{aligned}
&\int_0^T \int_{-\infty}^{V_F} p(v,t) \left[-\frac{\partial \phi}{\partial t} - \frac{\partial \phi}{\partial v} h(v,N) - a\frac{\partial^2 \phi}{\partial v^2} \right] dv dt \\
&= \int_0^T N(t) \left[\phi(V_R, t) - \phi(V_F, t) \right] dt \\
&+ \int_{-\infty}^{V_F} p^0(v)\phi(0,v)dv - \int_{-\infty}^{V_F} p(v,T)\phi(T,v)dv.
\end{aligned}$$

Here, the space $L^p(\Omega)$, $1 \leq p < \infty$, refers to the space of functions such that f^p is integrable in Ω, while L^∞ corresponds to the space of bounded functions in Ω. The set of infinitely differentiable functions in Ω is denoted by $C^\infty(\Omega)$ used as test functions in the notion of weak solution. The blow-up of solution and a priori estimates are given in [122]. We here just state the results.

Theorem 1.1. (Blow-up) Assume that the drift and diffusion coefficients satisfy

$$h(v,N) + v \geq bN \quad \text{and} \quad a(N) \geq a_m > 0, \tag{2.6}$$

for all $-\infty < v \leq V_F$ and all $N \geq 0$, and let us consider the average-excitatory network where $b > 0$. Choose $\mu > \max\left(\frac{V_F}{a_m}, \frac{b}{1}\right)$. If the initial data is concentrated enough around $v = V_F$, in the sense that

$$\int_{-\infty}^{V_F} e^{\mu v} p^0(v) dv$$

is close enough to $e^{\mu V_F}$, then there are no global-in-time weak solutions to (2.3)–(2.5).

Lemma 1.2 (A priori estimates)**.** *Assume $h(v, N) = -v + bN$, $a(N) = a_0 + a_1 N$ on the drift and diffusion coefficients and that (p, N) is a global-in-time solution of (2.3)–(2.5) in the sense of Definition 1.1 fast decaying at $-\infty$, then the following a priori estimates hold for all $T > 0$:*

1. *If $b \geq V_F - V_R$, then*

$$\int_{-\infty}^{V_F} (V_F - v) p(v, t) dv \leq \max\left(V_F, \int_{-\infty}^{V_F} (V_F - v) p^0(v)\, dv\right),$$

$$(b - V_F + V_R) \int_0^T N(t) dt \leq V_F T + \int_{-\infty}^{V_F} (V_F - v) p^0(v) dv.$$

2. *If $b < V_F - V_R$, then*

$$\int_{-\infty}^{V_F} (V_F - v) p(v, t)\, dv \geq \min\left(V_F, \int_{-\infty}^{V_F} (V_F - v) p^0(v)\, dv\right).$$

Moreover, if in addition a is constant, then

$$\int_0^T N(t) dt \leq (1 + T)\, C(V_F, V_R, a, p^0).$$

In a latest work [122], it was demonstrated that the problem (2.3)–(2.5) can produce a finite time blow-up solution for excitatory networks $b > 0$ when the initial data is concentrated near sufficient to the threshold voltage. This result was obtained by giving no information about the behavior at the blow-up time. In a recent work [126], we state the theorem gives a characterization of this blow-up time when it occurs for $b > 0$.

Theorem 1.3. Let $p^0(v)$ be a non-negative $C^1((-\infty, V_F) \bigcap L^1(-\infty, V_F)$ function such

that $p^0(V_F) = 0$ and

$$\frac{\partial p^0}{\partial v} = 0.$$

There exist a classical solution of (2.3-2.5) in the time interval $[0, T^*)$ with $T^* > 0$. The maximal existence time $T^* > 0$ can be characterized as

$$T^* = \sup\{t > 0 : N(t) < \infty\}.$$

Moreover, when $b \leq 0$ we have that $T^* = \infty$, while for $b > 0$ there exist classical solutions which blow up at a finite time T^* and consequently have diverging mean firing rate as $t \uparrow T^*$. We now state the main result on steady states from [122].

Theorem 1.4. Let $h(v, N) = bN - v$, $a(N) = a_0 + a_1 N$ with $a_0, a_1 > 0$.

1. Under either the conditions $b > 0$ and $2a_0 b + 2a_1 V_R < (V_F - V_R)^2 V_R$, or the condition $b < V_F - V_R$, then there exists at least one steady state solution to (2.3)–(2.5).

2. If both $2a_0 b + 2a_1 V_R < (V_F - V_R)^2 V_R$ and $b > V_F - V_R$ hold, then there are at least two steady states to solution to (2.3)–(2.5).

3. There is no steady state to (2.3)–(2.5) under the high connectivity condition'

$$b > \max(2(V_F - V_R), 2V_F I(0)). \tag{2.7}$$

2 Finite Element Approximation

We construct the numerical approximation of the problem given in (2.3) and (2.4) in two ways: First we use FEM for space discretization that provides a system of ODEs, which is then solved by Euler's backward difference for time. Spatial discretization involves the construction of a weak formulation of problem over a given domain $\Omega = [v_0, v_n]$ with specified BCs at $v = v_0$ and $v = v_n$. Weak formulation of the problem (2.3) and (2.4) is obtained by multiplying the equation with some test function $w(v)$ and integrating over Ω,

$$\int_\Omega w(v) \Big\{ \frac{\partial p}{\partial t} + \frac{\partial}{\partial v}\big(h(v, N)p\big) + a(N(t))\frac{\partial^2 p}{\partial v^2} \Big\} dv = N(t) \int_\Omega w(v)\, \delta(v - V_R)\, dv. \tag{2.8}$$

In the present study, the mean firing rate $N(t)$ is approximated by using backward FDM. Performing the integration by parts in above equation, we get the following equa-

tion:

$$\int_{\Omega} \Big\{ w\frac{\partial p}{\partial t} - \Big(h(v,N)\, p\, \frac{\partial w}{\partial v} \Big) + a(N(t))\, \frac{\partial p}{\partial v}\, \frac{\partial w}{\partial v} \Big\} dv = N(t) \int_{\Omega} w(v)\, \delta(v - V_R)\, dv. \quad (2.9)$$

This resulting integral (2.9) is called weak formulation because it allows approximate function with less continuity (or differentiability) than the strong form given in Equation (2.3). Once we obtained the weak formulation, next step is to discretize the weak form for the easy representation and to capture the local effects more precisely. Weak form discretization consists of dividing the entire domain into set of elements, then developing the finite element model by seeking the approximation of a solution over a typical element. This discretization is tackled by taking n non-overlapping elements say $D_i = [v_i, v_{i+1}]$ for $i = 1, 2, \ldots, n$ with step size h given by :

$$\int_{v_i}^{v_{i+1}} \Big\{ w\frac{\partial p}{\partial t} - \Big(h(v,N)\, p\, \frac{\partial w}{\partial v} \Big) + a(N(t))\, \frac{\partial p}{\partial v}\, \frac{\partial w}{\partial v} \Big\} dv = N(t) \int_{v_i}^{v_{i+1}} w(v)\, \delta(v - V_R)\, dv. \quad (2.10)$$

The unknown function $p(v,t)$ must be approximated in a manner so that continuity or differentiability demands by weak formulation can be met. Since the weak formulation contains the first-order derivative of p, any function with a non-zero first derivative would be a candidate for approximation. If we choose the N^{th} order basis function for the approximation, there are $N+1$ nodes per element. Thus there are $N+1$ shape functions for the N^{th} order approximation

$$\psi_i = \prod_{j=1,\, j\neq i}^{N+1} \frac{(v - v_j)}{v_i - v_j}, \quad i = 1, 2, \ldots, N+1. \quad (2.11)$$

In this chapter, we use the linear ($N = 1$) basis function to describe the implementation of the numerical approximation, thus the semi discretization consists of finding

$$p_i = \sum_{j=i}^{i+1} \hat{p}_j(t)\psi_j(v), \quad (2.12)$$

where $\hat{p}_j$ are the nodal values and ψ_j are the basis functions given by

$$\begin{aligned} \psi_i(v) &= \frac{v_{i+1} - v}{h}, \\ \psi_{i+1}(v) &= \frac{v - v_i}{h}. \end{aligned} \quad (2.13)$$

There are many choices of weight function $w(v)$ to be used. Particular choice for the weight function $w(v)$ in Galerkin approach is the same as the choice of basis function $\psi_j(v)$. Thus, substituting weight function $w = \psi_l(x)$, $l = i, i+1$ and approximation for the solution defined by Equation (2.12) in weak formulation obtained in Equation (2.10) leads to the following equa-

tion:

$$\int_{v_i}^{v_{i+1}} \left[\psi_l \left(\sum_{j=i}^{i+1} \frac{d\hat{p}_j}{dt} \psi_j \right) - h(v,N) \frac{d\psi_l}{dv} \left(\sum_{j=i}^{i+1} \hat{p}_j \psi_j \right) + a(N(t)) \, \frac{d\psi_l}{dv} \left(\sum_{j=i}^{i+1} \hat{p}_j \frac{\psi_j}{dv} \right) \right] dv$$
$$= N(t) \int_{v_i}^{v_{i+1}} \delta(v - V_R) \, \psi_l \, dv.$$

On simplification of the above, we get as follows

$$\sum_{j=i}^{i+1} \left[\left(\int_{v_i}^{v_{i+1}} \psi_l \, \psi_j \, dv \right) \frac{d\hat{p}_j}{dt} - \left(\int_{v_i}^{v_{i+1}} h(v,N) \psi_j \frac{d\psi_l}{dv} \, dv \right) \hat{p}_j + a(N(t)) \left(\int_{v_i}^{v_{i+1}} \frac{d\psi_l}{dv} \, \frac{d\psi_j}{dv} \, dv \right) \hat{p}_j \right] \tag{2.14}$$
$$= N(t) \int_{v_i}^{v_{i+1}} \delta(v - V_R) \, \psi_l \, dv.$$

Solving Equation (2.14), we get the system of ODEs for $\hat{p} = (\hat{p}_0, \hat{p}_1)^T$, which can be expressed in matrix notation given by

$$A \, \hat{p}_t(t^k) + \Big(B - C + D \Big) \hat{p}(t^k) = f, \tag{2.15}$$

where

$$A = \int_{v_i}^{v_{i+1}} \psi_l \, \psi_j \, dv \quad = \quad \frac{h}{6} \begin{bmatrix} 2 & 1 \\ 1 & 2 \end{bmatrix},$$

$$B = \int_{v_i}^{v_{i+1}} v \, \psi_l' \, \psi_j \; dv = \frac{1}{6h^2} \begin{bmatrix} -a_1 & -a_2 \\ a_1 & a_2 \end{bmatrix}, \quad \text{where} \quad \begin{cases} a_1 = 3v_i h^2 + h^3 \\ a_2 = 3 \, v_i h^2 + 2h^3 \end{cases}$$

$$C = b \, N(t^{k-1}) \int_{v_i}^{v_{i+1}} \psi_l' \, \psi_j \, dv = b \, N(t^{k-1}) \begin{bmatrix} -1/2 & -1/2 \\ 1/2 & 1/2 \end{bmatrix},$$

$$D = \frac{a(N(t^{k-1}))}{h} \int_{v_i}^{v_{i+1}} \psi_l' \, \psi_j' \, dv = \frac{a(N(t^{k-1}))}{h} \begin{bmatrix} 1 & -1 \\ -1 & 1 \end{bmatrix},$$

$$f = N(t^{k-1}) \int_{v_i}^{v_{i+1}} \delta(v - V_R) \, \psi_l \, dv = N(t^{k-1}) \begin{bmatrix} \delta_{(i)V_R} \\ \delta_{(i+1)V_R} \end{bmatrix}.$$

By assembling the contribution from all elements, we get the following system for the global nodal vector $p = [p_0, p_1, \ldots, p_n]^T$ on the entire domain

$$A \, p_t(t^k) + \Big(B - C + D \Big) p(t^k) = f, \tag{2.16}$$

where f is the column vector with all entries are zero except at reset potential V_R. Ordinary differential Equation (2.16) requires implicit and stable time-stepping method to avoid extremely small time-step. Firstly we discretize the time domain $[0, T]$ into m sub-intervals with time step Δt. We use the Euler's backward difference in time and get the following system from Equation (2.16):

$$M\, p^k = \frac{A}{\Delta t} p^{k-1} + f, \quad \text{where} \quad M = \frac{A}{\Delta t} + B - C + D, \tag{2.17}$$

this algebraic system (2.17) can be solved for p_j.

3 Numerical Experiments

Here, we use some numerical examples to demonstrate the behavior of the solutions of the nonlinear NLIF model. The performance of the developed scheme is tested by comparing our results with the existing scheme in the literature. Consider the system (2.3) and (2.4) with initial data as follows

$$p(v, 0) = \frac{1}{\sigma_0 \sqrt{2\,\pi}} e^{\frac{-(v-v_0)^2}{2\,\sigma_0^2}}, \tag{2.18}$$

where change in mean v_0 and variance σ_0^2 describe different scenario of a solution.

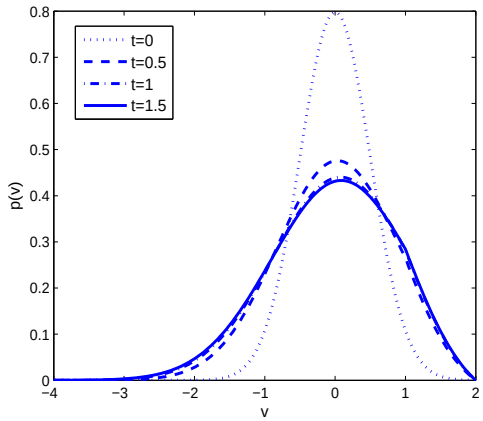

(a) Numerical simulation for $p(v, t)$ using FEM at different time level.

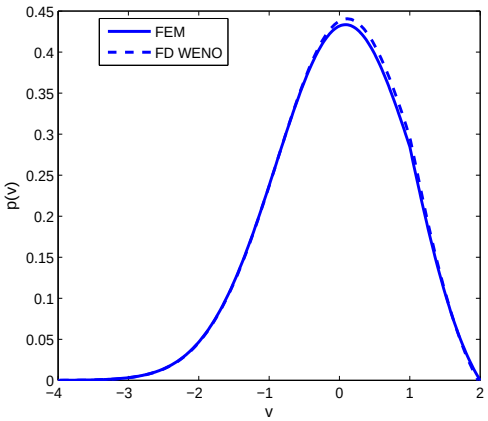

(b) Comparison of the existing scheme and FEM for $p(v, t)$ at $t = 1.5$.

Figure 2.1: The approximate solution $p(v, t)$ for initial data (2.18) with mean $v_0 = 0$ and variance $\sigma_0^2 = 0.25$. The system is considered for the excitatory case i.e. by taking $b = 0.5 > 0$ with activity dependent noise $a(N(t)) = a_0 = 1$.

We notice that the behavior of the solution depends upon the value of excitatory ($b > 0$) and inhibitory ($b < 0$) average network. First we take constant diffusion coefficient $a(N) = a_0$ and find the effect on solution with change in value of b.

In Figure 2.1a, we find that after some time the solution $p(v,t)$ goes to steady state by taking excitatory case i.e., $b = 0.5 > 0$ small enough.
The approximate solution $p(v,t)$ for $v \in [-4,2]$ at different time levels $t > 0$ is graphically represented in Figure 2.1 with a reset potential $V_R = 1$. From Figure 2.1a, we see that height of impulse decreases as time increases and after some time it reaches a steady state. In Figure 2.1b, we perform numerical approximation based upon FEM and compare the results obtained in [122] at a final time $t = 1.5$.
The evolution of the rate of firing denoted as $N(t)$ with the time $t > 0$, is graphically represented in Figure 2.2. We find that the rate of firing has a different range with change in $b > 0$ excitatory case as well as the inhibitory case $b < 0$. In Figure 2.2a, we consider the case when the initial data is centred at $v_0 = 0$ with $b = 0.5$. We observe that the solution reaches a steady state. We also take the cases when the initial data is centred at $v_0 = -1$ and different values of $b = 3, 1.5, -1.5$, to find different phenomena based on these values in Figure 2.2. In Figure 2.3a, we performed numerical approximation based upon FEM and compared the results obtained in [122] at a time $t = 0.0408$. The evolution of firing rate $N(t)$ with the time $t > 0$, is graphically represented in Figure 2.3b, which describes the blow-up situation when the initial data is concentrated around $v_0 = 1.5$ with $b = 1.5 > 0$. Tables 4.3 and 4.4 gives the different error values at the final time $t = 0.0408$ for the same data that is graphically represented in Figure 2.6.
Errors of the numerical solution $p(v,t)$ are calculated in different norms $\|\cdot\|_1, \|\cdot\|_2, \|\cdot\|_\infty$, norms which are defined as follows

$$\begin{aligned} \|\cdot\|_1 &= \Delta v \sum_i |(p_{\Delta v})_i - (p^*)_i|, \\ \|\cdot\|_2 &= \sqrt{\Delta v \sum_i |(p_{\Delta v})_i - (p^*)_i|^2}, \\ \|\cdot\|_\infty &= \max |(p_{\Delta v})_i - (p^*)_i|, \end{aligned}$$

where p^* is the numerical solution at finest grid N^*. For the numerical experiments, we find the errors with the finest grid being $N^* = 320$. Our test outcomes show that the error defined above is sure a monotone decreasing function as N increases i.e., $N = 20, 40, 80, 160$.
The errors for the approximate solution simulated in Figures 2.1, 2.3 and 2.4 are graphically represented in Figures 2.5–2.7 respectively. From Figure 2.4a, it is clear that when initial data is concentrated enough near the threshold point V_F, solution blows up at a finite time $t = 0.0025$, which is earlier than the phenomena described in Figure 2.3b. This happens because initial data is centered sufficiently close to the certain threshold point i.e., $v_0 = 1.83$, with $b = 0.5 > 0$ small enough. For different error values and CPU time for the data graphically represented in Figure 2.4, see Tables 4.5 and 4.6. In Figure 2.8, we treat the cases for $a(N) = a_0 + a_1 N(t), a_0, a_1 > 0$ type activity dependence noise.Figure 2.8a shows that by taking $b = 0.5$ and $a(N(t)) = 0.5 + N(t)/8$ solution goes to steady state. This further indicates that solution goes to a steady state earlier than the solution behavior provided in Figure 2.8b by

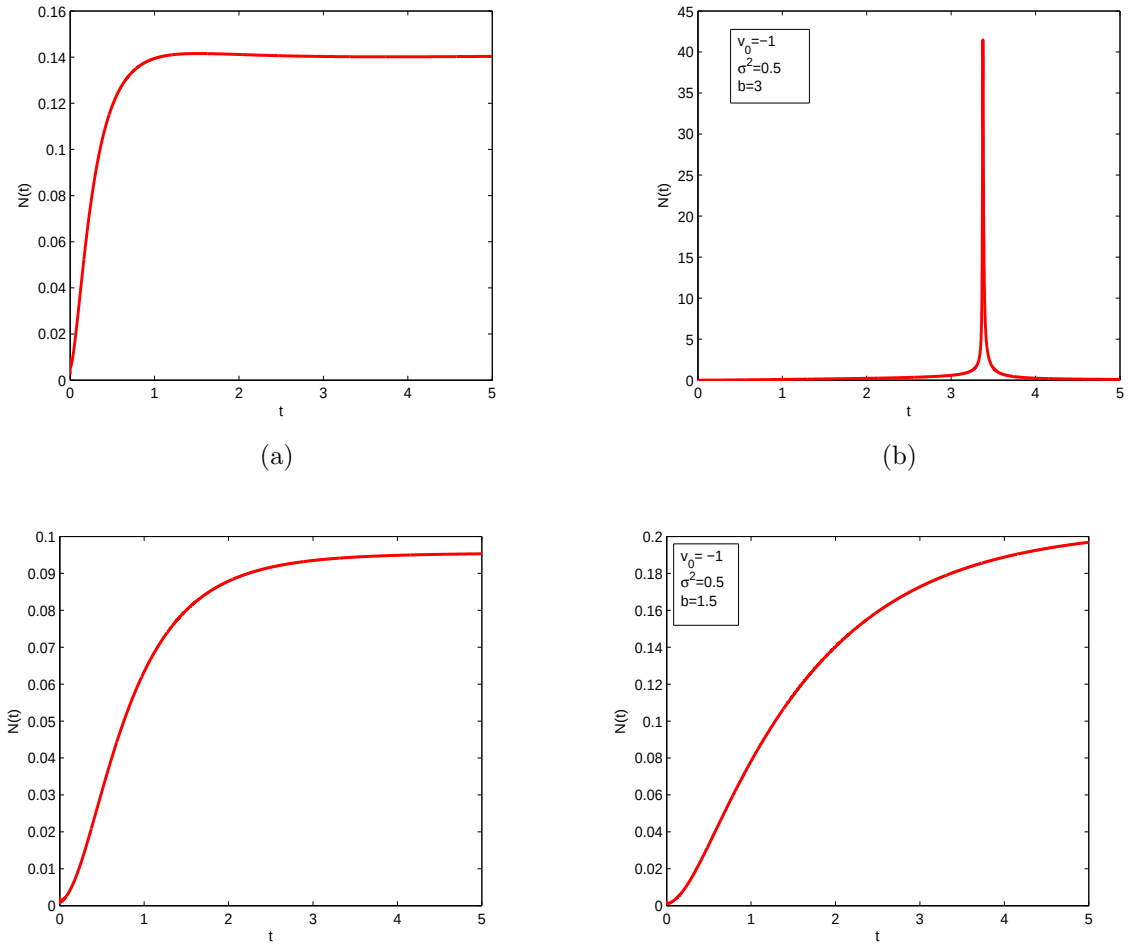

(a) (b)

(c) (d)

Figure 2.2: Firing rates N(t) for $a_0 = 1$ with initial data given in Eq. (2.18). Top left: $b = 0.5$ with: $v_0 = 0$ and $\sigma^2 = 0.25$. Top right: $b = 3$ with: $v_0 = -1$ and $\sigma^2 = 0.5$. The top right case seems to illustrate a blow-up phenomena. Bottom left: $b = -1.5$ with: $v_0 = -1$ and $\sigma^2 = 0.25$. Bottom right: $b = 1.5$ with: $v_0 = -1$ and $\sigma^2 = 0.25$.

taking $a(N(t)) = 0.4 + N(t)/100$. Figure 2.8c shows blow-up situation of a solution by taking $b > 1$ and $a(N(t)) = 0.5 + N(t)/8$. From Figure 2.8d, we find that by reducing the noise factor $a(N(t)) = 0.4 + N(t)/100$, solution goes to steady state.

The behavior of the solution by taking noise factor $a(N(t)) = 1 + N(t)/100$ for both the cases of EI are represented in Figure 2.9. From Figure 2.10a, we find that solution blows up in a finite time and right figure indicate the situation of steady state by reducing the noise factor.

Table 2.1: Error estimates for the numerical solution $p(v,t)$ graphically represented in Figure 2.1 by using FEM at time $t = 1.5$ with the finest grid being $N^* = 320$.

N	$\|\cdot\|_1$	$\|\cdot\|_2$	$\|\cdot\|_\infty$	CPU time(sec)
20	0.010161	0.005158	0.004335	0.067127
40	0.003960	0.001973	0.001516	0.371851
80	0.001542	0.000773	0.000542	3.080583
160	0.000489	0.000247	0.000171	33.034109

Table 2.2: Estimates of error for the approximate solution $p(v,t)$ graphically represented in Figure 2.1 by using WENO-FDM at a time $t = 1.5$ with the finest grid being $N^* = 320$.

N	$\|\cdot\|_1$	$\|\cdot\|_2$	$\|\cdot\|_\infty$	CPU time(sec)
20	0.289460	0.325151	0.283239	1.037672
40	0.135309	0.151787	0.039987	6.045227
80	0.047782	0.051424	0.009268	46.438833
160	0.013548	0.012541	0.001921	361.179426

Table 2.3: Error norms for the numerical solution $p(v,t)$ graphically represented in Figure 2.3 by using FEM at a time $t = 0.0408$ with the finest grid being $N^* = 320$.

N	$\|\cdot\|_1$	$\|\cdot\|_2$	$\|\cdot\|_\infty$	CPU time(sec)
20	0.159578	0.182739	0.283239	0.039572
40	0.022391	0.023427	0.039987	0.109250
80	0.005192	0.005395	0.009268	0.751499
160	0.001122	0.001127	0.001921	8.015343

Table 2.4: Error norms for the numerical solution $p(v,t)$ graphically represented in Figure 2.3 by using WENO-FDM at a time $t = 0.0408$ with the finest grid being $N^* = 320$.

N	$\|\cdot\|_1$	$\|\cdot\|_2$	$\|\cdot\|_\infty$	CPU time(sec)
20	0.289460	0.325151	0.538803	0.431218
40	0.135309	0.151787	0.262857	1.588952
80	0.047782	0.051424	0.089970	10.601858
160	0.013548	0.012541	0.018749	83.066463

Table 2.5: Error estimates using FEM for the approximate solution $p(v,t)$ graphically represented in Figure 2.4, at a final time $t = 0.00255$ with the finest grid being $N^* = 320$.

N	$\|\cdot\|_1$	$\|\cdot\|_2$	$\|\cdot\|_\infty$	CPU time(sec)
20	0.319312	0.568807	1.260046	0.024043
40	0.170528	0.221119	0.466656	0.031783
80	0.082213	0.119544	0.305763	0.079694
160	0.021068	0.030539	0.073327	0.536440

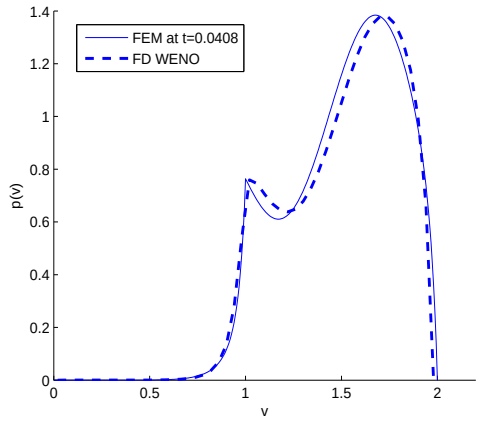

(a) Comparison of the existing scheme and FEM for the numerical Solution $p(v,t)$.

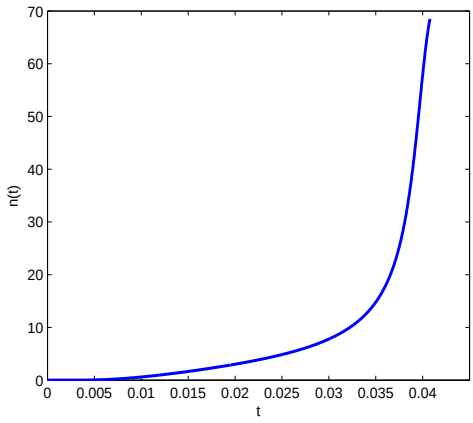

(b) Evolution in time of the firing rate $N(t)$

Figure 2.3: Left: The approximate solution $p(v,t)$, Right: Firing rate $N(t)$ for initial data given in Eq. (2.18) with mean $v_0 = 1.5$ and variance $\sigma_0^2 = 0.005$. The system is considered for the excitatory case i.e. by taking $b = 1.5 > 0$ with activity dependent noise $a(N(t)) = a_0 = 1$.

Table 2.6: Error estimates using WENO-FDM for the approximate solution $p(v,t)$ graphically represented in Figure 2.4, at a final time $t = 0.00255$ with the finest grid being $N^* = 320$.

N	$\|\cdot\|_1$	$\|\cdot\|_2$	$\|\cdot\|_\infty$	CPU time(sec)
20	0.372501	0.536629	1.056888	0.295874
40	0.173326	0.253474	0.501970	0.375890
80	0.073974	0.109328	0.221484	0.967150
160	0.024875	0.036970	0.075089	5.550542

4 Summary

We have presented a finite element method to find the approximate solution of the non-linear NLIF model. The performance of the proposed method is validated by comparing it with an existing scheme in the literature. The approximate solutions determined by the Galerkin finite element method have the same accuracy as achieved by a finite difference scheme (WENO-FDM). The proposed scheme takes less computational time compared to WENO-FDM. The reason behind that the existing scheme contains many computational factors such as smoothness indicator functions and non-negativity weights etc. Moreover, we also included the role of both excitatory and inhibitory impulses in the model equation. The behavior of the solution is simulated by taking some test examples. The results reveal that the continuous Galerkin FEM is better than the WENO-FDM for simulating dynamics of neuronal networks in the brain.
The next chapter presents a numerical study for the EI population density model based on LIF neurons with the effect of the refractory period and transmission delays.

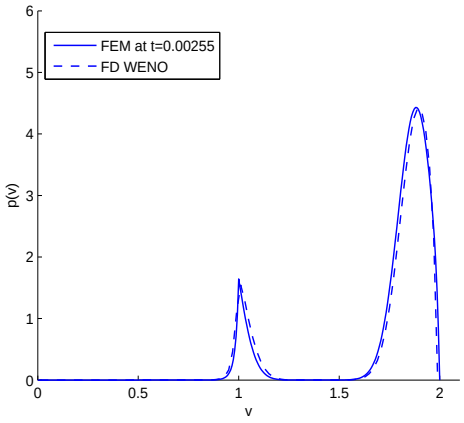

(a) Comparison of existing scheme and FEM for numerical Solution $p(v,t)$.

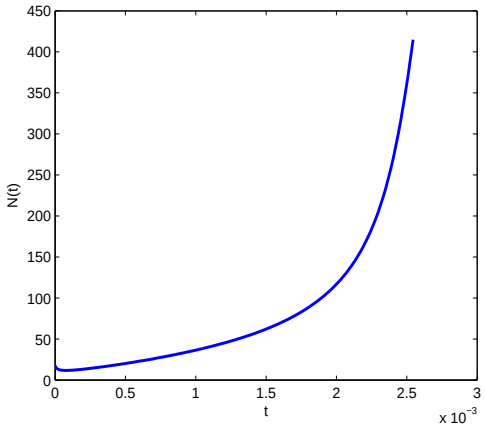

(b) Time evolution of the firing rate $N(t)$

Figure 2.4: Left: The approximate solution $p(v,t)$, Right: Firing rate $N(t)$ for initial data given in Eq. (2.18) with mean $v_0 = 1.83$ and variance $\sigma_0^2 = 0.003$. The system is considered for the excitatory case i.e. by taking $b = 0.5 > 0$ with activity dependent noise $a(N(t)) = a_0 = 1$.

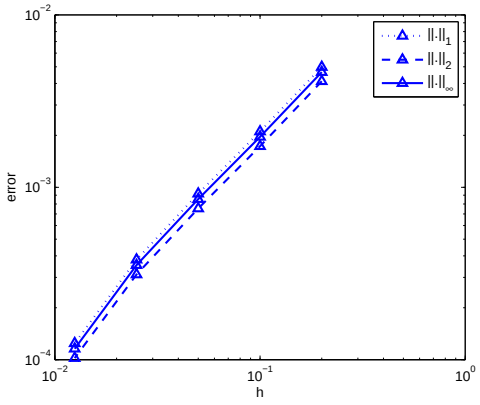

Figure 2.5: Error estimates for the approximate solution $p(v,t)$ graphically represented in Figure. 2.1.

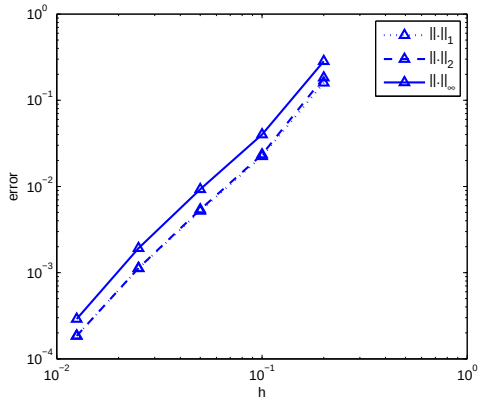

Figure 2.6: Error estimates for the approximate solution $p(v,t)$ graphically represented in Figure 2.3.

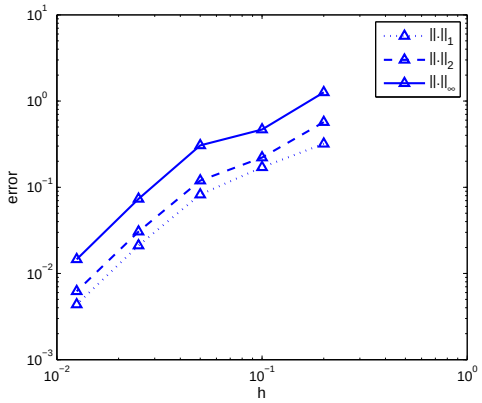

Figure 2.7: Error estimates for the approximate solution $p(v,t)$ graphically represented in Figure 2.4.

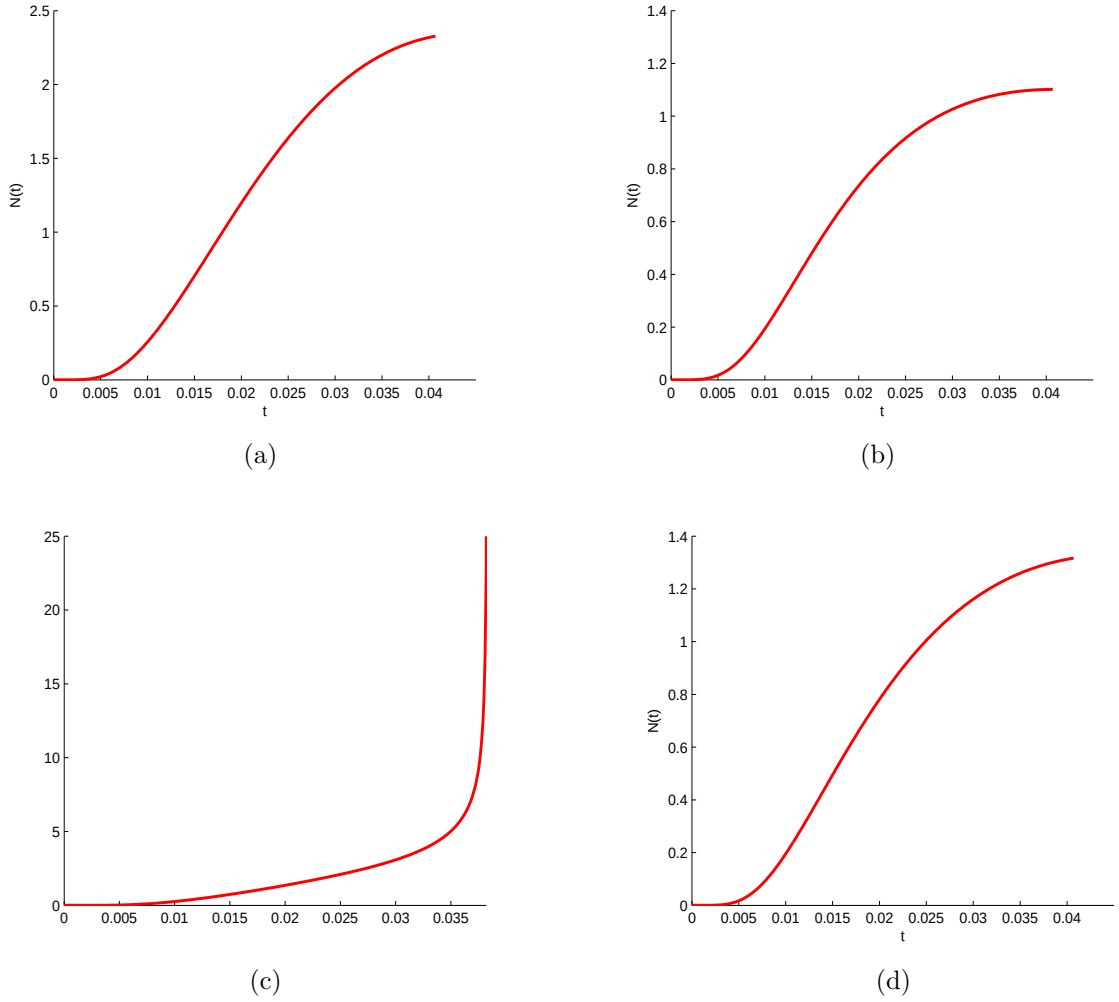

Figure 2.8: The N(t) for the initial data given in Eq. (2.18) having $v_0 = 1.5$ and $\sigma^2 = 0.005$ and activity dependence noise $a(N) = a_0 + a_1\, N(t)$, $a_0, a_1 > 0$. Top left: $b = 0.5$ and $a(N(t)) = 0.5 + N(t)/8$. Top right: $b = 0.5$ and $a(N(t)) = 0.4 + N(t)/100$. The bottom left case seems to depict a blow-up phenomena. Bottom left: $b = 1.2$ and $a(N(t)) = 0.5 + N(t)/8$. Bottom right: $b = 1.2$ and $a(N(t)) = 0.4 + N(t)/100$.

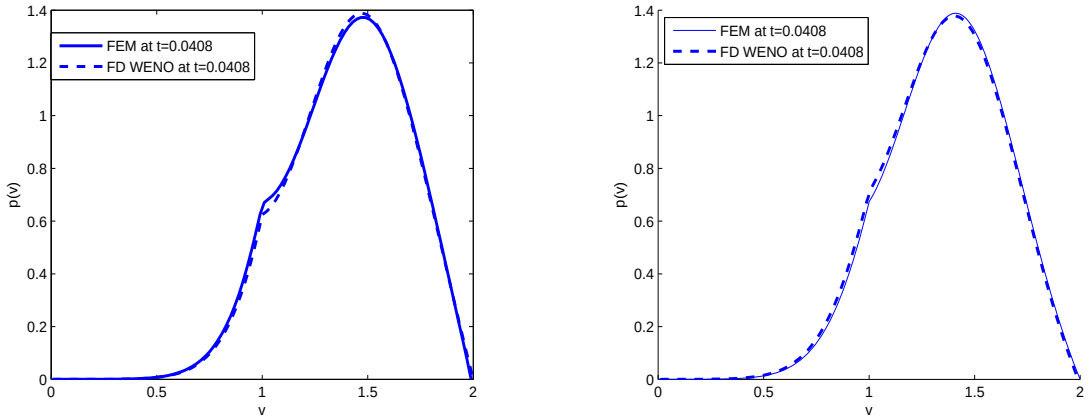

(a) (b)

Figure 2.9: The numerical simulation of $p(v,t)$ for initial data given in Eq. (2.18) with mean $v_0 = 1.5$ and variance $\sigma_0^2 = 0.005$ and with activity dependent noise $a(N(t)) = 1 + N(t)/100$. Left: The system is considered for the excitatory case i.e. by taking $b = 0.5 > 0$. Right: The system is considered for the inhibitory case i.e. by taking $b = -0.5 < 0$.

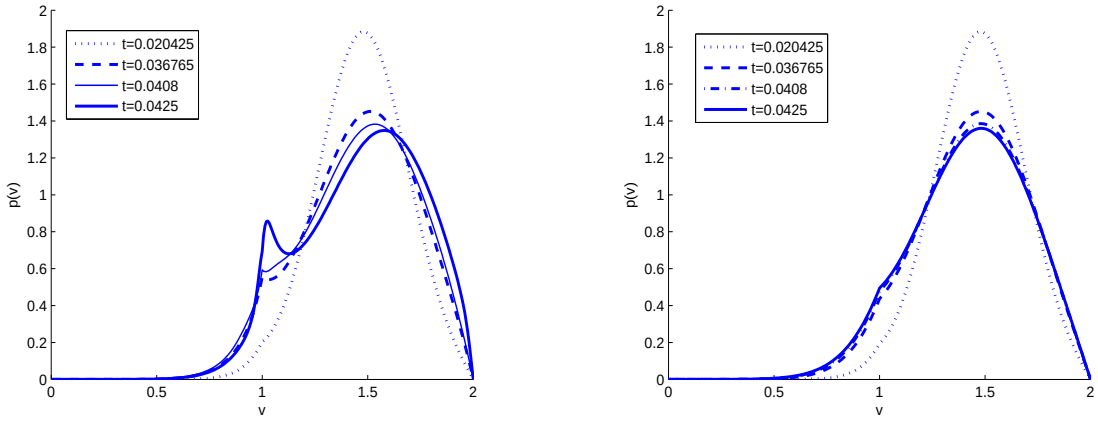

(a) (b)

Figure 2.10: The approximate solution $p(v,t)$ using FEM for the initial data given in Eq. (2.18) having $v_0 = 1.5$ and $\sigma^2 = 0.005$ and activity dependence noise $a(N) = a_0 + a_1\, N(t)$, $a_0, a_1 > 0$. Top left: $b = 1.2$ and $a(N(t)) = 0.5 + N(t)/8$. Top right: $b = 1.2$ and $a(N(t)) = 0.4 + N(t)/100$.

Chapter 3

A Numerical Approximation for the Excitatory-Inhibitory Networks with Delay and Refractory Periods [1]

The previous chapter discussed a FEM to find the approximate solution of the nonlinear NLIF model. This chapter introduces a non-linear NLIF model in the presence of a refractory period and transmission delay. For the numerical approximation, the DG scheme is applied for the spatial discretization, and discussed for the stability analysis. Moreover, the strong stability-preserving explicit Runge-Kutta (SSPERK) method is executed for temporal discretization. The proposed scheme is compared with the existing finite difference approach namely the weighted essentially non-oscillatory (WENO) scheme. Numerical results depict that the proposed scheme demands less computational time compared to the existing scheme which is demonstrated by taking some numerical test examples.

1 Introduction

The neuron network models are broadly used tools in computational neuroscience. In 1907, Lapicque introduced the most simplest and now widely used IF model of neurons in which incoming potential of postsynaptic potential generates an action potential when their sums reach a threshold. Afterward many authors investigated various IF models, for a single neuron and later on describe the dynamic behavior of a population of neurons ([9, 53, 80, 120]). Despite, from a computational approach, it is difficult to tackle a large network of neurons. In the recent past, a population density approach of IF neurons have been developed for the simulation of large neural network [54, 154]. It describes the population density function $p(v, t)$ to determine a neuron in a voltage v at a time t considering each neuron follows from a simple IF dynamics and the coupling changes in the current. The description of the properties of these neurons can be mathematically modeled using ODEs and/or PDEs. A various type of numerical schemes have been designed to solve these types of model equation[132, 155–157].
In this chapter, we examine the LIF model from a numerical perspective. The simplest NNLIF model which is widely analyzed for one population in the absence of refractory state and delays,

[1] Dipty Sharma and Paramjeet Singh *"Discontinuous Galerkin Approximation for an Excitatory-Inhibitory Networks with Delay and Refractory Periods"*, International Journal of Modern Physics C, **31(3)**, 2050041, 2020.

is given in [127, 158]. Moreover, the addition of a refectory period just after the membrane potential (voltage) hits threshold level (V_F), provides more realistic LIF dynamics (see [74, 124]). These authors provide the theoretical and numerical analysis about the blow-up criteria and the presence of steady states of the NNLIF model with the effect of the refractory period.
We study the more realistic NNLIF model for the description of the neural network considering only one type of population either average-excitatory or average-inhibitory with the effect of the refractory period and transmission delays [124]. We will follow that at a minimum one steady-state is produced by the presence of the refractory stage, while in the lack of a refractory state, there are some argument values for which the model has no steady states. Moreover, where there are transmission delays, global-in-time solutions exist for the average-excitatory population (see [123]). Following, we review the model equation of the population density function of IF neurons.
This model equation consists of an ODE in which all the interactions of the neurons (excitatory and inhibitory) with a network is modeled in its simplest form using synaptic input current $I_\alpha(t)$. The membrane potential $V_\alpha(t)$, describe the dynamics of neuron (either excitatory i.e. $\alpha = E$ or inhibitory neuron i.e. $\alpha = I$) is defined in the following equation

$$\tau_m \frac{dV_\alpha}{dt} = -V_\alpha(t) + I_\alpha(t), \tag{3.1}$$

with the membrane time constant τ_m. The interactions with other neurons provoke the neuron to fire when $V_\alpha(t)$ at a time t reaches certain threshold V_F, and $V_\alpha(t)$ reset to reset potential $V_R < V_F$ (firing potential). The synaptic current $I_\alpha(t)$ is described by the following stochastic process

$$I_\alpha(t) = J_E^\alpha \sum_{n=1}^{N_E} \sum_m \delta(t - t_{E_m}^n - \mathcal{D}_E^\alpha) - J_I^\alpha \sum_{n=1}^{N_I} \sum_m \delta(t - t_{I_m}^n - \mathcal{D}_I^\alpha), \quad \alpha = E, I,$$

where, delta function is used to describe every spike response. Moreover, the terms $\mathcal{D}_E^\alpha, \mathcal{D}_I^\alpha \geq 0$ are the synaptic delays ([6, 124]). Here, $t_{E_m}^n$ and $t_{I_m}^n$ for EI neurons denotes the time of receiving the m^{th}-spike from n^{th}-presynaptic neuron. Moreover, the terms N_E and N_I are the connection from the neurons in a network and J_k^α for $(\alpha, k = E, I)$ are the synapses strengths. Recently, several authors [54, 80, 154] described the synaptic input current $I_\alpha(t)$ as a continuous in time stochastic process of Ornstein-Uhlenbeck type given below

$$I_\alpha(t)dt \approx \mu_c^\alpha dt + \sigma_c^\alpha \, d_{B_t}, \quad \alpha = E, I. \tag{3.2}$$

Initially, it is supposed that the spike generation of each neuron is defined by Poisson process with stationary and independent increments [54]. Due to the use of these assumptions, the mean value of the current $(\mu_c^\alpha(t))$ and its variance $(\sigma_c^\alpha(t))$ are given by

$$\mu_c^\alpha(t) = N_E \, J_E^\alpha \, r_E(t - \mathcal{D}_E^\alpha) - N_I \, J_I^\alpha \, r_I(t - \mathcal{D}_I^\alpha),$$

$$\sigma_c^{\alpha}(t) = N_E\,(J_E^{\alpha})^2\ r_E(t-\mathcal{D}_E^{\alpha})\ - N_I\ (J_I^{\alpha})^2\ r_I(t-\mathcal{D}_I^{\alpha}).$$

Further, the standard firing rate $r_\alpha(t)$ is given below as discussed in [55]

$$r_\alpha(t) = N_{\alpha,ext} + N_\alpha(t),$$

where $N_\alpha(t)$ is the mean firing rate of the network and $N_{\alpha,ext}$ is the frequency of the external input. Here, the term $N_{I,ext} = 0$, as the external connections are with excitatory neurons. Comprising the continuous form of $I_\alpha(t)$ in SDE model (3.1), we obtain

$$\tau_m\, dV_\alpha(t) = (-V_\alpha(t) + \mu_c^{\alpha}(t))\, dt + \sigma_c^{\alpha}(t)\, dB_t,\ V_\alpha \le V_F,\ t \ge 0,$$

with $\tau_m = 1$. The term B_t is the standard Brownian motion with the assumption that, whenever the voltage of a neuron at a time t_o^-, arrives at a threshold level i.e. $V_\alpha(t_o^-) = V_F$ and then suddenly it reaches the resting potential, i.e., $V_\alpha(t_o^+) = V_R,\ V_R < V_F$. Further, using the equations (3.1) and (3.2), one can write the associated Fokker-Planck equation (FPE) (have a glimpse of [124] for details). Thus, the population density function $p(v,t) \ge 0$ of neurons with voltage $v \in (-\infty, V_F]$, at a time $(t \ge 0)$ is described by the following equation

$$\frac{\partial}{\partial t}p(v,t) + \frac{\partial}{\partial v}[h(v,N(t-\mathcal{D}))p(v,t)] - a(N(t-\mathcal{D}))\frac{\partial^2}{\partial v^2}p(v,t) \quad = \quad M(t)\,\delta(v-V_R), \tag{3.3}$$

where, $h(v,N(t)) = -v + b\ N(t) + N_{ext}$ and $a(N(t)) = a_0 + a_1\ N(t)$ with $a_0 > 0$, $a_1 \ge 0$. Here, the value of the connectivity parameter b depend on the neuron population type i.e. b is positive for the excitatory neuron population and negative for inhibitory neuron population. We have Dirac mass in the source term of Eq. (3.3), as all the neurons at the time $t \ge 0$ fired, delivered the signal on the network and then reset to the voltage $V_R < V_F$ and remains in a refractory state for some period $\tau > 0$. There are many choices available in literature for $M(t)$, as $M(t) = N(t-\tau)$ proposed in [54] or $M(t) = \dfrac{R(t)}{\tau}$, as defined in [74]. The ODE is therefore provided below for the probability density $R(t)$ of neurons in a refractory state

$$\frac{d}{dt}R(t) = N(t) - M(t). \tag{3.4}$$

In this dynamical system, when the neurons trigger spikes and transmit the signals over the network, their voltage reset instantly to the reset potential V_R. Since at the resting time, no neuron has the voltage of firing, the initial and boundary conditions are provided as

$$p(v,0) = p^0(v) \ge 0,\ p(-\infty,t) = 0,\ p(V_F,t) = 0,\ R(0) = R^0 > 0. \tag{3.5}$$

In the above equation, the conservative property of the neurons is often easily verified by identifying the average firing rate of the network. Since the term $N(t)$ is the neuron flux at V_F,

its value is provided by

$$N(t) = -a(N(t-\mathcal{D}))\frac{\partial p(V_F,t)}{\partial v} \geq 0. \tag{3.6}$$

Additionally, the nonlinearity of Eq. (3.3) comes from $N(t)$, as it is described in terms of BCs on the distribution function $p(v,t)$. Since, R denotes the probability and Eq.(3.3) describe the probability density function, then

$$\int_{-\infty}^{V_F} p(v,t)dv + R(t) = \int_{-\infty}^{V_F} p^0(v)dv + R^0 = 1. \tag{3.7}$$

The problem (3.3) together with Eqs.(3.4-3.5) is a second-order nonlinear time-dependent PDE. Due to nonlinearity and having delayed term, this model equation can not be solved analytically [128, 158–169]. Therefore, the numerical schemes normally used are: the technique of finite difference as discussed in [170–172], finite element method provided in [141, 143], meshless method [173] and a numerical collacation method as proposed in [174, 175]. In recent work, Cáceres and Schneider used the finite difference WENO scheme to get the approximate solution of the model equation (see [124]). This existing scheme uses a reconstruction procedure to recover the degree polynomial values at cell boundaries from the cell averages of the cell itself and several adjacent cells; the discontinuous Galerkin method does not need any reconstruction as it stores and evolves the whole degree polynomial in each cell. where other methods don't provide accurate solutions or even fail.

For all the above reasons, this chapter presents a numerical technique based on the DG method to find a more accurate solution in the sense of accuracy and computational approach. This method provides local approximation flexibility by using discontinuous piecewise polynomials as a basis function and thus, can be designed for the higher order of accuracy which is then determined locally by using a higher-order polynomial approximation within an element. An elementary introduction to the discontinuous Galerkin (DG) approach can be found in [115, 176]. Reed and Hill first introduced it in 1973 as a scheme for solving linear time-dependent hyperbolic equations [177], and further to solve nonlinear equations by Cockburn et al. [178, 179]. Applying the DG technique directly to the higher-order equations is hard or somehow impossible.

Therefore, the local discontinuous Galerkin (LDG) method is used to find the approximate solution for the second-order nonlinear Eq.(3.3-3.5) as introduced by Cockburn and Shu [178]. More precisely, the approach used in this technique is to rewrite the higher-order equation into a first-order system and then apply the classical DG method on the reduced system. This concept is motivated by the successful numerical results performed by Bassy and Rebay [180]. The LDG method is somehow the same as the general DG method with a different approach is to design the numerical flux to ensure the stability of the scheme [115]. We hereby brief out the above discussion and the work done in this chapter:

- The population density approach of IF neurons is being used to describe the neuronal

variability.

- We examined the general NNLIF model outlined by the Eq. (3.3-3.5) in the influence of refectory period and transmission delays.

- DG approximation is proposed to solve the model equations and the stability analysis is then discussed in detail.

- The detailed comparison of the third-order WENOFD and the third-order RKDG method is presented by using some test examples.

- We have chosen a third-order version of both schemes to compare just as examples, in practice, higher-order versions can be and often used.

- The performance of the constructed scheme is displayed via some numerical simulations.

1.1 Preliminaries

Here, we provide some fundamental definitions and additional results that are already known (see [74, 124, 158]). Firstly, we begin with the concept of a weak solution as we are dealing with the nonlinearity of the model equation.

Definition 1.1. *A set of non-negative functions* (p, N, R) *with* $p \in L^\infty(\mathbb{R}^+; L^1_+(-\infty, V_F))$, $N \in L^1_{loc,+}(\mathbb{R}^+)$ *and* $R \in L^\infty_+(\mathbb{R}^+)$ *is a weak solution of (3.3)-(3.5) if for any test function* $\phi(v,t) \in C^\infty((-\infty, V_F) \times (0,T))$ *such that* $\dfrac{\partial^2\phi}{\partial v^2}, v\dfrac{\partial\phi}{\partial v} \in L^\infty((-\infty, V_F) \times (0,T))$, *we have*

$$\begin{aligned}
&\int_0^T \int_{-\infty}^{V_F} p(v,t)\left[-\frac{\partial\phi}{\partial t} - \frac{\partial\phi}{\partial v}h(v, N(t-\mathcal{D})) - a(N(t-\mathcal{D}))\frac{\partial^2\phi}{\partial v^2}\right] dvdt \\
&= \int_0^T M(t)\,\phi(V_R,t) - N(t)\,\phi(V_F,t)\,dt \\
&+ \int_{-\infty}^{V_F} p^0(v)\phi(v,0)dv - \int_{-\infty}^{V_F} p(v,T)\phi(v,T)dv,
\end{aligned}$$

and R *is the solution of the ODE provided in Eq. (3.4). Here, the space* $L^p(\Omega)$, $1 \le p < \infty$, *refers to the space of functions such that* f^p *is integrable in* Ω, *while* L^∞ *corresponds to the space of bounded functions and* L^∞_+ *denotes the space of non-negative bounded functions in* Ω. *The set of infinitely differentiable functions in* Ω *is denoted by* $C^\infty(\Omega)$ *used as test functions in the notion of weak solution and* $L^1_{loc,+}(\Omega)$ *indicates the set of non-negative functions that are locally integrable.*

Moreover, we state the result of the steady-state and finite time blow-up with the effect of

refractory state and no transmission delays, i.e $\mathcal{D} = 0$. We just provide the outcomes for the case of one population model as given in [124], described by the below-mentioned theorems.

Theorem 1.1. *(Long time behavior) Supposed that a small enough parameter of connectivity, $|b| \ll 1$, a constant diffusion coefficient, $a(N) = a_m > 0$, with no transmission delay, $\mathcal{D} = 0$, and the initial data is near enough to the unique steady state $(p_\infty, R_\infty, N_\infty)$,*

$$\int_{-\infty}^{V_F} p_\infty(v) \left(\frac{p^0(v) - p_\infty(v)}{p_\infty(v)}\right)^2 dv + R_\infty \left(\frac{R(0)}{R_\infty} - 1\right)^2 \leq \frac{1}{2|b|}. \tag{3.8}$$

Then, there exist $\mu > 0$ for fast decaying solution to (3.3-3.5) in the sense of Definition 1.1, the following a priori estimates hold for all $t > 0$:

$$\begin{aligned}
&\int_{-\infty}^{V_F} p_\infty(v) \left(\frac{p(v) - p_\infty(v)}{p_\infty(v)}\right)^2 dv + \frac{(R(t) - R_\infty)^2}{R_\infty} \\
&\leq e^{-\mu t} \left[\int_{-\infty}^{V_F} p_\infty(v) \left(\frac{p^0(v) - p_\infty(v)}{p_\infty(v)}\right)^2 dv + \frac{(R^0 - R_\infty)^2}{R_\infty}\right].
\end{aligned}$$

The delay terms in the results shown above are assumed to vanish, moreover, for the model with small non-zero values of the delays, a similar procedure could be used to prove the fast exponential convergence to steady-state (see [124]). As the above results show the long-time behavior of the solution, the following result shows the finite-time blow-up solution with the lack of the delay term.

Theorem 1.2. *(Blow-up in excitatory case) Assume that the drift and diffusion coefficients satisfy*

$$h(v, N) + v \geq bN \quad \text{and} \quad a(N) \geq a_m > 0, \tag{3.9}$$

for all $-\infty < v \leq V_F$ and all $N \geq 0$. Let us consider the two cases for the average-excitatory network :

1. *For fixed initial data $p^0 \neq 0$ with $b > 0$ large enough.*
2. *For fixed $b > 0$, choose $\mu > \max\left(\frac{V_F}{a_m}, \frac{1}{b}\right)$ with the initial data is concentrated enough around $v = V_F$, in the sense that*

$$\int_{-\infty}^{V_F} e^{\mu v}\, p^0(v)\, dv \geq \frac{e^{\mu V_F}}{b\mu},$$

then global-in-time weak solutions does not exist to (3.3-3.5).

From our numerical simulation, we find that only a period of the refractory state is not sufficient to keep off the blow-up. The numerical results depict the finite-time blow-up phenomena since

the transmembrane potentials of the population (fully excitatory) are near enough to the certain threshold level, or if there is a sufficiently large connectivity parameter $b > 0$. Thus, it is necessary to add some transmission delay between excitatory neurons to achieve the global-in-time existence of the solution [181].

Definition 1.2. *At the nth time level, the total variation (TV) of a discrete scaler solution is described as*

$$TV(\mathcal{P}^n) = \sum_i |\mathcal{P}^n_{i+1} - \mathcal{P}^n_i|,$$

and the scheme is called TVD (total variation diminishing) if the following holds

$$TV(\mathcal{P}^{n+1}) \leq TV(\mathcal{P}^n).$$

In addition, the scheme is called total variation bounded (TVB) if the growth in total variation is bounded that is

$$TV(\mathcal{P}^n) \leq M,$$

for all n and for some constant $M > 0$.

2 The Numerical Scheme

Here, we develop the numerical approximation using the DG approach to solve the model (3.3-3.5) described by the following equation

$$\frac{\partial}{\partial t}p(v,t) + \overbrace{\frac{\partial}{\partial v}[h(v, N(t-\mathcal{D}))p(v,t)]}^{\text{Drift}} - \overbrace{a(N(t-\mathcal{D}))\frac{\partial^2}{\partial v^2}p(v,t)}^{\text{Diffusion}} = \overbrace{M(t)\,\delta(v - V_R)}^{\text{Reset}}, \quad (3.10)$$

as the problem under consideration is a second order nonlinear time-dependent PDE, we use the LDG approach [178]. Using this approach, firstly we reduce the Eq.(3.10) into a first-order system by introducing an additional variable q as follows:

$$\begin{aligned} \frac{\partial p(v,t)}{\partial t} + \frac{\partial}{\partial v}\left(h(v, N(t-\mathcal{D}))\, p(v,t) - \sqrt{a(N)}\, q(v,t)\right) &= M(t)\delta(v - V_R), \\ q(v,t) &= \sqrt{a(N)}\frac{\partial p(v,t)}{\partial v}. \end{aligned} \quad (3.11)$$

Now we will apply a classical DG approach to the above reduced system (3.11) for the efficient numerical solution. In this approach, the spatial discretization for $v \in D := [-V_{left}, V_F]$ is tackled by taking K non-overlapping elements say $D_k = [v_k, v_{k+1}]$, for $k = 1, 2, \ldots, K$, where size of each element is defined as $\Delta v_k = v_{k+1} - v_k$ and $\Delta v = \max_{1 \leq k \leq K} \Delta v_k$. In more general form

the above Eq.(3.11) can be read as

$$\begin{aligned} \frac{\partial p(v,t)}{\partial t} + \frac{\partial}{\partial v}\left(f(p(v,t)) - \sqrt{a(N)}q(v,t)\right) - M(t)\delta(v - V_R) &= 0, \\ q(v,t) - \sqrt{a(N)}\frac{\partial p(v,t)}{\partial v} &= 0, \end{aligned} \tag{3.12}$$

where $f(p(v,t)) = h(v, N(t-\mathcal{D}))\ p(v,t)$. Initially, assume that the local solution $p^k(v,t)$ is then represented in each element by a local polynomial approximation $p_h^k(v,t)$ which belongs to the following finite dimensional space

$$V_h = \{\psi_h : \psi_h|_{D_k} \in P^N(D_k); \quad k = 1, \ldots, K\},$$

i.e., as the space of piecewise polynomial functions of degree no more than $N \geq 1$ over D_k. This function space is admissible to have discontinuities across element interfaces which describes the flexibility of the proposed scheme. Local polynomials $p_h^k(v,t)$ and $q_h^k(v,t)$ in general framework of degree N with $Np = N + 1$ grid points say v_i over D_k are expressed as follows:

$$p_h^k(v,t) = \sum_{i=1}^{N_p} p^k(v_i^k, t) l_i^k(v) = \sum_{n=1}^{N_p} \hat{p}_n^k(t)\psi_n(v),$$

$$q_h^k(v,t) = \sum_{i=1}^{N_p} q^k(v_i^k, t) l_i^k(v) = \sum_{n=1}^{N_p} \hat{q}_n^k(t)\psi_n(v),$$

where $\psi_n(v)$ is the Legendre basis functions and $l_i(v)$ is the Lagrange fundamental polynomial. In the above expression, $\hat{p}_n^k(t)$ and $\hat{q}_n^k(t)$ are the modal coefficients defined on the k-th element. In this approach, the basis functions should be chosen carefully give rise to perfectly conditioned Vandermonde matrices. We have to choose the basis functions just as the resulting interpolation is well-behaved in the sense of best fit. A polynomial basis such as monomials $\psi_n(v) = v^{n-1}$ will generate linearly dependent basis, and then the condition number for the Vandermonde matrix grows exponentially as order of polynomial increases. To describe computationally stable approach, we recover an orthonormal basis using Gram-Schmidt orthogonalization approach given by

$$\psi_n(r) = \frac{P_{n-1}(r)}{\sqrt{\gamma_{n-1}}}, \quad \gamma_{n-1} = \frac{2}{2n+1},$$

where $P_n(r)$ are the classic Legendre polynomial of order n, which are orthogonal on $I = [-1, 1]$ and γ_n is the orthonormalizing weight. The above approach has been rediscovered on various occasions by various researchers, see ([115]). We also need to bother about the choice of discrete points of approximation as the accuracy of the method is based on the order of the local polynomial interpolation. We choose the grids point v_i^k, $i = 1, \ldots, N_p$, by introducing the

following affine mapping :

$$v \in D_k : v(r) = v_k + \frac{1+r}{2}\Delta v_k, \quad \text{where } \Delta v_k = v_{k+1} - v_k,$$

with the reference variable $r \in I = [-1, 1]$. By choosing appropriate r_i as a quadrature point, we ensure that resulting interpolation is well behaved in the sense of well-conditioned Vendermonde matrix. We choose the quadrature points as Gauss-Lobatto points for the interpolation, which have the property that they are exact fit for a polynomial of degree $2N_p - 1$ [182]. Thus grid distribution becomes the Legendre-Gauss-Lobatto (LGL) distribution along the edges of the element. We define as given below, the vector of nodal and modal values on D_k

$$p_h^k = [p_1^k, \ldots, p_{Np}^k], \quad \hat{p}_h^k = [\hat{p}_1^k, \ldots, \hat{p}_{Np}^k],$$

and the vector of local Lagrange polynomials and shape functions on D_k are

$$l_N^k = [l_1^k, \ldots, l_{Np}^k], \quad \psi_N^k = [\psi_1^k, \ldots, \psi_{Np}^k].$$

The Vandermonde matrix defined as $V_{ij} = \tilde{P}_{j-1}(v_i)$, implies the connection between modal and nodal representation as

$$p_h^k = V\hat{p}_h^k, \quad \hat{p}_h^k = V^{-1}p_h^k, \quad V^T l_N^k = \psi_N^k.$$

In order to approximate the solution (p_h, q_h), firstly we multiply the system (3.12) by a test function and then integrate over a element D^k. By taking again integration by parts results in the following equation: Find $p_h^k, q_h^k \in V_h$, such that the proposed scheme leading to

$$\begin{aligned}
\int_{D_k} \partial_t p_h^k \; l_j^k(v)\, dv &= -\int_{D_k} \partial_v g_h^k \; l_j^k(v)\, dv + M(t) \int_{D_k} (\delta(v - V_R)) l_j^k(v)\, dv + \left[g_h^k - (g_h^k)^*\right] \; l_j^k(v)\Big|_{v_l}^{v_r}, \\
\int_{D_k} q_h^k \; l_j^k(v)\, dv &= \int_{D_k} \sqrt{a(N)}\; \partial_v p_h^k \; l_j^k(v)\, dv - \left[\sqrt{a(N)} p_h^k - (\sqrt{a(N)} p_h^k)^*\right] \; l_j^k(v)\Big|_{v_l}^{v_r},
\end{aligned} \tag{3.13}$$

for all the test function $l_j^k(v)$ and $g_h^k = f_h^k(p) - \sqrt{a(N)} q_h^k$. In this approximation due to the lack of the continuity of the test functions at the element interfaces, solution is not unique exactly at these boundary points. These element interface values must be replaced by the numerical flux to guarantee stability and convergence. The critical ingredient for developing an accurate and stable scheme is the right design of these fluxes. Thus $(g_h^k)^*$ and $\left(\sqrt{a(N)} p_h^k\right)^*$ at the interface is given by a single valued monotone numerical flux, therefore it should be a function of $g_h^k(v_l^k, t)$ and $g_h^{k-1}(v_r^{k-1}, t)$ at the left end and it should depend upon $g_h^k(v_r^k, t)$ and $g_h^{k+1}(v_l^{k+1}, t)$ at the right end of the element D^k (see [115]). Well known monotonic flux satisfies the consistency, continuity and monotonicity conditions is Lax-Friedrichs flux. We split the flux and define a

jump along normal $\hat{n}$ is given by

$$f^*(a,b) = \frac{f(a)+f(b)}{2} + \hat{n}\frac{\alpha}{2}(a-b) \quad \text{where} \quad \alpha = \max_p |f'(p)|. \tag{3.14}$$

Moreover, the above defined flux can be represented as

$$f^*(a,b) = \begin{cases} f^+(a) + f^-(b), & \hat{n} = 1 \\ f^-(a) + f^+(b), & \hat{n} = -1, \end{cases}$$

where

$$f^+(a) = \frac{1}{2}\left(f(a) + \alpha a\right), \quad f^-(b) = \frac{1}{2}\left(f(b) - \alpha b\right).$$

Additionally, the subscript "$-$" is used for the interior information within the element and "$+$" is used for the exterior information within the neighboring element. Further, homogeneous Dirichlet BCs are also imposed through numerical flux [115]. Moreover, following are the mass and stiffness matrices for the element D^k

$$M_{ij}^k = \int_{D_k} l_i(v) l_j(v)\, dv, \qquad S_{ij}^k = \int_{D_k} l_i(v) l_j'(v) dv,$$

and the matrices correspond to the reference interval $[-1,1]$ are given below

$$M_{ij} = \int_{-1}^{1} l_i(r) l_j(r) dr, \qquad S_{ij} = \int_{-1}^{1} l_i(r) l_j'(r) dr,$$

where $l_i(r)$ is the ith Lagrange polynomial at the LGL nodes r_i on reference interval $[-1,1]$. Using these matrices, we find the following relation

$$M_{ij}^k = \frac{1}{2}(v_r^k - v_l^k) M_{ij}, \qquad S_{ij}^k = S_{ij}.$$

Now, we will use the integral property of the delta function located at the element interface D^k and D^{k+1}

$$\int_{D^k} \delta(v - V_R) l_j(v)\, dv = \delta_{(Np)j}, \quad \int_{D^{k+1}} \delta(v - V_R) l_j(v)\, dv = \delta_{1j}, \quad \text{where} \quad \delta_{ij} = \begin{cases} 1, & i = j \\ 0, & i \neq j \end{cases}$$

where δ_{1j} reads a single Lagrange polynomial, say $l_1^{k+1}(v)$ correspond to rightward wave propagation over D^{k+1} and $l_{N_p}^k(v)$ correspond to the leftward wave propagation over D^k. Using the monotonic flux and the above terminology of local mass and stiffness matrices, we get the

element-wise reduced scheme for (3.10) can be expressed as

$$\begin{aligned} M^k \frac{dp_h^k}{dt} + S^k\, g_h^k &= \left[g_h^k - (g_h^k)^*\right] l_j^k(v)\Big|_{v_l}^{v_r} + M(t)\delta_{ij}, \\ M^k q_h^k - S^k \sqrt{a(N)} p_h^k &= -\left[\sqrt{a(N)} p_h^k - (\sqrt{a(N)} p_h^k)^*\right] l_j^k(v)\Big|_{v_l}^{v_r}. \end{aligned} \tag{3.15}$$

Thus, we can write the approximate system of the model equation (3.10), as the following ordinary differential equation

$$\begin{aligned} \frac{d\,p}{dt} &= L(p,t), \quad \forall t \geq 0, \quad \forall v \in [-V_{left}, V_F] \\ p(v,0) &= p^0(v) \quad \forall v \in [-V_{left}, V_F], \end{aligned}$$

where L is the sum of the approximations of the drift, diffusion, and the source term. The resulting ODE is then solved by the using of time discretization techniques provided in [183, 184]. In practice, we want a higher-order time discretization scheme that still satisfies the stability property, when coupled with nonlinear stability preserving spatial discretization scheme. Explicit methods can be directly used for this and the step size for time is, however, confined for these techniques. The connection between the Δt (maximum time step) and the Δv (minimum element size) is acknowledged as CFL-condition. More precisely, for the method of lines they look like:

$$c\frac{\Delta t}{\Delta v} \leq CFL,$$

where c is the magnitude of the largest wave velocity of the hyperbolic system and CFL a constant depending on the time step and spatial discretization. Further, for a DG method with the use of polynomials degree N and $N+1$ stages RK method, the upper bound of this CFL number implies as

$$\text{CFL} = \frac{1}{2N+1},$$

is optimal for $N = 0$ and $N = 1$. For $N \geq 2$, it is numerically shown that this upper bound is less than 5% smaller than the optimal CFL number [179]. This is a necessary condition for non-linear flux functions. We use the SSPERK higher-order time discretization approach. This method ensure the TVD property with possible different step size (time), if whenever the first order forward Euler time discretization of method of lines is strongly stable under a predefined norm with suitable time step restriction [184]. The time evolution of the solution p is thus approximated by a widely used approach in DG as the following third order explicit

strong-stability preserving (SSP) RK method

$$\begin{aligned} p^1 &= p^n + dt\, L(t_n, p^n), \\ p^2 &= \frac{3}{4}p^n + \frac{1}{4}p^1 + \frac{1}{4}dtL\left(t_n + dt, p^1\right), \\ p^{n+1} &= \frac{1}{3}p^n + \frac{2}{3}p^2 + \frac{2}{3}dtL\left(t_n + \frac{1}{2}dt, p^2\right), \end{aligned}$$

where $p^n = p(v, t_n), n = 0, 1, 2, \ldots$ and $t_n = n\ dt$. We dynamically choose the term dt based on the the CFL condition

$$dt \leq \min_{i,k} \frac{CFL(\Delta v_i^k)^2}{|h(v_i^k, N(t - \mathcal{D}))|}.$$

Through the time evolution of the solution for each time t, we require the value of N at $(t - \mathcal{D})$. Thus we set a time step dt and identify an array of $P = \dfrac{\mathcal{D}}{dt}$ values of $N(t)$ for the time interval $[k\mathcal{D}, (k+1)\mathcal{D}), k = 0, 1, 2, \ldots$. Thereafter these values being utilized to find $N(t - \mathcal{D})$ (delayed values) for the interval of time $[(k+1)\mathcal{D}; (k+2)\mathcal{D})$ using linear interpolation. Initially all the array values are zero as $N(t) = 0, \forall t < 0$, therefore all the recovered values are zero for $(k = 0)$.

3 Stability Analysis

Here, the stability analysis of the designed scheme (3.15) is discussed for the case of positive drift coefficient $h(v, N) > 0$, and the similar process can be used for $h(v, N) < 0$. Thus, we have the following stability result of the numerical scheme proposed for this chapter.

Proposition 3.1. *The DG approach with monotonic Lax-Friedrichs flux approximation (3.14) for the equation (3.3-3.5) is stable.*

Proof. We consider a local element-wise operator β_h over a single interval k, bounded by $[v_k, v_{k+1}]$, using the shape functions $\psi_h, \varphi_h \in V_h$ (space of piecewise polynomial functions). Local operator β_h by summing up the equalities in Eq. (3.15) after multiply by ψ_h^T and φ_h^T, is given by

$$\begin{aligned} \beta_h(p_h, q_h, \psi_h, \varphi_h) &= \psi_h^T M^k \frac{dp_h^k}{dt} + \psi_h^T\ S^k\ g_h^k - \left[\psi_h \left(g_h^k - (g_h^k)^*\right)\right]_{v_l}^{v_r} + M(t) 1_{v=V_R} \\ &+ \varphi_h^T M^k q_h^k - \varphi_h^T S^k \sqrt{a(N)}\, p_h^k + \left[\varphi_h \left(\sqrt{a(N)}\, p_h^k - (\sqrt{a(N)} p_h^k)^*\right)\right]_{v_l}^{v_r}, \end{aligned}$$

where $g_h^k = \left(f_h^k(p) - \sqrt{a(N)} q_h^k\right)$. Initially, we find that if (p_h, q_h) suffice the numerical approach, then trivially we get

$$\beta_h(p_h, q_h, \psi_h, \varphi_h) = 0, \quad \forall (\psi_h, \varphi_h) \in V_h.$$

Besides, if we choose the test function as $\psi_h = p_h$ and $\varphi_h = q_h$, we realize that

$$p_h^T M^k p_h = \int_{D_k} \sum_{i=1}^{N+1} p_h^k(v_i) l_i^k(v) \sum_{j=1}^{N+1} p_h^k(v_j) l_j^k(v) dv = ||p_h^k||_{D_k}^2,$$

and proceeding in the same way to simplify the term $q_h^T M^k q_h$, we get the following

$$q_h^T M^k q_h = \int_{D_k} \sum_{i=1}^{N+1} q_h^k(v_i) l_i^k(v) \sum_{j=1}^{N+1} q_h^k(v_j) l_j^k(v) dv = ||q_h^k||_{D_k}^2.$$

Moreover,the term $p_h^T S^k p_h$, implies

$$\begin{aligned} p_h^T S^k p_h &= \int_{D_k} \sum_{i=1}^{N+1} p_h^k(v_i) l_i^k(v) \sum_{j=1}^{N+1} p_h^k(v_j) \frac{dl_j^k}{dv} dv = \int_{D_k} p_h^k(v)\ (p_h^k(v))' dv, \\ &= \frac{1}{2}\left[\left(p_h^k\right)^2\right]_{v_l}^{v_r}. \end{aligned}$$

After doing some mathematical calculations, we get

$$p_h^T S^k q_h + q_h^T S^k p_h = [pq]_{v_l}^{v_r}.$$

Using the above simplifications and some algebraic manipulation, we immediately recover the following

$$\frac{d}{dt}\|p_h^k\|_{D_k}^2 + \|q_h^k\|_{D_k}^2 + \Theta_r - \Theta_l = 0, \tag{3.16}$$

where

$$\Theta = -\frac{h}{2}(p_h^k)^2 + \sqrt{a(N)} p_h^k q_h^k + p_h^k (f_h^k(p))^* - \sqrt{a(N)}\left(p_h^k (q_h^k)^* + q_h^k (p_h^k)^*\right) + M(t) 1_{v=V_R}.$$

Here, we denoted the term $h(v, N)$ by h just for a simplicity. Now, taking value of p_h^k and q_h^k as internal value at the element interfaces v_r and central flux approximation for both $p_h^{k^*}$ and $q_h^{k^*}$. For the function $(f_h^k(p))^*$, we used the Lax-Friedrichs flux approximation as given in Eq.(3.14) and assuming h is continuous over D_k, we recover

$$\begin{aligned} \Theta_r &= -\frac{h}{2}(p_r^k)^2 + \sqrt{a(N)} p_r^k q_r^k + h\, p_r^k \left(\frac{p_r^k + p_l^{k+1}}{2} + \frac{\alpha}{2}\left(p_r^k - p_l^{k+1}\right)\right) \\ &\quad - \frac{\sqrt{a(N)}}{2}\left(p_r^k \left(\frac{q_r^k + q_l^{k+1}}{2}\right) + q_r^k \left(\frac{p_r^k + p_l^{k+1}}{2}\right)\right), \\ &= \frac{h}{2}(p_r^k\ p_l^{k+1}) + \frac{\alpha h}{2}\left((p_r^k)^2 - p_r^k\ p_l^{k+1}\right) - \frac{\sqrt{a(N)}}{2}\left(p_r^k\, q_l^{k+1} + p_l^{k+1}\, q_r^k\right). \end{aligned}$$

Similarly we can recover Θ_l as given below

$$\Theta_l = \frac{h}{2}(p_l^k\ p_r^{k-1}) + \frac{\alpha h}{2}\left(p_l^k\ p_r^{k-1} - (p_l^k)^2\right) - \frac{\sqrt{a(N)}}{2}\left(p_l^k\ q_r^{k-1} + p_r^{k-1}\ q_l^k\right) + M(t)1_{v=V_R},$$

where $p_r^k = p_h^k(x_r^k)$ denotes the internal value say (p^-) and $p_l^{k+1} = p_h^k(x_l^{k+1})$ is for external value say (p^+) of the right end of element k. For the stability, we must require that

$$\frac{d}{dt}||p_h||^2 + ||q_h||^2 \leq 0, \tag{3.17}$$

i.e. $(\Theta_r - \Theta_l) \geq 0$. Now taking $p^- = p^+$ and $q^- = -q^+$ at boundary points and summing over all the elements we recover the global energy condition

$$\frac{d}{dt}\|p_h\|^2 + \|q_h\|^2 = -\frac{\alpha h}{2}\sum_{k=1}^{K-1}\left(p_h^k(v_r^k) - p_h^k(v_l^{k-1})\right)^2 - \frac{h}{2}\left(\left(p_h^K(v_r^K)\right)^2 - \left(p_h^1(v_l^1)\right)^2\right) + M(t)1_{v=V_R} \leq 0,$$

with strong control on BCs and the function $M(t)$ at $v = V_R$. ■

4 Numerical Experiments

We now depict the behavior of the solutions of the NNLIF model using some test problems. The validation of the constructed scheme examined by its comparison with the existing technique in the literature [124]. For the numerical experiments, we used the second order polynomial approximation for each cell and the third order SSPRK time discretization for both of the schemes. We consider the problem (3.3) along with initial approximation

$$p(v,0) = \frac{c}{\sqrt{2\,\pi}} e^{\frac{-(v-v_0)^2}{2\,\sigma_0^2}}, \tag{3.18}$$

with a constant c ensure that $\int_{-V_{left}}^{V_F} p^0(v)\ dv \approx 1$. We consider an average-excitatory/inhibitory population model with the connectivity parameter $b > 0$ and $b < 0$ along with the other parameter as $V_F = 2, V_R = 1$ and $a(N) = 1$. In the influence of refractory state and transmission delays, we consider the following different cases to examine the behavior of the solution.

4.1 Average-excitatory population in the presence of transmission delays without refractory state

Firstly we will describe the behavior of the solution for the excitatory case $(b > 0)$ without a refractory period and find how the transmission delay affects the blow-up phenomenon of the solution.

The results illustrated in Figure 3.1a and 3.2a describes the behavior of excitatory neurons in the absence of transmission delays and finite time blow-up phenomena of the solution. From our

numerical simulations, we find that global-in-time solution present for excitatory neurons with the addition of the delay in transmission (Figure 3.1a and 3.2b). Thus, the numerical solution presented in Figure 3.1 and Figure 3.2 depicts how the transmission delay prevents the solution from blowing up even though the situation with no steady-state.

Example 1. *We consider the model* (3.3)-(3.5) *with the initial data* (3.18) *over the domain* $D = [0, 2]$ *and the following coefficients*

$$b = 0.5, \quad v_0 = 1.83 \quad \sigma_0 = 0.0003,$$

together with the BCs

$$p(0, t) = 0, \quad p(2, t) = 0.$$

In the Example 1, we consider the excitatory population without refractory state and the corresponding numerical solutions plotted in Figure 3.1 with $b = 0.5 > 0$. From Figure 3.1a, we find the finite time blows-up solution with the absence of delay i.e. ($\mathcal{D} = 0$) and get a steady state in the presence of delay as $\mathcal{D} = 0.1$ (Figure 3.1b).

Example 2. *Consider the system* (3.3)-(3.5) *with the same parameters and functions as defined in Example 1 with different value of the connected parameter* $b = 2.2$ *is large enough.*

We consider the highly connected excitatory population for the given system along with the other parameters as defined in the Example 1. From Figure 3.2a, if the excitatory neurons are concentrated near a threshold point V_F, we find the blows-up phenomenon with no transmission delay $\mathcal{D} = 0$ and the connectivity parameter i.e. $b = 2.2$ is large enough. This type of blow-up phenomenon can be avoided with the addition of transmission delay as we can observe in Figure 3.2b with $\mathcal{D} = 0.1$, the firing rate seems to rise without blowing up in finite time.

4.2 Average-excitatory population with the influence of refractory state and the transmission delays

In the above description, the excitatory system (3.3)-(3.5) analyzed in the absence of the refractory period. Now we will describe the behavior of excitatory neurons by taking $M(t) = \dfrac{R(t)}{\tau}$.

Example 3. *Consider the data as given in* (3.18) $\forall v \in [0, 2]$ *with the following coefficients*

$$b = 0.5, \quad v_0 = 1.83 \quad \sigma_0 = 0.0003, \quad R(0) = 0.2, \quad \tau = 0.025, \quad \mathcal{D} = 0.07$$

together with the BCs

$$p(0, t) = 0, \quad p(2, t) = 0.$$

In Figure 3.3, we analyzed the excitatory neuron network with the influence refractory period

that is $M(t) = \frac{R(t)}{\tau}, \tau = 0.025$. We find that only a refractory state is not enough to prevent the blow-up situation (Figure 3.3a). The numerical simulations sound that, it is essential to add some delay in transmission to obtain the global-in-time solution existence. Figure 3.3b depicts that the solution goes to the steady-state for the excitatory network with the effect of transmission delay.
Furthermore, we find that the delay in transmission also generates periodic solutions along with the prevention of blow-up situations. Here we present some examples to describe the situation to get periodic solutions.

Example 4. *We consider the above example with different parameters as* $b = 1.5, \mathcal{D} = 0.1$ *and studied the system for the initial approximation of data concentrated around two different voltage level as* $v_0 = 1.83$ *and* $v_0 = 1.5$.

Here, we examined the effect of the delay for the average-excitatory population. From Figure 3.4a, we observe that the solutions are periodic if the initial datum concentrated around V_F, and the goes to a steady-state if it is far from V_F (Figure 3.4b).

4.3 Average-inhibitory population with the influence of refractory state and the presence of transmission delays

Previously, we analyzed the behavior of the solution for the excitatory network ($b > 0$) and examined the situations for which the solution has three different states blow-up, steady, and periodic. Now we will consider the average-inhibitory population for the connected parameter that is $b < 0$ and $M(t) = \dfrac{R(t)}{\tau}$, for which the neurons are restricted to get stimulated. Following, we present an example to examine the behavior of an average-inhibitory population.

Example 5. *We consider average-inhibitory population with transmission delay for the initial data given in* (3.18) *with other parameters as follows*

$$b = -4, \quad \tau = 0.025, \quad R(0) = 0.2, \quad \mathcal{D} = 0.1, \quad N_{ext} = 20,$$

For the Example 5, we examine the biological phenomena for the given data with $D = [0, 2]$ and two different values of v_0 as $v_0 = 1.83$ and $v_0 = 1.5$ with the external firing rate $N_{ext} = 20$. In Figures 3.5a, we observe that for the initial approximation that is sufficiently close to the certain potential level V_F, gives the periodic solution. We also get the same for the average-inhibitory population even with the initial data that is away from the maximum voltage level along with the high value of N_{ext} (see Figure 3.5b).

Following are the errors estimates $\epsilon_{\Delta v}$ for the approximate solution $p(v,t)$ in different norms

$$\begin{aligned}
\|\epsilon_{\Delta v}\|_1 &= \Delta v \sum_i |(p_{\Delta v})_i - (p^\star)_i|, \\
\|\epsilon_{\Delta v}\|_2 &= \sqrt{\Delta v \sum_i |(p_{\Delta v})_i - (p^\star)_i|^2}, \\
\|\epsilon_{\Delta v}\|_\infty &= \max |(p_{\Delta v})_i - (p^\star)_i|,
\end{aligned}$$

where $p^\star$ is the approximate solution at the finest grid $N^\star$ and for the numerical simulations, we get the errors at the finest grid being $N^* = 320$. Our test results demonstrate that the error estimates described above is sure a monotone decreasing function as N rises i.e. $N = 20, 40, 80, 160$. In addition, the formula we used to calculate the accuracy rate of the designed scheme is provided as

$$r = \log_2 \frac{\epsilon^N}{\epsilon^{2N}},$$

where ϵ^N is the error at the N-th grid cells.

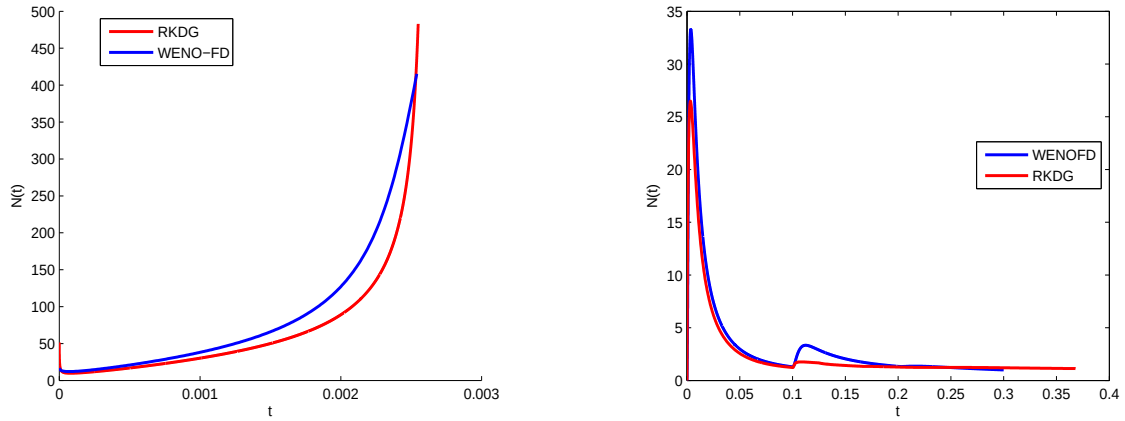

(a) (b)

Figure 3.1: Average-excitatory population for the system (3.3)-(3.5) provides the blow-up in the absence of the delay term. This simulation use the initial approximation as given in (3.18) with other parameter values as $v_0 = 1.83, \sigma^2 = 0.0003$ and $b = 0.5$. Left: $\mathcal{D} = 0$ and Right: $\mathcal{D} = 0.1$.

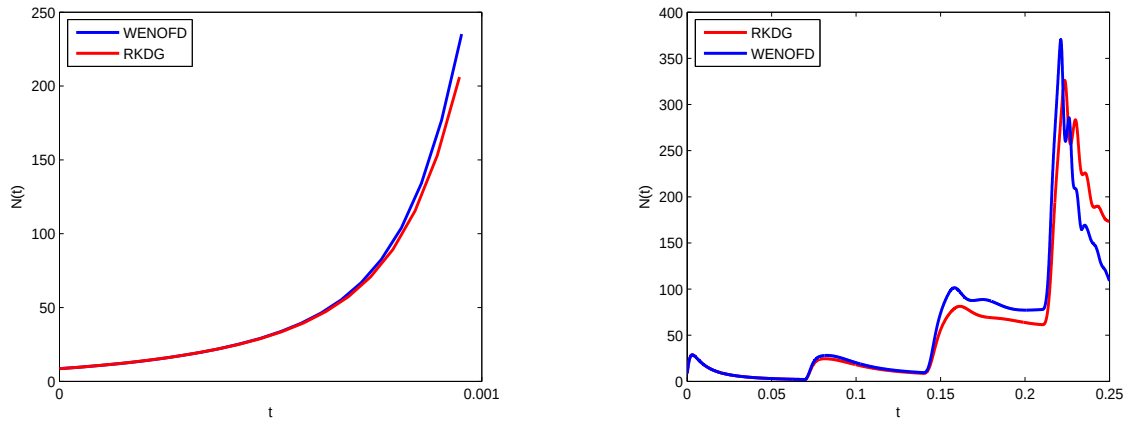

(a) (b)

Figure 3.2: Consider the Eq. (3.18) with $v_0 = 1.83, \sigma^2 = 0.003$ and the parameter of connectivity $b = 2.2$. Left: absence of transmission delay $\mathcal{D} = 0$ and Right: $\mathcal{D} = 0.1$, firing rate seems to rise but not to blow-up in finite time.

Table 3.1: Example 1: RKLDG method, T=0.00255

N	$\|\epsilon_{\Delta v}\|_1$	r	$\|\epsilon_{\Delta v}\|_2$	r	$\|\epsilon_{\Delta v}\|_\infty$	r	CPU Time (s)
10	0.62625E-02		0.70634E-02		0.10483E-01		0.04
20	0.10426E-02	2.59	0.13693E-02	2.37	0.27253E-02	1.94	0.10
40	0.12332E-03	3.08	0.21208E-03	2.69	0.67048E-03	2.02	0.40
80	0.94093E-05	3.71	0.16776E-04	3.66	0.53542E-04	3.65	2.17
160	0.51286E-06	4.20	0.90733E-06	4.21	0.31926E-05	4.06	22.34

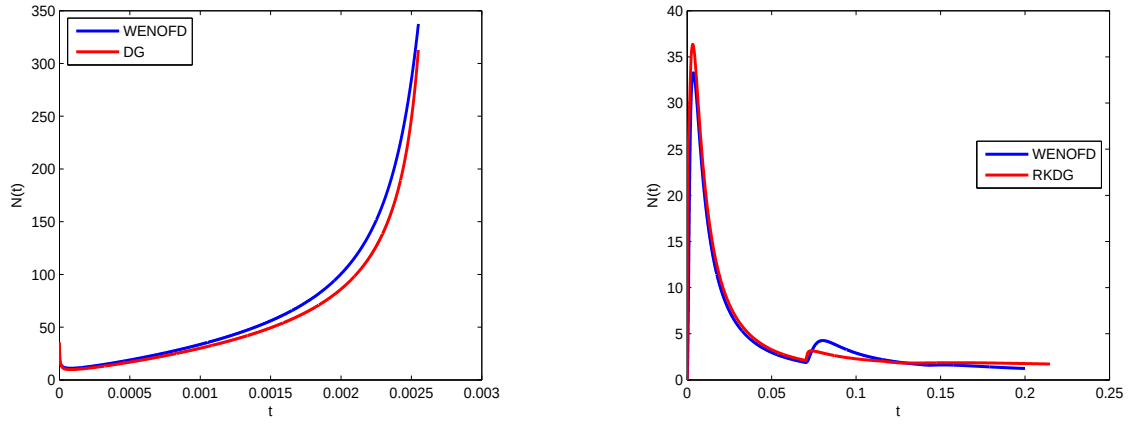

(a) (b)

Figure 3.3: We consider the average-excitatory population in the influence of both transmission delays and refractory period using (3.18) with $v_0 = 1.83, \sigma^2 = 0.0003$ and $b = 0.5$. Left: $R(0) = 0.2,\ \tau = 0.025\ \mathcal{D} = 0$ and Right: $R(0) = 0.2,\ \tau = 0.025\ \mathcal{D} = 0.07$

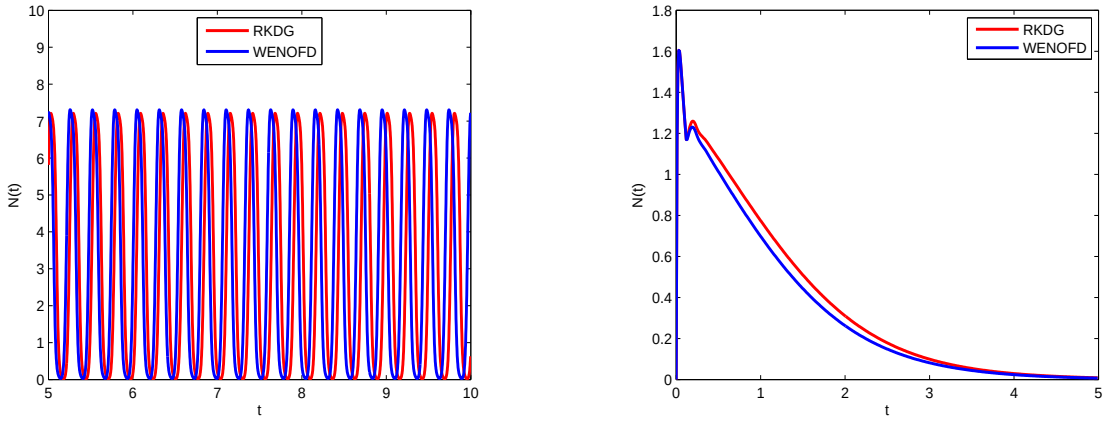

(a) (b)

Figure 3.4: Simulation of Example (4) for $M(t) = \dfrac{R(t)}{\tau}$. We consider the initial data (3.18) with $b = 1.5,\ \tau = 0.025,\ R(0) = 0.2,\ \mathcal{D} = 0.1$. Left: $v_0 = 1.83$, Right: 1.5.

Table 3.2: Example 1: WENOFD method, T=0.00255

N	$\|\epsilon_{\Delta v}\|_1$	r	$\|\epsilon_{\Delta v}\|_2$	r	$\|\epsilon_{\Delta v}\|_\infty$	r	CPU Time (s)
10	0.16167E-01		0.18051E-01		0.27274E-01		0.08
20	0.38089E-02	2.08	0.48183E-02	1.91	0.962971E-02	1.50	0.27
40	0.10443E-02	1.87	0.15689E-02	1.62	0.46353E-02	1.05	1.26
80	0.53858E-04	4.28	0.91344E-04	4.10	0.33646E-03	3.78	6.97
160	0.41185E-05	3.71	0.59497E-05	3.94	0.24458E-04	3.78	88.02

Table 3.3: Example 2: RKLDG method, T=0.001

N	$\|\epsilon_{\Delta v}\|_1$	r	$\|\epsilon_{\Delta v}\|_2$	r	$\|\epsilon_{\Delta v}\|_\infty$	r	CPU Time (s)
10	0.59143E-02		0.66103E-02		0.11931E-01		0.02
20	0.50100E-03	3.56	0.70075E-03	3.24	0.14638E-02	3.02	0.07
40	0.62825E-04	2.99	0.12091E-03	2.53	0.43047E-03	1.76	0.26
80	0.55604E-05	3.50	0.12099E-04	3.32	0.45161E-04	3.25	1.44
160	0.33774E-06	4.04	0.73253E-06	4.05	0.30611E-05	3.88	10.38

Table 3.4: Example 2: WENOFD method, T=0.001

N	$\|\epsilon_{\Delta v}\|_1$	r	$\|\epsilon_{\Delta v}\|_2$	r	$\|\epsilon_{\Delta v}\|_\infty$	r	CPU Time (s)
10	0.16838E-01		0.18660E-01		0.27788E-01		0.15
20	0.43380E-02	1.96	0.54354E-02	1.78	0.10849E-01	1.35	0.34
40	0.14103E-02	1.62	0.21041E-02	1.36	0.61095E-02	0.83	1.48
80	0.85894E-04	4.03	0.13946E-03	3.91	0.49193E-03	3.63	7.92
160	0.50606E-05	4.08	0.79033E-05	4.14	0.35371E-04	3.80	83.32

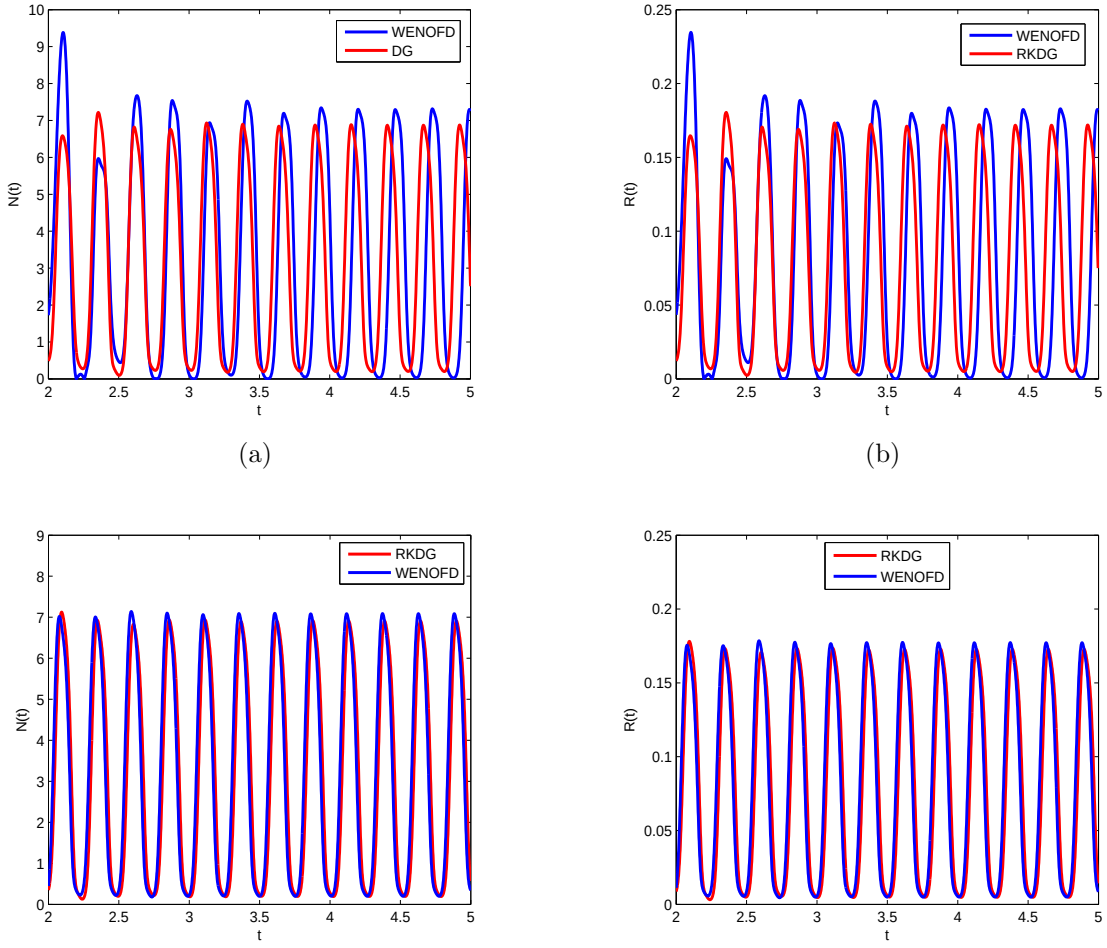

Figure 3.5: Average-inhibitory population for the system (3.3)-(3.5) provides the periodic solutions for the initial data (3.18) using $N_{ext} = 20,\ \tau = 0.025,\ \mathcal{D} = 0.1,\ R(0) = 0.2$ and the connectivity parameter $b = -4$. Top: initial data concentrated at $v_0 = 1.83$ and $N_{ext} = 20$. Bottom: $v_0 = 1.5, N_{ext} = 20$.

Table 3.5: Example 3: RKLDG method, T=0.003

N	$\|\epsilon_{\Delta v}\|_1$	r	$\|\epsilon_{\Delta v}\|_2$	r	$\|\epsilon_{\Delta v}\|_\infty$	r	**CPU Time (s)**
10	0.10965E-01		0.11869E-01		0.17779E-01		0.07
20	0.16939E-02	2.69	0.23065E-02	2.36	0.48218E-02	1.88	0.15
40	0.21262E-03	2.99	0.32247E-03	2.84	0.93048E-03	2.37	0.66
80	0.14361E-04	3.88	0.21835E-04	3.88	0.62583E-04	3.89	5.66
160	0.10726E-05	3.74	0.17891E-05	3.61	0.63746E-05	3.30	38.66

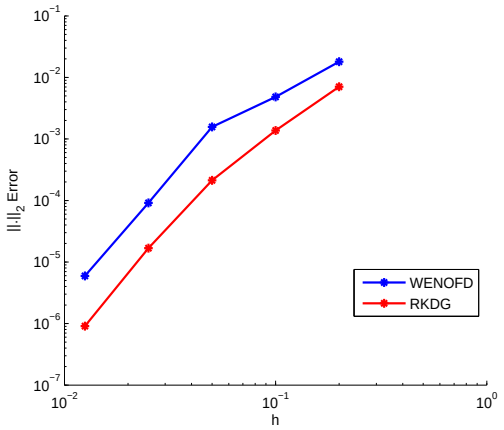

(a) $||.||_2$ Error versus number of cells.

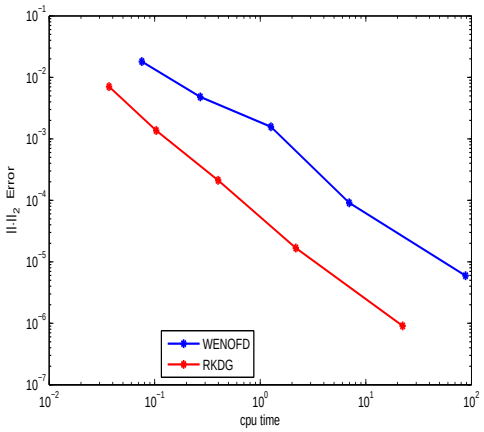

(b) $||.||_2$ Error versus CPU time.

Figure 3.6: Comparison of WENOFD and RKDG for Example 1

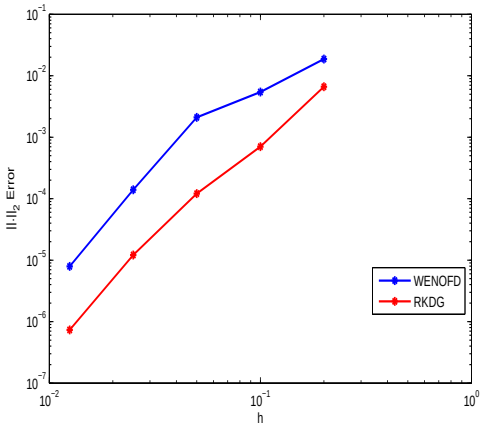

(a) $||.||_2$ Error versus number of cells.

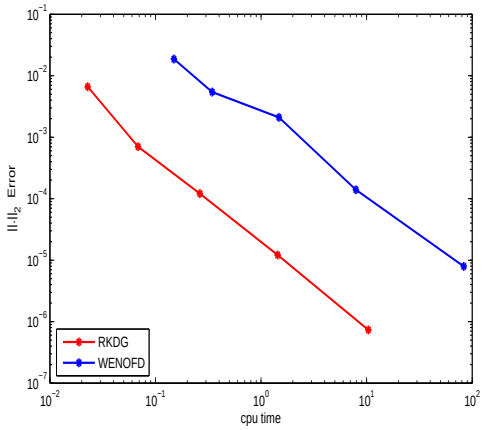

(b) $||.||_2$ Error versus CPU time.

Figure 3.7: Comparision of WENOFD and RKDG for Example 2

Table 3.6: Example 3: WENOFD method, T=0.003

N	$\|\epsilon_{\Delta v}\|_1$	r	$\|\epsilon_{\Delta v}\|_2$	r	$\|\epsilon_{\Delta v}\|_\infty$	r	**CPU Time (s)**
10	0.17367E-01		0.19441E-01		0.29063E-01		0.11
20	0.54786E-02	1.66	0.67692E-02	1.52	0.13505E-01	1.11	0.33
40	0.23270E-02	1.23	0.33932E-02	1.00	0.93957E-02	0.52	1.63
80	0.17288E-03	3.75	0.25797E-03	3.72	0.87243E-03	3.42	9.09
160	0.78238E-05	4.46	0.15529E-04	4.05	0.87841E-04	3.31	124.28

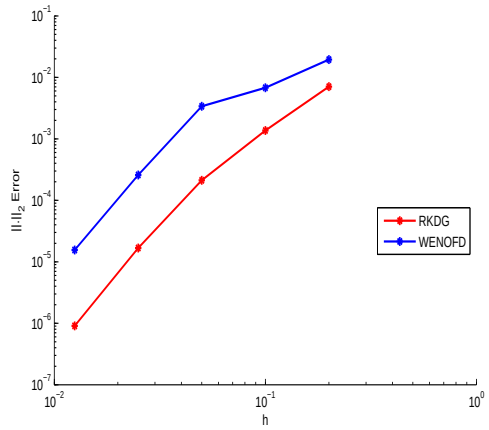

(a) $||.||_2$ Error versus number of cells.

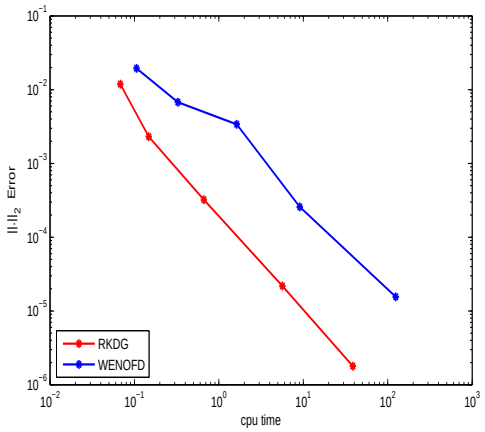

(b) $||.||_2$ Error versus CPU time.

Figure 3.8: Comparison of WENOFD and RKDG for Example 3

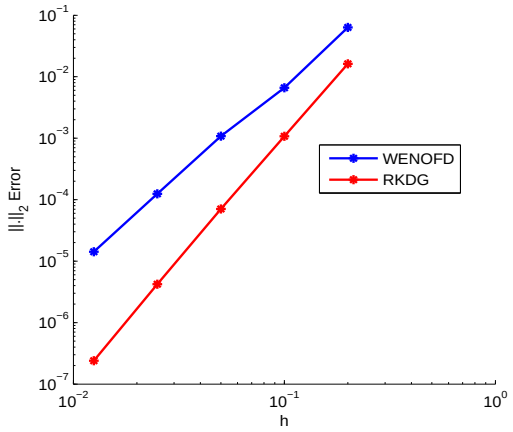

(a) $||.||_2$ Error versus number of cells.

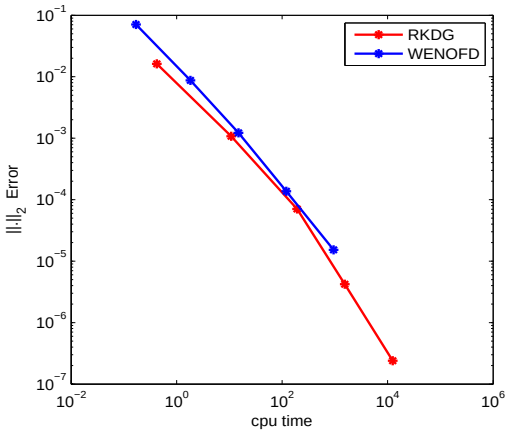

(b) $||.||_2$ Error versus CPU time.

Figure 3.9: Comparison of WENOFD and RKDG for Example 4

Table 3.7: Example 4: WENOFD method, T=2

N	$\|\epsilon_{\Delta v}\|_1$	r	$\|\epsilon_{\Delta v}\|_2$	r	$\|\epsilon_{\Delta v}\|_\infty$	r	**CPU Time (s)**
10	0.58916E-01		0.63542E-01		0.95939E-01		0.17
20	0.51615E-02	3.51	0.66129E-02	3.26	0.13328E-02	2.85	1.83
40	0.70832E-03	2.87	0.10794E-02	2.62	0.31159E-03	2.10	14.86
80	0.75857E-04	3.22	0.12462E-03	3.11	0.37892E-04	3.04	120.66
160	0.84812E-05	3.16	0.14189E-04	3.13	0.47337E-05	3.00	943.32

Table 3.8: Example 4: RKLDG method, T=2

N	$\|\epsilon_{\Delta v}\|_1$	r	$\|\epsilon_{\Delta v}\|_2$	r	$\|\epsilon_{\Delta v}\|_\infty$	r	**CPU Time (s)**
10	0.14271E-01		0.16179E-01		0.23042E-01		0.42
20	0.78449E-03	4.18	0.10729E-02	3.91	0.21656E-02	3.41	10.81
40	0.318490E-04	4.62	0.70600E-04	3.92	0.27975E-03	2.95	192.43
80	0.17584E-05	4.17	0.42056E-05	4.06	0.16551E-04	4.07	1545.16
160	0.82622E-07	4.41	0.23951E-06	4.13	0.13879E-05	3.57	12516.15

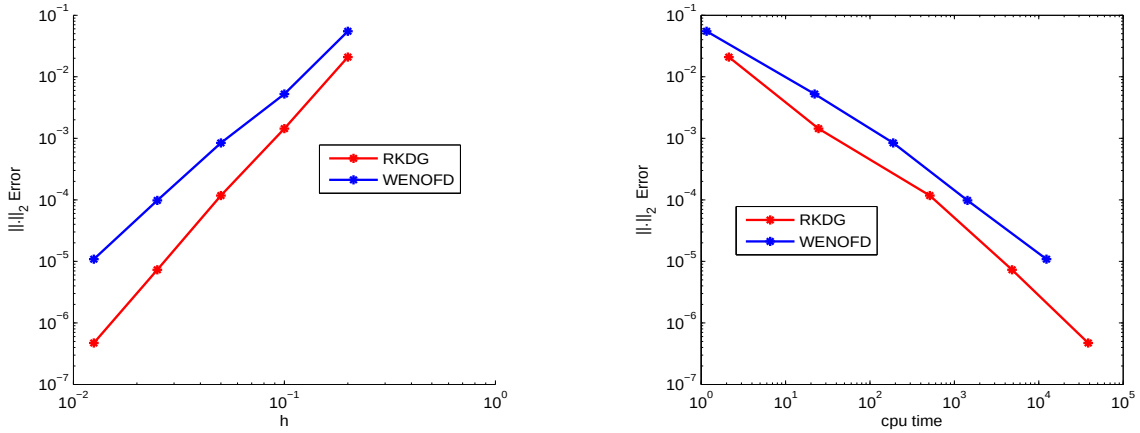

(a) $||.||_2$ Error versus number of cells.

(b) $||.||_2$ Error versus CPU time.

Figure 3.10: Comparison of WENOFD and RKDG for Example 5

Table 3.9: Example 5: WENOFD method, T=5

N	$\|\epsilon_{\Delta v}\|_1$	r	$\|\epsilon_{\Delta v}\|_2$	r	$\|\epsilon_{\Delta v}\|_\infty$	r	**CPU Time (s)**
10	0.50562E-01		0.54850E-01		0.83001E-01		1.16
20	0.40322E-02	3.64	0.52462E-02	3.38	0.10456E-01	2.99	22.13
40	0.51881E-03	2.95	0.84255E-03	2.64	0.26277E-02	1.99	188.72
80	0.54497E-04	3.25	0.97890E-04	3.11	0.32526E-03	3.01	1432.43
160	0.58237E-05	3.22	0.10871E-04	3.17	0.41368E-04	2.98	12378.02

Table 3.10: Example 5: RKLDG method, T=5

N	$\|\epsilon_{\Delta v}\|_1$	r	$\|\epsilon_{\Delta v}\|_2$	r	$\|\epsilon_{\Delta v}\|_\infty$	r	**CPU Time (s)**
10	0.18446E-01		0.20880E-01		0.30168E-01		2.13
20	0.10846E-02	4.08	0.14397E-02	3.85	0.27719E-02	3.44	24.60
40	0.55816E-04	4.28	0.11760E-04	3.61	0.45495E-03	2.60	512.32
80	0.31199E-05	4.16	0.73074E-05	4.00	0.28903E-04	3.98	4825.44
160	0.17183E-06	4.18	0.47253E-06	3.95	0.26073E-05	3.47	38564.07

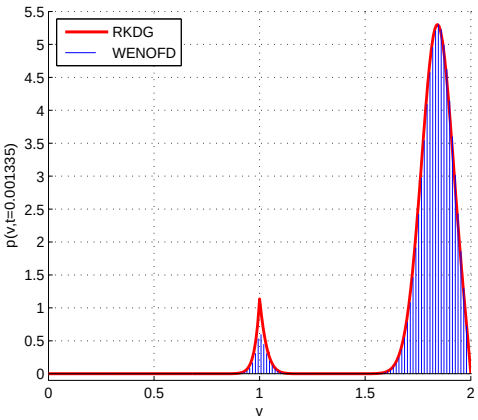

(a)

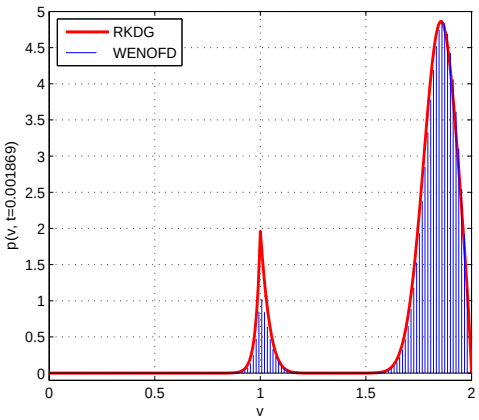

(b)

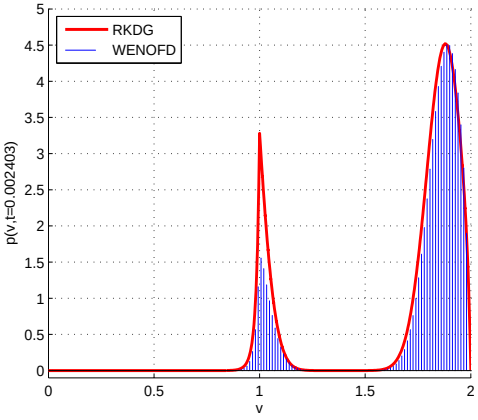

(c)

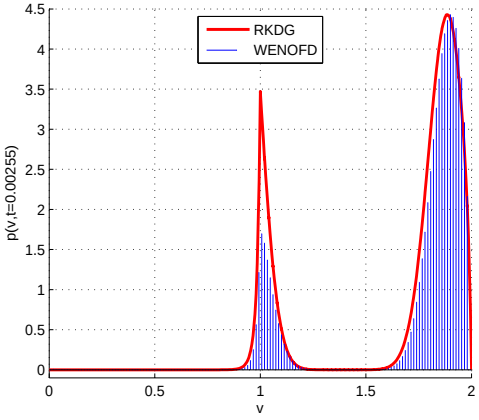

(d)

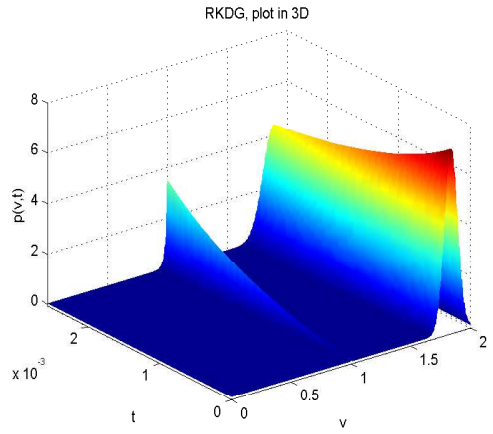

(e)

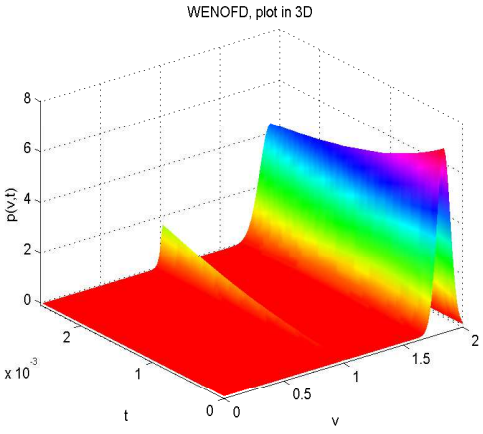

(f)

Figure 3.11: we consider the excitatory population without refractory state for the initial approximation (3.18) with $b = 0.5,\ v_0 = 1.83,\ \sigma^2 = 0.0003,\ \mathcal{D} = 0$. The excitatory system (3.3)-(3.5) depicts the blow-up in the absence of transmission delays.

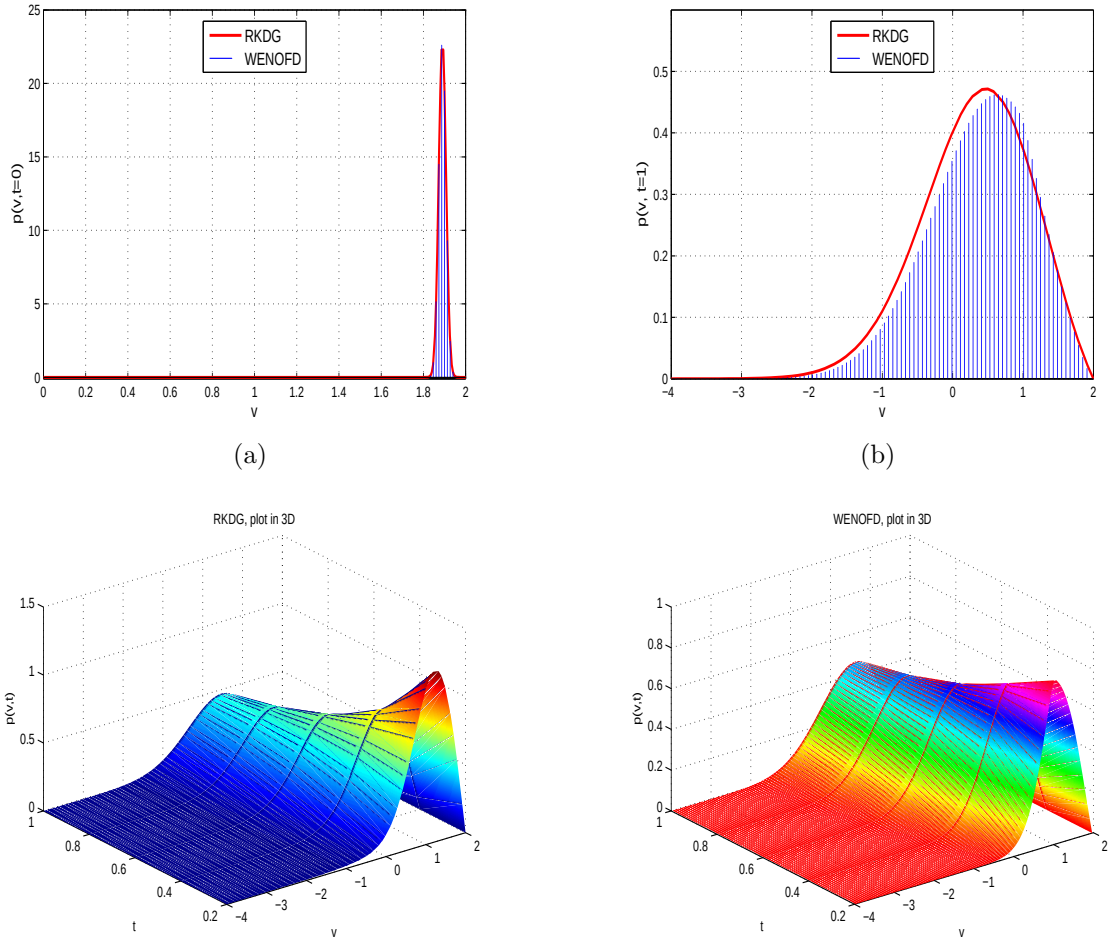

(a) (b)

(c) (d)

Figure 3.12: we consider the excitatory population with refractory state for the initial approximation (3.18) with other parameter values
$b = 0.5,\ v_0 = 1.83,\ \sigma^2 = 0.0003, \mathcal{D} = 0.1$. The excitatory system (3.3)-(3.5) avoids finite time blow-up phenomena in the presence of transmission delays.

Figure 3.11 simulates the behavior of a population of neurons in the absence of refractory period and transmission delay. From our numerical simulations, we observe a blow-up phenomenon for excitatory neurons which are more concentrated near a threshold value V_F. We observe that only the addition of refractory state is not enough to prevent blow-up (Figure 3.3). Therefore, in Figure 3.12, we show the behavior of neurons under the presence of transmission delay and we find the solution that prevents the finite-time blow-up phenomena.

5 Discussions

We provided an application of the RKDG for the NNLIF model and comparison with WENOFD validates the performance of the proposed scheme. Here, we find that the accuracy rate of the designed scheme (RKDG) and the existing scheme (WENOFD) are almost the same. Moreover, the designed scheme requires less computational time compared to the existing technique in literature as it includes many computational factors such as non-negativity weights and smoothness indicator functions, etc. The analysis of the stability of the proposed technique demonstrates that the scheme is conditionally stable. Some test examples are included to simulate the behavior of the solution and the results reveal that the RKDG method performs nicely for the simulation of the neural network dynamics.
The next chapter presents a numerical study of the biological model of the tumor cell population dynamics based on an age-structured approach.

Chapter 4

A Numerical Study of the Tumor Cell Population Model based on Age-structured Approach [1]

The previous chapter presented the numerical study of the NLIF model based on the population density approach. This chapter describes a nonlinear age-structured tumor cell population model with the application of the discontinuous Galerkin (DG) method to study its dynamical behaviors. The DG numerical approximation is used for the spatial discretization and then the SSPERK technique is applied for the temporal discretization. This chapter aims to establish more efficient results in the sense of computational approach and compare these with analogous estimates for the WENO scheme. Eventually, some test examples and numerical simulations are provided to illustrate theoretical results and to study the behavior of the solution.

1 Introduction

The mathematical study of an age-structured population is a very important part of population dynamics. Aging is a vital and essential quality in the population structuring approach. Numerous internal aspects are determined by age because different behaviors, the different reproduction rates, and the difference in the capacity of survival are due to the difference in ages. Previously such type of analysis was limited to demography, but these days the age-structured mathematical approach is useful in epidemiology, the simulation of cancer, neurons, and ecological systems, and numerous other areas, see [14, 16–20, 22, 185–187].

Firstly, Lotka and McKendrick proposed the linear model of the age-structured population which supports exponential solution [84, 188] that was later extended by Gurtin and MacCamy for non-linear models [14]. The authors constructed a non-linear structure using the factors of mortality and fertility that rely on the total population size. In recent years, numerous experts [18, 87–89] developed various algorithms that are used to solve this type of modeled equation of population dynamics. To simplify the analysis of the model equation, numerous authors supposed that the death rate and some other variables are bounded wherever few models use

[1] Dipty Sharma and Paramjeet Singh *"Discontinuous Galerkin method for a nonlinear age-structured tumor cell population model with proliferating and quiescent phases."*, International Journal of Modern Physics C, **32(03)**, 2150039, 2021.

maximum age as a factor which can not be touched and also required mortality rate to be unbounded at that age [189, 190].

It is well-known that the solution is smooth whereas the maximum age is infinite, and derivatives are bounded if some conditions of compatibility are met [14]. On the other side, the solution can be stiff as the maximum age is finite depends on the function of mortality, even though all the conditions of compatibility are fulfilled. In such a case (near the maximum age), many numerical schemes existing in the literature are not working well.

A linear model which is having a finite life span can induce significant outcomes of population change for a short duration of advanced ages. Nevertheless, the nonlinear model with a maximum age that is finite produces both types of i.e. quantitative and qualitative analysis of population dynamics. Thereby, in the next section, we explore the model of tumor cell population dynamics based on an age-structured approach where each cell has a maximum age that is finite. The key purpose of this type of simulation method, when used with the population model, is to build the estimates of the growth of the population for the future. Iannelli and Milner [18] concluded that the numerical methods where the standard order is lower can not be appropriate for the model equations of population dynamics. To see the long-term phenomenon, it would be ideal to choose suitable higher-order methods and, thus the DG method is a decent choice among these types of equations. Additionally, our schemes are appropriate for various types of functions of mortality that can be used in population modeling. Some other high-order schemes are available in the literature which can be used to solve the governing equation given in [153, 191].

In this chapter, we purpose a nonlinear Lotka–McKendrick equation to describe the tumor cell population dynamics with quiescent and proliferating states. Several researchers have drawn great attention to the development and invasion of the tumor cell population model and have been thoroughly examined for the past few decades. The theoretical analysis performed on tumor evolution in vitro or vivo is one essential way to deal with tumor study, which is generally used to examine extensive dynamical evolution at three levels: molecular, cellular , and tissue, either one at a time or comprehensively [192–196]. Furthermore, tumor progression is categorized into three distinct phases based on different circumstances of dispersal and different growth rates: avascular, vascular, and metastatic. In this chapter, we examine the evolutionary model of a tumor cell population dynamics in vitro condition and at the stage of avascular. The proliferating cell's division rate is supposed to be nonlinear because of nutrient and space limitations. Moreover, this model applies to other circumstances where an inadequate resource is provided at the metastatic or vascular stage. In the recent past, the model with vital dynamics is evolving as provided in [194, 197, 198] and shown schematically in Figure 4.1. From the $G1$ phase, proliferating cells continue through phases of S and $G2$, giving birth to new cells when the cycle of the cell reaches its end i.e. (M phase). Such type of newborn cells can either stay in proliferating stage or can enter the quiescent stage, while the quiescent cells do not promote

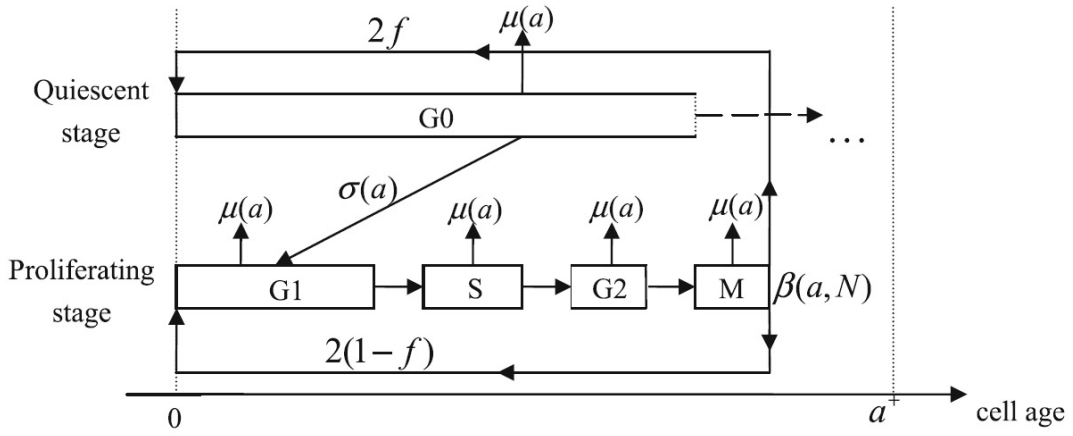

Figure 4.1: The diagram of the quiescent cells in $G0$ phase and the proliferating cells in $G1$ phase (first gap), S (synthesis), $G2$ (second gap) and M (mitosis) of the cell cycle correlated with cell age, (this image is taken from [4].)

or split but migrated to the proliferative stage or remain in phase $G0$ till it reaches its end and also removed from the tissue. For both types i.e. quiescent and proliferating, their age starts with the time when the cell was just split and its age is related to the stage of the cell cycle (for proliferating). Further-also consider that for time t, da/dt i.e. evolution speed of physiological age a is constant (symbolized by k). Such as, if $k = 0.5$, implies the age of biology develops twice and it is as slow as real-time t. Moreover, there is a ratio of newborn cells at the time cells divide and entered quiescence at 0 age. This type of proportion may reflect the dosage of drugs like erlotinib as described in [199] that erlotinib's main effect on cells (cancer) is to get enter into quiescence (see [198]). This fraction is represented by f, therefore, $1 - f$ indicates a portion that still exists in the proliferating stage. Next, presume that if there is not any joining to quiescent cells besides a member of the daughter cells (age 0) i.e. with age $a > 0$, all proliferating cells will not be able to enter into the quiescent stage. Moreover, we also believe that the existence of transit rate from quiescent phase to proliferating phase that is produced by fluctuation of the source supply for some irregular period. Therefore, we propose the model, where the age density evolution $q(t, a)$ and $p(t, a)$ with finite maximum age $a \in [0, a^+]$ and at time t which is expressed by the given system:

$$\begin{aligned} \frac{\partial p}{\partial t} + k\frac{\partial p}{\partial a} &= -\mu(a)p(a,t) - \beta(a, N(t))p(a,t) + \sigma(a)q(a,t), \\ \frac{\partial q}{\partial t} + k\frac{\partial q}{\partial a} &= -\mu(a)q(a,t) - \sigma(a)q(a,t), \end{aligned} \tag{4.1}$$

for the quiescent and proliferating cells. In the above system $\beta(., N)$, $\mu(a)$ and $\sigma(a)$ denotes the division rate, death rate and transition rate respectively with the following assumptions

- $\mu(.) \in L^1_{+,loc}([0, a_{\max}))$ and $\int_0^{a_{\max}} \mu(s)\, ds = \infty$. Further, the boundness on the death rate for the age interval $[0, a^+]$ is assumed by replacing $a_{\max}$ with $a^+ = a_{\max} - \epsilon_0$, $\epsilon_0 > 0$. Therefore, $\mu(.)$ is non-negative and essentially bounded in $[0, a^+]$.
- The assumption that all the cells will not divide earlier than arriving at maximum survival age a^+, implies boundness on dividing rate $\beta(., N) \in L^\infty[0, a^+] > 0$.
- $\sigma(.) \in L^\infty[0, a^+] > 0$ and $N \in \mathbb{R} \geq 0$.

Additionally, following initial and BCs completes the given model

$$\begin{cases} p(0,t) = 2(1-f) \int_0^{a^+} \beta(a, N(t))\, p(a,t) da, \\ q(0,t) = 2f \int_0^{a^+} \beta(a, N(t))\, q(a,t) da. \end{cases} \tag{4.2}$$

$$p(a,0) = p_0(a), \quad q(a,0) = q_0(a). \tag{4.3}$$

Furthermore, $\int_{a_1}^{a_2} p(a,t)da$ and $\int_{a_1}^{a_2} q(a,t)da$ denotes the number of cells (proliferating and quiescent respectively) for age interval $[a_1, a_2]$. Then, the total number of cells denoted by $P(t)$ and $Q(t)$ for the proliferating cells and the quiescent cells respectively at a time t are defined

$$P(t) = \int_0^{a^+} p(a,t)da,$$
$$Q(t) = \int_0^{a^+} q(a,t)da,$$

and their addition described by $N(t) = P(t) + Q(t)$ denotes total cell populations. When problem (4.1) organized with Eqs. (4.2-4.3) it is called first-order nonlinear hyperbolic PDE. This type of model equation cannot be solved analytically [96, 128, 200–202] due to the term nonlinearity. So, the numerical scheme are usually used for; finite difference technique of which is covered in [171, 203], method of finite element provided in [141, 143] and the method for numerical collacation proposed in [174, 204]. Moreover, solutions to (4.1) can be discontinuous, i.e. when there is discontinuous initial data or when this type of solution not met with an inflow boundary condition at the origin. Furthermore, in addition to this, if the mortality rate and the division rate are stepwise functions, the particular solution can be regular only piecewise. All these make it extremely desirable to impose the discretization scheme that may tackle irregular solutions with an expected design. A various type of numerical techniques have been proposed to solve population growth model, and even for a more general age-structured population dynamical equations (see [205]). All this type of method remains of fixed order (see [206]) and the furthermost of these methods have been examined with some restrictive assumption (smoothness of data and the solution). Thus, to efficiently handle these types of solutions (irregular) with a certain pattern, we go for another class of approximation techniques. To Achieve this

purpose, DG method may be efficiently applied for the simulation of the population growth model.

The basic introduction to the DG approach provided in the previous chapter and the interested reader can find more details about the method herein [115, 176]. Moreover, this method offers flexibility for local approximation as it uses discontinuous piecewise polynomials (basis function). Therefore, the higher-order accurate scheme may be designed with the help of higher-order polynomial approximation within an element. Furthermore, as there is no need for continuity, across the element interfaces, the basis function on every element may be chosen and to be orthogonal, that again produces a well-conditioned algebraic system for higher-order approximations using FEM approach [116, 207]. In the recent study, convergence and error evaluations of the semi-discrete DG scheme for a linear age-structured population model is presented by Kim [208], but there are no outcomes for the nonlinear system and fully-discrete scheme. Therefore, we proposed the numerical technique based on the DG approach and that can be used to find the solution which is more accurate in terms of accuracy and computational approach. The numerical analysis for the proposed DG method for the nonlinear system (4.1) is even more problematic and has a consequence in both application of the nonlinear system and numerical analysis of population growth in biology.

1.1 Preliminaries

We provide some of the definitions which are fundamental and some additional outcomes which are already known. Additionally, throughout the work done in this chapter, we always assume that

A1. The term $\sigma(.),\ \mu(.),\ \beta(.,N) \in L^{\infty}[0,a^{+}] \geq 0$ and $N \in \mathbb{R}\geq 0$.

A2. $\beta(a,N)$ is differentiable with respect to N.

A3. Special form of division rate as $\beta(a,N(t)) = \beta(a),\phi(N(t))$ with the assumption that $\phi(x)$ is continuous, differentiable and strictly decreasing in $x \in [0,+\infty]$ and $\phi(0) = 1, \lim_{x\to+\infty}\phi(x) = 0$.

Local and global stabilities of trivial steady state: Let $\bar{E}(a) = (\bar{p}(a), \bar{q}(a))$ is the steady state of time independent system of (4.1) and some other terms used are defined as

$$s_1(a) = \exp\left(-\int_0^a \mu(\xi)d\xi\right),$$
$$s_2(a) = \exp\left(-\int_0^a \beta(\xi,N)d\xi\right),$$
$$s_3(a) = \exp\left(-\int_0^a \sigma(\xi)d\xi\right).$$

We just provide the result as verified in [4], described by the following theorems.

Theorem 1.1. *(Locally asymptotically stable) Let assumptions* $(A1)$ *and* $(A2)$ *be satisfied and*

$$2\int_0^{a^+}\beta(a)s_1(a)s_2(a)\left(1-f+f\int_0^a\bar{\sigma}(\xi)s_3(\xi)s_2^{-1}(\xi)d\xi\right)da<1,$$

then, trivial steady state $\bar{E}_0:=(0,0)$ *is locally asymptotically stable, where* $s_2(a)=s_2(a,N)|_{N=0}$ *and* $\beta(a)=\beta(a,N)|_{N=0}$

Theorem 1.2. *(Globally asymptotically stable) Let the assumptions* $(A1)$ *and* $(A3)$ *holds and additionally if*

$$2\int_0^{a^+}\beta(a)s_1(a)\,da<1,$$

then trivial steady state $\bar{E}_0:=(0,0)$ *is globally asymptotically stable.*

Remark 1.1. *The local stability of positive steady state can be gained by improving assumption* $(A2)$ *that is* $\beta(a,N)$ *is differentiable with respect to* N *and* $\dfrac{\partial\beta(a,N)}{\partial N}$ *is bounded on* $[0,a^+]$ *(see [4]).*

We demonstrate the stability and the existence of positive steady state numerically in the Section 4. From these simulations, we find that system is really locally asymptotically stable positive steady state if appropriate values are taken by the coefficients of the considered system. Here, we construct the numerical approximation based on DG approach for the system (4.1) which can be written in standard form described by

$$\begin{aligned}\frac{\partial p}{\partial t}+k\frac{\partial p}{\partial a} &= \widehat{S1}(p,q,a,t),\\ \frac{\partial q}{\partial t}+k\frac{\partial q}{\partial a} &= \widehat{S2}(p,q,a,t),\end{aligned}\tag{4.4}$$

where $\widehat{S1}(p,q,a,t)=-\mu(a)p(a,t)-\beta(a,N(t))p(a,t)+\sigma(a)q(a,t)$ and $\widehat{S2}(p,q,a,t)=-\mu(a)q(a,t)-\sigma(a)q(a,t)$ are the source terms. The spatial discretization reduce the above system into ODE system which is then solved by explicit higher order RK method. Firstly, space discretization is done by taking partition of the entire domain as follows.

1.2 Domain Partition

In this approach, consider a partition of the entire domain $a\in\Omega:=[0,a^+]$ into M disjoint elements say $\Omega_m=[a_m,a_{m+1}]$, for $m=1,2,\ldots,M$, with element size being $\Delta a_m=a_{m+1}-a_m$ and $\Delta a=\max\limits_{1\le m\le M}\Delta a_m$. Initially, we will approximate the solution inside each element by a polynomial of degree N. Since the accuracy of the scheme is depend upon the order of local polynomial interpolation so there is a need to care about the choice of discrete points of

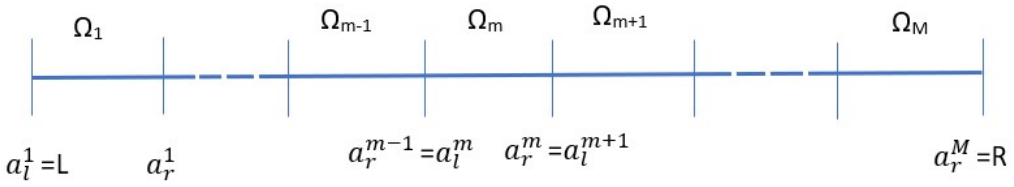

Figure 4.2: Partition of the domain Ω

approximation. Thus, consider the following affine mapping

$$a \in \Omega_m : a(r) = a_i^m + \frac{1+r}{2}\Delta a_m, \quad \text{where } \Delta a_m = a_{m+1} - a_m,$$

where a_i^m, $i = 1, \ldots, N^p$, for $N^p = (N+1)$ are the grids point over the reference interval $r \in I = [-1, 1]$. Since Gauss quadrature has the property of exact fitted for the polynomial with degree $2N^p - 1$, we choose the Gauss-Lobatto discrete points (r_i) for the interpolation. Moreover, let $a_i \in \Omega_m$ denote the physical locations of the Gauss-Lobatto points.

1.3 Semi-discrete DG Scheme

Here, we specify the finite dimensional space of the piecewise polynomial functions for the discretization of the purposed scheme,

$$V_h = \{\psi_h : \psi_h|_{\Omega_m} \in P^N(\Omega_m); \quad m = 1, \ldots, M\},$$

which consist the polynomials of degree up to $N \geq 1$ over Ω_m. Further, Local polynomials $p_h^m(a,t)$ and $q_h^m(a,t)$ are represented as

$$p_h^m(a,t) = \sum_{i=1}^{N^p} p^m(a_i^m, t) l_i^m(a) = \sum_{n=1}^{N^p} \hat{p}_n^m(t)\psi_n(a),$$

$$q_h^m(a,t) = \sum_{i=1}^{N^p} q^m(a_i^m, t) l_i^m(a) = \sum_{n=1}^{N^p} \hat{q}_n^m(t)\psi_n(a),$$

where, the modal coefficients ($\hat{p}_n^m(t)$ and $\hat{q}_n^m(t)$) are defined over the m-th element. Moreover, the Legendre basis function is denoted as $\psi_n(a)$ and $l_i(a)$ describes the Lagrange polynomial. Using Gram-Schmidt orthogonalization approach, one can recover an orthonormal basis as defined

$$\psi_n(r) = \frac{P_{n-1}(r)}{\sqrt{\gamma_{n-1}}}, \quad \gamma_{n-1} = \frac{2}{2n+1},$$

which are orthogonal on $I = [-1, 1]$ and $(P_n(r))$ is the classical Legendre polynomial with order n. The term γ_n in the above expression is the orthonormalizing weight see([115]). The term $V_{ij} = \tilde{P}_{j-1}(a_i)$ (Vandermonde matrix), defines the following relation between nodal and modal representation

$$p_h^m = V\hat{p}_h^m, \quad \hat{p}_h^m = V^{-1}p_h^m, \quad V^T l_N^m = \psi_N^m.$$

Now to apply the DG approximation for the solution (p_h, q_h), first thing is to multiply the system (4.4) by a test function and then integrate over element say Ω^m. Further, taking integration by parts again results in the equation for $p_h^m, q_h^m \in V_h$,

$$\begin{aligned}
\int_{\Omega_m} \partial_t p_h^m \; l_j^m(a)\, da &= -k \int_{\Omega_m} \partial_a p_h^m \; l_j^m(a)\, da + \int_{\Omega_m} \widehat{S1}_h^m l_j^m(a)\, da + [p_h^m - (p_h^m)^*] \; l_j^m(a)\Big|_{a_l}^{a_r}, \\
\int_{\Omega_m} \partial_t q_h^m \; l_j^m(a)\, da &= -k \int_{\Omega_m} \partial_a q_h^m \; l_j^m(a)\, da + \int_{\Omega_m} \widehat{S2}_h^m l_j^m(a)\, da + [q_h^m - (q_h^m)^*] \; l_j^m(a)\Big|_{a_l}^{a_r},
\end{aligned} \tag{4.5}$$

with all the test function $l_j^m(a)$. As there is lack of the continuity of test functions at element interfaces, the solution is not exactly unique at these boundary points in this approximation. To guarantee convergence and stability there is a need to replace the element interface values by the numerical flux . So the right design of these fluxes is the main component to develop an accurate and the stable scheme.

1.4 Flux approximation

At the element interfaces, the densities p^* and q^* are presented by a monotonic flux so that, the continuity, monotonicity and consistency conditions hold. Thus, we use the well known monotonic flux (Lax-Friendrichs) with a jump along the normal $\hat{n}$ as described

$$f^*(p_h^-, p_h^+) = \frac{f(p_h^-) + f(p_h^+)}{2} + \hat{n}\frac{\kappa}{2}(p_h^+ - p_h^-) \quad \text{where} \quad \kappa = \max_p |f'(p)|. \tag{4.6}$$

The expression p_h^- and p_h^+ are denoted for the interior and exterior boundary values respectively. Moreover, the BCs are enforced through numerical flux [115]. Further, the mass and stiffness matrices over element Ω^m are defined

$$M_{ij}^m = \int_{\Omega_m} l_i(a) l_j(a)\, da, \qquad S_{ij}^m = \int_{\Omega_m} l_i(a) l_j'(a) da,$$

and follwing are the matrices for the reference interval $[-1, 1]$

$$M_{ij} = \int_{-1}^{1} l_i(r) l_j(r) dr, \qquad S_{ij} = \int_{-1}^{1} l_i(r) l_j'(r) dr.$$

The $l_i(r)$ used in the above expression is the ith Lagrange polynomial for the Legendre Gauss-Lobatto (LGL) nodes r_i. Using these matrices, one can obtain the following relation

$$M_{ij}^m = \frac{1}{2}(a_r^m - a_l^m)M_{ij}, \qquad S_{ij}^m = S_{ij}.$$

After applying the above terminology, we get the following element-wise reduced system for (4.1)

$$\begin{aligned} M^m \frac{dp_h^m}{dt} &= -S^m\, p_h^m + [p_h^m - (p_h^m)^*]\, l_j^m(a)\Big|_{a_l}^{a_r} + M^m \widehat{S1}_h^m, \\ M^m \frac{dq_h^m}{dt} &= S^m q_h^m + [q_h^m - (q_h^m)^*]\, l_j^m(a)\Big|_{a_l}^{a_r} + M^m \widehat{S2}_h^m. \end{aligned} \tag{4.7}$$

Thus, the above semidiscrete estimate of model equation (4.1) can be write as following system of ordinary differential equation

$$\frac{d\, u_h}{dt} = L_h(u_h, t), \quad \forall t \geq 0, \quad \forall a \in [0, a^+],$$

where u_h is the vector of solution coefficients and L_h is the R.H.S of the system (4.7). The time discretization techniques are then used to get the approximate solution from the derived system of ODE as described in [183, 184].

1.5 Temporal discretization (strong stability-preserving method)

The higher-order explicit strong-stability preserving (SSP) time discretization approach is used for the temporal discretization. For this approach, firstly consider the partition of time domain $[0, T]$ as $\{t^k\}_{k=0}^K$ with time step $\Delta t^k = t^{k+1} - t^k$, $k = 0, 1, \ldots, K-1$ and the procedure of $s-$ stage explicit RK method is as follows

$$\begin{cases} v^{(0)} = u_h^k \\ i = 1, \ldots, s : v^{(i)} = \sum_{j=0}^{i-1} \alpha_{ij} v^{(j)} + \beta_{ij} \Delta t L(v^{(j)}, t^n + \gamma_j\, \Delta t). \\ u_h^{k+1} = v(s), \end{cases}$$

where α_{ij}, β_{ij} all are positive and for the consistency, we must have $\sum_{l=0}^{i-1} \alpha_{il} = 1$. Moreover, if the scheme is total variational diminishing or bounded (TVD/TVB) for Δt_E using forward Euler method i.e.

$$u_h^{k+1} = u_h^k + \Delta t L_h(u_h^k, t^k), \quad |u_h^{k+1}|_{TV} \leq |u_h^k|_{TV}.$$

Then, one can obtain that result for the higher order provided

$$\Delta t_{RK} \leq \min_{ij} \frac{\alpha_{ij}}{\beta_{ij}} \Delta t_E.$$

We use the third order SSPERK method for the numerical simulations which is defined as follows

$$\begin{aligned} u^1 &= u^n + \Delta t\, L(t_n, u^n), \\ u^2 &= \frac{3}{4}u^n + \frac{1}{4}u^1 + \frac{1}{4}\Delta t L\left(t_n + \Delta t, u^1\right), \\ u^{n+1} &= \frac{1}{3}u^n + \frac{2}{3}u^2 + \frac{2}{3}\Delta t L\left(t_n + \frac{1}{2}\Delta t, u^2\right), \end{aligned}$$

where $u^n = u(a, t_n), n = 0, 1, 2, \ldots$ and $t_n = n\ \Delta t$.

2 Numerical Experiments

Here, we provide some of the numerical simulation to study the impact of variables on nonlinear tumor growth model (4.1) in this Section. The vital arguments that effect the model dynamics are k i.e. evolution speed, f i.e. the proportion of new born cells which enters the quiescent phase at the age 0 and μ (death rate). For the numerical examples , we use $a^+ = 72$ hrs i.e. maximum survival age of the cells, $\sigma(a) = 0.02$ and $\beta(a, N) = \beta(a)\phi(N)$ with

$$\beta(a) = \left\{ \begin{array}{ll} 0, & \text{if } a \leq \bar{a}, \\ \dfrac{1}{\vartheta}\dfrac{(a-\bar{a})^2}{2\vartheta^2 + 2\vartheta(a-\bar{a}) + (a-\bar{a})^2}, & \text{if } a > \bar{a} \end{array} \right\}$$

and $\phi(N) = 10^7(N + 10^7)$ for all $N \geq 0$. The time from proliferating cells begins to divide is demonstrated by $\bar{a}$ and takes the value $\bar{a} = 50$ and (the variance constant denoted by ϑ) being $\vartheta = 2$ for the numerical simulations. Further the death rate $\mu(a)$ is described as follows

$$\mu(a) = \left\{ \begin{array}{ll} \mu, & \text{if } a \leq \bar{a}, \\ \mu + \mu(a-\bar{a})^2, & \text{if } a > \bar{a} \end{array} \right\}.$$

We consider the model (4.1)-(4.3) with parameter values as $k = 1,\ f = 0.3,\ \mu = 0.011$ and initial data as

$$p(0, a) = q(0, a) = 4(a^+ - a)10^5/a^+. \tag{4.8}$$

The simulations described by Figures 4.3 and 4.4, show the effect of death rate for the initial data as given in (4.8). We observe that the maximum value of the total number of cells is less than $3x10^7$. Further, the presence of steady-state for both p and q for the long time (larger than

600 hrs) with initial data

$$p(0,a) = q(0,a) = (a^+ - a)10^5/a^+, \tag{4.9}$$

can be found in Figure 4.5. Next, the trends for q and p for dissimilar age values are demonstrated in Figure 4.6. From, Figures 4.6a and 4.6b, we can analyze that the system is stable for different initial values as the curves of newborn cells tend to the same line. The stability of the total number of cells can be found in Figure 4.6c. The change of cell numbers concerning the effect of two parameters k and f shown in Figure 4.7 under the exact rate of death as $\mu = 0.001$. Figure 4.7 shows that cell numbers are increasing with effect of k i.e larger the cell evolution speed leads the increase in all number of cells. Figure 4.7b, we can observe the rise in quiescent cell population and fall off in the proliferating cell population as the proportion f increases.

The errors estimates $\epsilon_{\Delta a}$ for the approximate solution $p(a,t)$ and $q(a,t)$ with different norms are described

$$\begin{aligned}
\|\epsilon_{\Delta a}\|_1 &= \Delta a \sum_i |(q_{\Delta a})_i - (q^\star)_i|, \\
\|\epsilon_{\Delta a}\|_2 &= \sqrt{\Delta a \sum_i |(q_{\Delta a})_i - (q^\star)_i|^2}, \\
\|\epsilon_{\Delta a}\|_\infty &= \max |(q_{\Delta a})_i - (q^\star)_i|.
\end{aligned}$$

In the above expression, $q^\star$ is the approximated solution at the finest grid $N^\star$. In order to perform numerical simulations, we used the finest grid being $N^* = 320$. The numerical result as demonstrated (see Table 4.1-Table 4.8) implies that the error estimates are a monotone decreasing function as N increases i.e. $N = 20, 40, 80, 160$. Additionally, we used the following formula for the calculation of the accuracy rate of the designed scheme

$$r = \log_2 \frac{\epsilon^N}{\epsilon^{2N}},$$

where ϵ^N is the error at the Nth grid cells.

Table 4.1: Error estimates for the numerical solution $p(a,t)$ using DG method at $T = 400$

$\boldsymbol{N}$	$\|\boldsymbol{\epsilon_{\Delta a}}\|_\mathbf{1}$	r	$\|\boldsymbol{\epsilon_{\Delta a}}\|_\mathbf{2}$	r	$\|\boldsymbol{\epsilon_{\Delta a}}\|_\boldsymbol{\infty}$	r
20	0.12097E-00		0.28734E-01		0.10456E-01	
40	0.15564E-01	2.96	0.46143E-02	2.63	0.26277E-02	1.99
80	0.16349E-02	3.25	0.53616E-03	3.10	0.32526E-03	3.01
160	0.17471E-03	3.22	0.59543E-04	3.17	0.41368E-04	2.97

Table 4.2: Error estimates for numerical solution $p(a,t)$ using WENO method at $T = 400$

N	$\|\epsilon_{\Delta a}\|_1$	r	$\|\epsilon_{\Delta a}\|_2$	r	$\|\epsilon_{\Delta a}\|_\infty$	r
20	0.32013E-00		0.60744E-01		0.20077E-01	
40	0.46899E-01	2.77	0.10249E-01	2.56	0.48241E-02	2.06
80	0.80497E-02	2.54	0.24642E-02	2.06	0.20210E-02	1.26
160	0.12817E-02	2.65	0.56352E-03	2.12	0.61753E-03	1.71

Table 4.3: Error estimates for the numerical solution $q(a,t)$ using DG method at $T = 400$

N	$\|\epsilon_{\Delta a}\|_1$	r	$\|\epsilon_{\Delta a}\|_2$	r	$\|\epsilon_{\Delta a}\|_\infty$	r
20	0.50311E-01		0.12306E-01		0.43918E-02	
40	0.44794E-02	3.49	0.15477E-02	2.99	0.10124E-02	2.12
80	0.38084E-03	3.55	0.14998E-03	3.37	0.10453E-03	3.27
160	0.29792E-04	3.68	0.12943E-04	3.53	0.11398E-04	3.19

3 Summary

In this chapter, we describe an implementation of the DG method for the nonlinear age-structured model to examine the tumor cell population dynamics. From our numerical simulation, we examine that the initial effort to design and analyze an accurate and stable method is suitable for long-time age distribution of $p(a,t)$ (proliferating cells) and $q(a,t)$ (quiescent cells). Numerical results are also provided to verify the accuracy of the proposed scheme. Finally, some test examples are included to demonstrate the behavior of the solution and the results reveal that the DG method performs nicely for the simulation of the age-structured tumor cell dynamics.

Table 4.4: Error estimates for the numerical solution $q(a,t)$ using WENO method at $T = 400$

N	$\|\epsilon_{\Delta a}\|_1$	r	$\|\epsilon_{\Delta a}\|_2$	r	$\|\epsilon_{\Delta a}\|_\infty$	r
20	0.28960E-00		0.54772E-01		0.16024E-01	
40	0.40507E-01	2.83	0.17634E-01	2.74	0.35987E-02	2.15
80	0.59128E-02	2.77	0.15774E-03	2.37	0.12368E-02	1.54
160	0.80986E-03	2.86	0.30603E-03	2.36	0.33866E-03	1.86

Table 4.5: Error estimates for the numerical solution $p(a,t)$ using DG method at $T = 1200$

N	$\|\epsilon_{\Delta a}\|_1$	r	$\|\epsilon_{\Delta a}\|_2$	r	$\|\epsilon_{\Delta a}\|_\infty$	r
20	0.17918E-00		0.41547E-01		0.15288E-01	
40	0.24920E-01	2.85	0.68271E-01	2.61	0.35868E-02	2.09
80	0.29730E-02	3.07	0.81196E-03	3.07	0.41217E-03	3.12
160	0.39308E-03	2.91	0.10663E-03	3.12	0.56631E-04	2.86

Table 4.6: Error estimates for the numerical solution $p(a,t)$ using WENO method at $T = 1200$

N	$\|\epsilon_{\Delta a}\|_1$	r	$\|\epsilon_{\Delta a}\|_2$	r	$\|\epsilon_{\Delta a}\|_\infty$	r
20	0.36650E-00		0.71670E-01		0.22801E-01	
40	0.73512E-01	2.31	0.15638E-01	2.19	0.57873E-02	1.97
80	0.85080E-02	3.11	0.25255E-02	2.63	0.20422E-02	1.50
160	0.14132E-02	2.59	0.57540E-03	2.13	0.61993E-03	1.72

Table 4.7: Error estimates for the numerical solution $q(a,t)$ using DG method at $T = 1200$

N	$\|\epsilon_{\Delta a}\|_1$	r	$\|\epsilon_{\Delta a}\|_2$	r	$\|\epsilon_{\Delta a}\|_\infty$	r
20	0.14214E-00		0.33187E-01		0.12078E-01	
40	0.21314E-01	2.73	0.59184E-02	2.48	0.31376E-02	1.94
80	0.25034E-02	3.09	0.74402E-03	2.99	0.41084E-03	2.93
160	0.32796E-03	2.93	0.97104E-04	2.93	0.57284E-04	2.84

Table 4.8: Error estimates for the numerical solution $q(a,t)$ using WENO method at $T = 1200$

N	$\|\epsilon_{\Delta a}\|_1$	r	$\|\epsilon_{\Delta a}\|_2$	r	$\|\epsilon_{\Delta a}\|_\infty$	r
20	0.27838E-00		0.55467E-01		0.18221E-01	
40	0.40454E-01	2.78	0.79469E-02	2.80	0.27499E-02	2.72
80	0.55642E-02	2.86	0.13323E-02	2.57	0.96376E-03	1.51
160	0.76599E-03	2.86	0.23631E-03	2.49	0.24815E-03	1.95

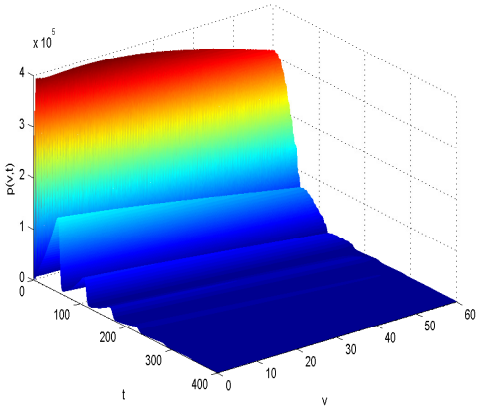

(a) Numerical Solution $p(a,t)$ determined by DG method

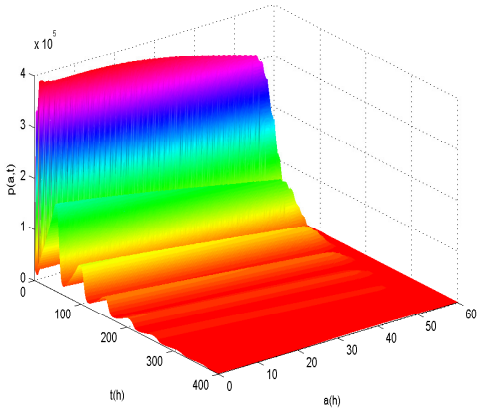

(b) Numerical Solution $p(a,t)$ determined by WENO method

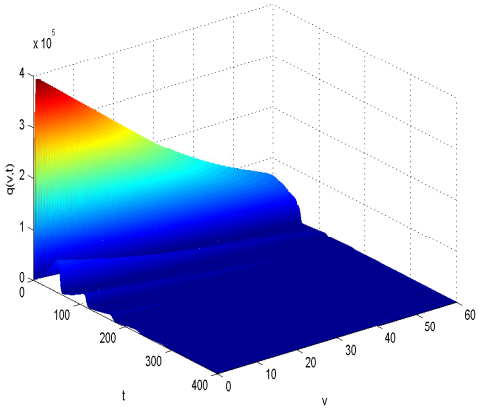

(c) Numerical Solution $q(a,t)$ determined by DG method

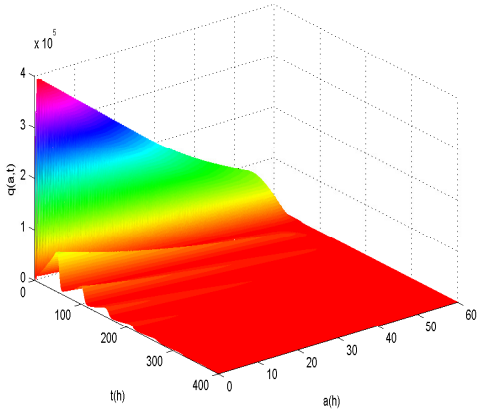

(d) Numerical Solution $q(a,t)$ determined by WENO method

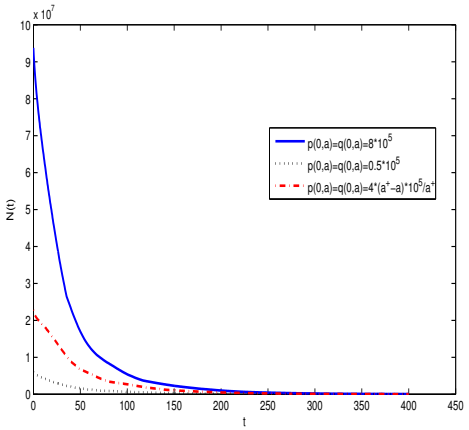

(e) Total Number of cells $N(t)$

Figure 4.3: (A,B) are the Numerical simulation for $p(a,t)$, (C,D) are for $q(a,t)$ for initial data $p(0,t) = q(0,t) = 4 * (a^+ - a) * 10^5/a^+$ and three key parameter are $f = 0.3, k = 1, \mu = 0.011$. The total number $N(t)$ is shown in (E) under three different initial conditions for the model (4.1)

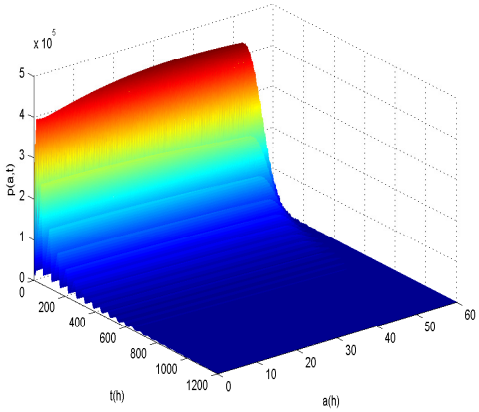

(a) Numerical Solution $p(a,t)$ determined by DG method

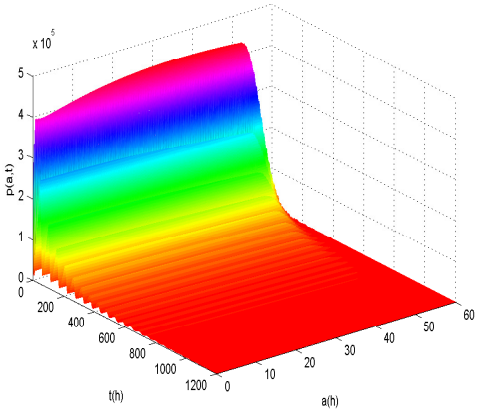

(b) Numerical Solution $p(a,t)$ determined by WENO method

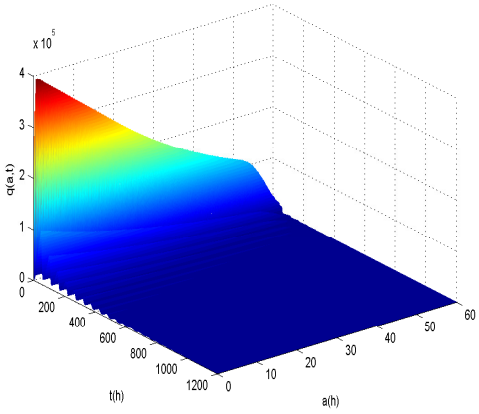

(c) Numerical Solution $q(a,t)$ determined by DG method

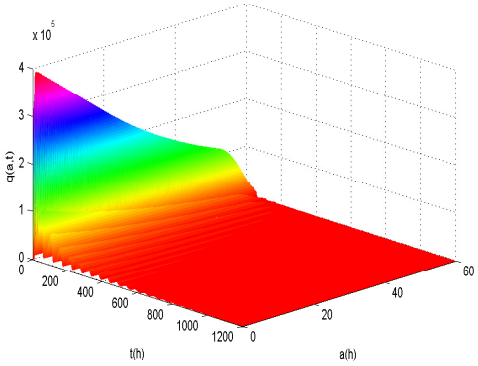

(d) Numerical Solution $q(a,t)$ determined by WENO method

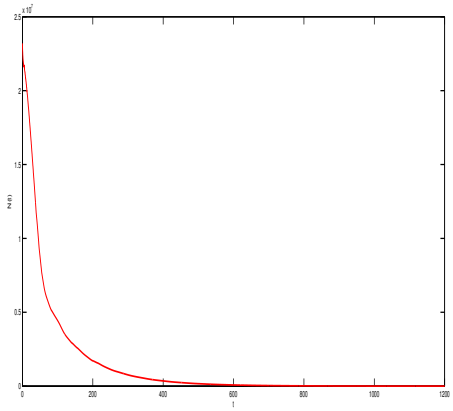

(e) Numerical Solution $N(t)$ determined by DG method

Figure 4.4: (A,B) are the Numerical simulation for $p(a,t)$, (C,D) are for $q(a,t)$ for initial data $p(0,t) = q(0,t) = 4 * (a^+ - a) * 10^5/a^+$ and three key parameter are $f = 0.3, k = 1, \mu = 0.006$. The total number $N(t)$ is shown in (E) for the model (4.1)

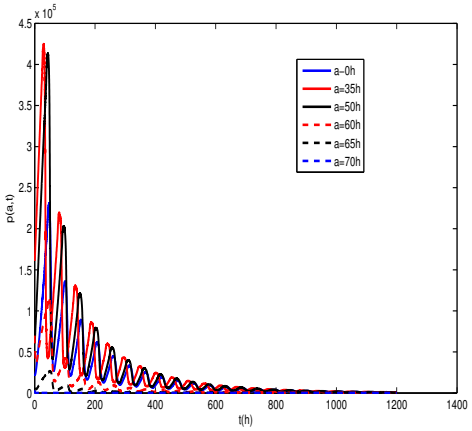

(a) Numerical Solution $p(a,t)$ determined by DG method

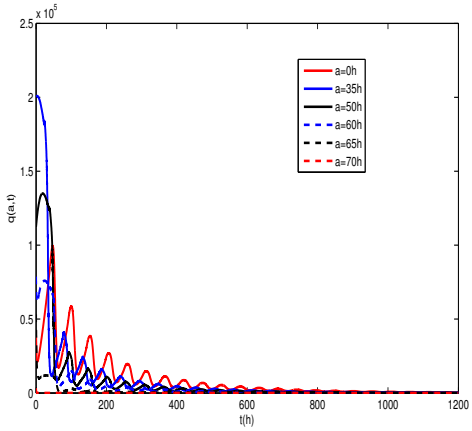

(b) Numerical Solution $q(a,t)$ determined by DG method

Figure 4.5: (A) are the Numerical simulation for proliferating cells $p(a,t)$, (B) are for quiescent cells $q(a,t)$ at fix ages $a = 0, 35, 50, 60, 65, 70$.

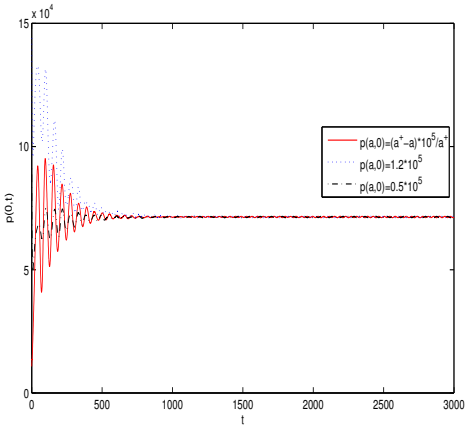

(a) Numerical Solution $p(a,t)$

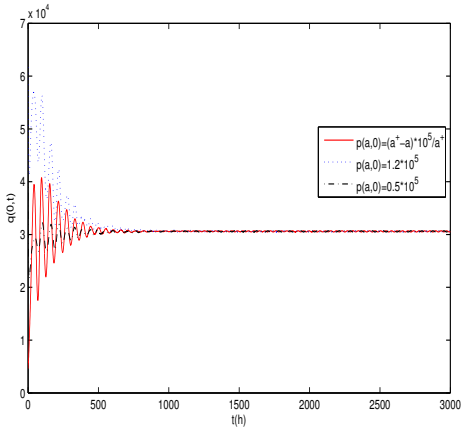

(b) Numerical Solution $q(a,t)$

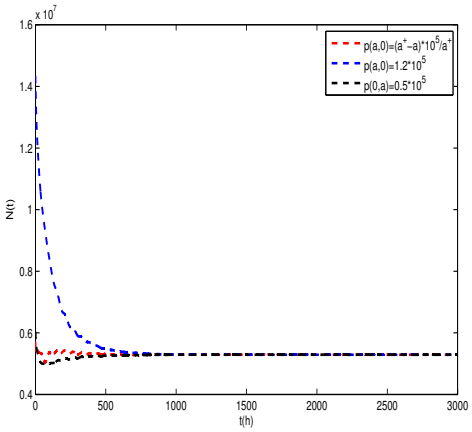

(c) Total Number of cells $N(t)$

Figure 4.6: (A,B) are the Numerical simulation for $p(a,t)$, and $q(a,t)$ for different initial data with three key parameter are $f = 0.3, k = 1, \mu = 0.001$. The total number $N(t)$ is shown in (C) for the model (4.1)

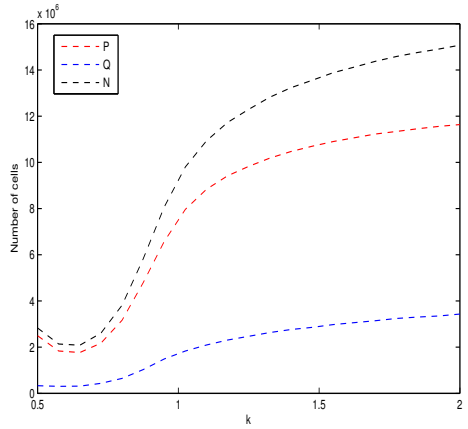

(a) Number of cells versus call evolution speed

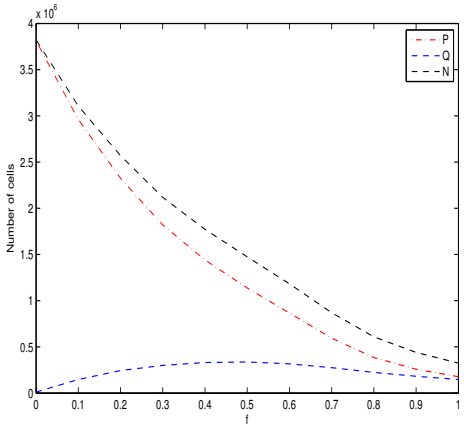

(b) Number of cells versus f

Figure 4.7: (A) describes the number of cells for different value of k and (B) demonstrate the number of cells against different values of f.

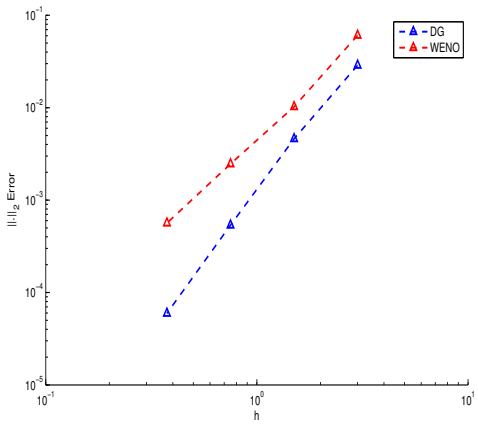

(a) Error estimates for $p(a,t)$ versus number of grids

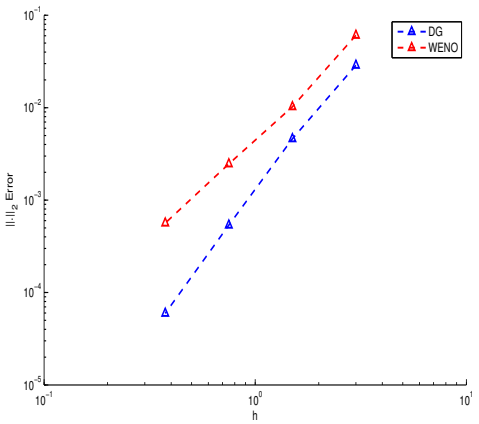

(b) Error estimates for $q(a,t)$ versus number of grids

Figure 4.8: (A) described the error estimates for $p(a,t)$ and (B) described for $q(a,t)$ at the time $t = 1200$.

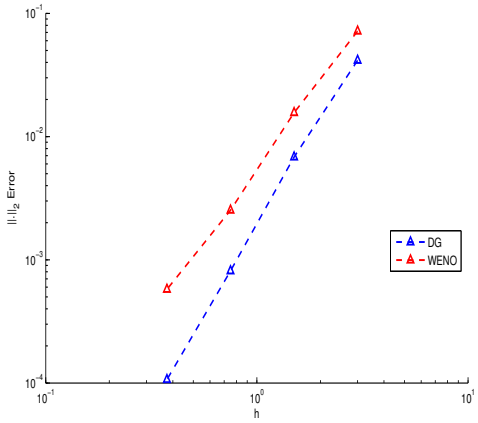

(a) Error estimates for $p(a,t)$ versus number of grids

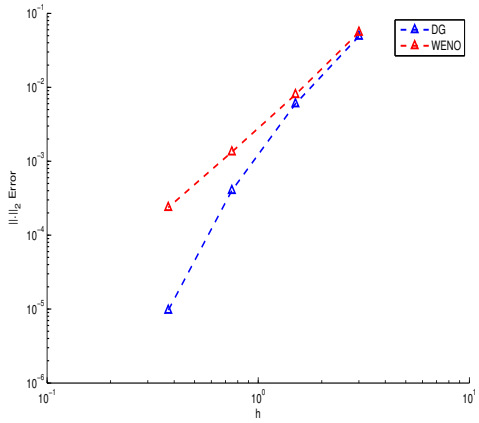

(b) Error estimates for $q(a,t)$ versus number of grids

Figure 4.9: (A) described the error estimates for $p(a,t)$ and (B) described for $q(a,t)$ at the time $t = 1200$.

Chapter 5

Conclusions and Future Scope

This chapter summarizes the thesis findings and conclusions. The chapter also provides recommendations and suggestions about future work.

1 Conclusions

This thesis aims to formulate, analyze, and implement DG methods for the partial differential equations arising from neuroscience and population dynamics. This study comes under the category of applied and computational mathematics. This area of research has become an appealing field in the present time and remained relatively unexplored until the discovery of high-speed computers. We examined biological models in the form of time-dependent PDEs and designed suitable numerical schemes, discussed the stability and convergence, and simulated, it on a computer to get the desired results in practice. The work has been published in the research articles [117, 118]. The objectives mentioned for this research work are completed in chapters. A brief summary of each chapter follows.

1. The first chapter is dedicated to the review and analysis of existing literature that has been accomplished to determine the gaps existing in the area of computational neuroscience and population dynamics. The resulting equations are time-dependent PDEs, thus the overview of the numerical techniques for the solution of these equations are composed in this chapter. Some preliminaries of neurons and their structures are also discussed.

2. The NLIF model plays an essential role in neuron biology to represent their biological phenomena. In Chapter 2, we used the nonlinear NNLIF model to discuss the neuronal behavior in more realistic manner. A suitable numerical approach based on the FEM approach has been used to determine the approximate solution of the governing equation and the performance of the proposed scheme over the existing schemes have been shown in the chapter. Relevant numerical examples were provided to validate the theoretical results.

3. The probability density approach in computational neuroscience has a long-standing history and it is used in various contexts. However, this approach is inadequate for the simulation of a large neural network. In Chapter 3, we used the population density

approach based on probability density function for the derivation of the population density model (excitatory and inhibitory) with delay and refractory period. An appropriate discontinuous Galerkin scheme has been designed and discussed in this chapter. The comparative results depict the performance of the designed scheme over the existing schemes for the resulting model equation.

4. The model equation based on the age-structure approach plays a vital role in population dynamics. Thus age-structured tumor cell population model has been studied in Chapter 4. The considered model is governed by a non-linear hyperbolic PDE to depict the tumor cell population dynamics based on an age-structured approach. The discontinuous Galerkin approximation has been employed to figure out the numerical solution of the model equation. Moreover, this scheme is also suitable for long-time behavior of the governing model equation.

2 Scope of the Future Work

Research is a continuous process. The work presented in this thesis is related to the numerical study of biological models. The aim is to understand the realistic biological phenomena concerning non-linear mathematical models, which are very difficult to solve analytically. Hence, we need numerical methods to find the approximate solutions. Further research directions in this area are listed below:

1. A neuron network model with adaptation and fatigue can be studied. Due to the high nonlinearities, it would be a challenge to provide the numerical study of the impact of the fragmentation term which appears due to the synchronization of neurons in the neural network.

2. For a better understanding of the complicated physical phenomenon of neuronal networks, it is necessary to introduce mathematical models which might show some features very similar to those of the original phenomenon. The resulting mathematical models suitably governed by the higher-order nonlinear PDEs have many difficulties to solve. Therefore, It is very difficult to apply the correct analytical approach for the expression of this variability. Therefore, suitable numerical methods are required to study the neuronal variability governed by the higher-order nonlinear PDEs.

3. The delay differential/partial equations play a vital role in mathematical biology to represent the complex biological phenomena. On the other side, it is very difficult to solve these model equations analytically. Therefore, a stable and efficient numerical method is needed to tackle these types of the model equation to figure out the dynamical behavior of these biological processes.

4. The problem of tumor growth and its monitoring has draw a substantial concern over the last few years. Tumor growth models generally consist of two or more equations in terms of the variables order parameter, chemical potential, and nutrient concentration, and many others. Therefore, these model equations are governed by a highly nonlinear system of PDEs which again needs a suitable approach to tackle these complicated phenomenons.

3 Recommendations about Future Work

One of the challenging issues in modern sciences is the modeling of physical phenomena arising in biological growth problems. The resulting mathematical models are governed by the higher-order nonlinear partial differential equations. Often, it is very difficult to solve these nonlinear equations explicitly for exact solutions. Thus, the numerical solutions of nonlinear systems governing biological phenomena are of great importance. The problem of tumor growth and its monitoring has attracted considerable attention over the last two decades.

Tumor growth models generally consist of Cahn-Hilliard type equations with transport and reaction terms which govern various types of cell concentrations. The reaction terms depend on the nutrient concentration (e.g., oxygen) which obeys an advection-reaction-diffusion equation coupled with the Cahn-Hilliard equations. In particular, we will examine a diffuse interface model of tumor growth for their numerical analysis.

A further study would be to investigate time-dependent higher-order PDEs arising in cancer biology, infectious disease transmission, and related areas. Possible extension of these models for higher space dimensions can be considered. Various type of numerical techniques has been proposed to solve the tumor growth model. All this type of method remains of fixed order and the furthermost of these methods have been examined with some restrictive assumption (smoothness of data and the solution). Thus, to efficiently handle these types of solutions (irregular) with a certain pattern, we go for another class of approximation techniques. To Achieve this purpose, the DG method may be efficiently applied for the simulation of the population growth model. The discontinuous Galerkin method is a new technique and provides adorable properties for the numerical approximation of the solution of various classes of PDEs. Further, applications of the discontinuous Galerkin methods could be explored to study complex biological and related phenomena.

References

[1] K. Pakdaman, B. Perthame, and D. Salort. Dynamics of a structured neuron population. *Nonlinearity*, **23**(1):55–75, 2010.

[2] Wikipedia. Neuron-Wikipedia, the free encyclopedia. `http://en.wikipedia.org/w/index.php?title=Neuron&oldid=778367135`, 2020. [Online; accessed 07-July-2019].

[3] L. F. Abbott. Lapicque's introduction of the integrate-and-fire model neuron (1907). *Brain Research Bulletin*, **50**(5-6):303–304, 1999.

[4] Z. Liu, J. Chen, J. Pang, P. Bi, and S. Ruan. Modeling and analysis of a nonlinear age-structured model for tumor cell populations with quiescence. *Journal of Nonlinear Science*, 28(5):1763–1791, 2018.

[5] E. R. Kandel, J. H. Schwartz, and T. M. Jessell. *Principles of Neural Science*. McGraw-Hill, New York, fourth edition, 2000.

[6] H. C. Tuckwell. *Introduction to Theoretical Neurobiology: Nonlinear and Stochastic Theories*, volume 2. Cambridge University Press, 1988.

[7] S. R. y Cajal. A new concept of the histology of the central nervous system. In: Rottenberg, Hochberg, editors, Neurological Classics in Modern Translation. New York: Hafner, 1977.

[8] W. Gerstner and W. M. Kistler. *Spiking Neuron Models: Single Neurons, Populations, Plasticity*. Cambridge University Press, Cambridge, 2002.

[9] E. M. Izhikevich. *Dynamical Systems in Neuroscience: The Geometry of Excitability and Bursting*. MIT Press, Cambridge, Massachusetts, 2007.

[10] G. B. Ermentrout and D. H. Terman. *Mathematical Foundations of Neuroscience*, volume 35. Springer Science & Business Media, Berlin; Heidelberg; New York, 2010.

[11] R. Q. Quiroga and S. Panzeri. *Principles of Neural Coding*. CRC Press, London, 2013.

[12] W. Gerstner, W. M. Kistler, R. Naud, and L. Paninski. *Neuronal Dynamics: From Single Neurons to Networks and Models of Cognition*. Cambridge University Press, Cambridge, 2014.

[13] B. Charlesworth. *Evolution in Age-Structured Populations*. Cambridge University Press, Cambridge, second edition, 1994.

[14] M. E. Gurtin and R. C. MacCamy. Non-linear age-dependent population dynamics. *Archive for Rational Mechanics and Analysis*, 54(3):281–300, 1974.

[15] K. O. Okosun and O. D. Makinde. Modelling the impact of drug resistance in malaria transmission and its optimal control analysis. *International Journal of Physical Sciences*, 6(28):6479–6487, 2011.

[16] J. D. Ferreira, A. M. P. Galvis, and V. S. H. Rao. Dynamic models of competition systems involving generalized functional response. *Differential Equations and Dynamical Systems*,

27(1-3):221–248, 2019.

[17] G. F. Webb. *Theory of Nonlinear Age-Dependent Population*. CRC Press, 1985.

[18] M. Iannelli and F. Milner. On the approximation of the Lotka-McKendrick equation with finite life-span. *Journal of Computational and Applied Mathematics*, 136(1-2):245–254, 2001.

[19] J. D. Ferreira, R. A. Garcia, and V. S. H. Rao. Bifurcation dynamics: Theory, Methods, and Applications, 2012.

[20] S. P. Luby, M. Rahman, B. F. Arnold, L. Unicomb, S. Ashraf, P. J. Winch, C. P. Stewart, F. Begum, F. Hussain, J. Benjamin-Chung, and E. Leontsini. Effects of water quality, sanitation, handwashing, and nutritional interventions on diarrhoea and child growth in rural Bangladesh: a cluster randomised controlled trial. *The Lancet Global Health*, 6(3):e302–e315, 2018.

[21] A. S. Waziri, E. S. Massawe, and O. D. Makinde. Mathematical modelling of HIV/AIDS dynamics with treatment and vertical transmission. *Appl. Math*, 2(3):77–89, 2012.

[22] M. Garbey, M. Rahman, and S. Berceli. A multiscale computational framework to understand vascular adaptation. *Journal of Computational Science*, 8:32–47, (2015).

[23] Y. Dong, Y. Takeuchi, and S. Nakaoka. A mathematical model of multiple delayed feedback control system of the gut microbiot-antibiotics injection controlled by measured metagenomic data. *Nonlinear Analysis: Real World Applications*, 43:1–17, 2018.

[24] A. V. Hill. Excitation and accommodation in nerve. *Proceedings of the Royal Society of London B: Biological Sciences*, **119**(814):305–355, 1936.

[25] G. Gerstein and B. Mandelbrot. Random walk models for the spike activity of a single neuron. *Biophysical Journal*, **4**(1):41–68, 1964.

[26] R. B. Stein. A theoretical analysis of neuronal variability. *Biophysical Journal*, **5**(2):173–194, 1965.

[27] R. B. Stein. Some models of neuronal variability. *Biophysical Journal*, **7**(1):37–68, 1967.

[28] B. W. Knight. Dynamics of encoding in a population of neurons. *The Journal of General Physiology*, **59**(6):734–766, 1972.

[29] V. I. Kryukov. Wald's identity and random walk models for neuron firing. *Advances in Applied Probability*, **8**(2):257–277, 1976.

[30] H. C. Tuckwell. On stochastic models of the activity of single neurons. *Journal of Theoretical Biology*, **65**(4):783–785, 1977.

[31] P. Lánskỳ. On approximations of Stein's neuronal model. *Journal of Theoretical Biology*, **107**(4):631–647, 1984.

[32] W. J. Wilbur and J. Rinzel. An analysis of Stein's model for stochastic neuronal excitation. *Biological Cybernetics*, **45**(2):107–114, 1982.

[33] H. C. Tuckwell. Neuronal interspike time histograms for a random input model. *Biophysical Journal*, **21**(3):289, 1978.

[34] H. C. Tuckwell. Synaptic transmission in a model for stochastic neural acttivity. *Journal of Theoretical Biology*, **77**:65–81, 1979.

[35] D. K. Cope and H. C. Tuckwell. Firing rates of neurons with random excitation and inhibition. *Journal of Theoretical Biology*, **80**(1):1–14, 1979.

[36] F. B. Hanson and H. C. Tuckwell. Diffusion approximations for neuronal activity including synaptic reversal potentials. *Journal of Theoretical Neurobiology*, **2**:127–153, 1983.

[37] M. Musila and P. Lánskỳ. On the interspike intervals calculated from diffusion approximations of Stein's neuronal model with reversal potentials. *Journal of Theoretical Biology*, **171**(2):225–232, 1994.

[38] S. Fusi and M. Mattia. Collective behavior of networks with linear (VLSI) integrate-and-fire neurons. *Neural Computation*, **11**(3):633–652, 1998.

[39] G. B. Ermentrout and N. Kopell. Parabolic bursting in an excitable system coupled with a slow oscillation. *SIAM Journal on Applied Mathematics*, **46**(2):233–253, 1986.

[40] E. M. Izhikevich. Class 1 neural excitability, conventional synapses, weakly connected networks, and mathematical foundations of pulse-coupled models. *IEEE Transactions on Neural Networks*, **10**(3):499–507, 1999.

[41] P. E. Latham, B. J. Richmond, P. G. Nelson, and S. Nirenberg. Intrinsic dynamics in neuronal networks. I. Theory. *Journal of Neurophysiology*, **83**(2):808–827, 2000.

[42] B. S. Gutkin and G. B. Ermentrout. Dynamics of membrane excitability determine interspike interval variability: a link between spike generation mechanisms and cortical spike train statistics. *Neural Computation*, **10**(5):1047–1065, 1998.

[43] G. B. Ermentrout. Type I membranes, phase resetting curves, and synchrony. *Neural Computation*, **8**(5):979–1001, 1996.

[44] B. Lindner, A. Longtin, and A. Bulsara. Analytic expressions for rate and CV of a type I neuron driven by white gaussian noise. *Neural Computation*, **15**(8):1761–1788, 2003.

[45] N. Brunel and P. E. Latham. Firing rate of the noisy quadratic integrate-and-fire neuron. *Neural Computation*, **15**(10):2281–2306, 2004.

[46] N. Fourcaud-Trocmé, D. Hansel, C. v. Vreeswijk, and N. Brunel. How spike generation mechanisms determine the neuronal response to fluctuating inputs. *Journal of Neuroscience*, **23**(37):11628–11640, 2003.

[47] N. Fourcaud-Trocmé and N. Brunel. Dynamics of the instantaneous firing rate in response to changes in input statistics. *Journal of Computational Neuroscience*, **18**(3):311–321, 2005.

[48] R. Brette and W. Gerstner. Adaptive exponential integrate-and-fire model as an effective description of neuronal activity. *Journal of Neurophysiology*, **94**(5):3637–3642, 2005.

[49] L. J. DeFelice. *Introduction to Membrane Noise*. Plenum, New York, 1981.

[50] G. C. Quarton, T. Melnechuk, and F. O. Schmitt. *The Neurosciences. A Study Program*. Rockefeller University Press, New York, 1967.

[51] A. V. Holden. *Models of the Stochastic Activity of Neurones*. Springer, 1976.

[52] L. F. Abbott and C. v. Vreeswijk. Asynchronous states in networks of pulse-coupled oscillators. *Physical Review E*, **48**(2):1483–1490, 1993.

[53] N. Brunel and V. Hakim. Fast global oscillations in networks of integrate-and-fire neurons

with low firing rates. *Neural Computation*, **11**(7):1621–1671, 1999.

[54] N. Brunel. Dynamics of sparsely connected networks of excitatory and inhibitory spiking neurons. *Journal of Computational Neuroscience*, 8(3):183–208, 2000.

[55] N. Brunel A. Renart and X.-J. Wang. Mean-field theory of irregularly spiking neuronal populations and working memory in recurrent cortical networks. *Computational neuroscience: A comprehensive approach*, pages 431–490, 2004.

[56] A. Faisal, L. Selen, and L. Wolpert. Noise in the nervous system. *Nature Reviews. Neuroscience*, **9**(4):292–303, 2008.

[57] A. Faisal, L. Selen, and L. Wolpert. Neuronal noise. *Scholarpedia*, **8**(9):1618, 2013.

[58] P. Singh, M. K. Kadalbajoo, and K. Sharma. Probability density function of leaky integrate-and-fire model with Lévy noise and its numerical approximation. *Numerical Analysis and Applications*, 9(1):66–73, 2016.

[59] A. N. Burkitt. A review of the integrate-and-fire neuron model: I. homogeneous synaptic input. *Biological Cybernetics.*, **95**(1):1–19, 2006.

[60] J. Arcede. Fundamental theorem of calculus for backwards Itô integral. *Matimyas Matematika, Proceedings of the 9th Philippines-Taiwan Symposium on Analysis*, **34**(01):1–9, 2011.

[61] J. Arcede. On integration-by-parts and Itô formula for backwards Itô integral. *The Mindanawan Journal of Mathematics*, **3**(02):112–131, 2012.

[62] D. Q. Nykamp and D. Tranchina. A population density approach that facilitates large-scale modeling of neural networks: Analysis and an application to orientation tuning. *Journal of Computational Neuroscience*, **8**(1):19–50, 2000.

[63] D. Q. Nykamp and D. Tranchina. A population density approach that facilitates large-scale modeling of neural networks: extension to slow inhibitory synapses. *Neural Computation*, 13(3):511–546, 2001.

[64] F. Apfaltrer, C. Ly, and D. Tranchina. Population density methods for stochastic neurons with realistic synaptic kinetics: firing rate dynamics and fast computational methods. *Network: Computation in Neural Systems*, **17**(4):373–418, 2006.

[65] C. Ly and D. Tranchina. Critical analysis of dimension reduction by a moment closure method in a population density approach to neural network modeling. *Neural Computation*, **19**(8):2032–2092, 2007.

[66] G. Dumont and J. Henry. Population density models of integrate-and-fire neurons with jumps: well-posedness. *Journal of Mathematical Biology*, **67**(3):453–481, 2012.

[67] C. Ly. A principled dimension-reduction method for the population density approach to modeling networks of neurons with synaptic dynamics. *Neural Computation*, **25**(10):2682–2708, 2013.

[68] G. Dumont and J. Henry. A density model for a population of theta neurons. *The Journal of Mathematical Neuroscience*, **4**(1):1–22, 2014.

[69] W. Nicola, C. Ly, and S. A. Campbell. One-dimensional population density approaches to recurrently coupled networks of neurons with noise. *SIAM Journal on Applied Mathe-*

matics, **75**(5):2333–2360, 2015.

[70] A. L. Hodgkin and A. F. Huxley. A quantitative description of membrane current and its application to conduction and excitation in nerve. *The Journal of Physiology*, **117**(4):500–544, 1952.

[71] J. Touboul. Bifurcation analysis of a general class of nonlinear integrate-and-fire neurons. *SIAM Journal on Applied Mathematics*, **68**(4):1045–1079, 2008.

[72] J. Touboul and R. Brette. Spiking dynamics of bidimensional integrate-and-fire neurons. *SIAM Journal on Applied Dynamical Systems*, **8**(4):1462–1506, 2009.

[73] K. A. Newhall, G. Kovačič, P. R. Kramer, and D. Cai. Cascade-induced synchrony in stochastically driven neuronal networks. *Physical Review E*, **82**(4):041903, 2010.

[74] M. J. Cáceres and B. Perthame. Beyond blow-up in excitatory integrate and fire neuronal networks: refractory period and spontaneous activity. *Journal of Theoretical Biology*, 350:81–89, 2014.

[75] M. Rahman, S. F. Previs, T. Kasumov, and R. G. Sadygov. Gaussian process modeling of protein turnover. *Journal of Proteome Research*, 15(7):2115–2122, 2016.

[76] W. J. Wilbur and J. Rinzel. A theoretical basis for large coefficient of variation and bimodality in neuronal interspike interval distributions. *Journal of Theoretical Biology*, **105**(2):345–368, 1983.

[77] Y. Kuramoto. A collective synchronization of pulse-coupled oscillators and excitable units. *Physica D: Nonlinear Phenomena*, **50**(1):15–30, 1991.

[78] Y. Kuramoto. A simple and stable numerical solution for the population density equation. *Neural Computation*, 15(9):2129–2146, 2003.

[79] D. Manin B. W. Knight and L. Sirovich. Dynamical models of interacting neuron populations in visual cortex. *Robot Cybern*, **54**:4–8, 1996.

[80] A. Omurtag, B. W. Knight, and L. Sirovich. On the simulation of large populations of neurons. *Journal of Computational Neuroscience*, 8(1):51–63, 2000.

[81] B. W. Knight A. Omurtag and L. Sirovich. Dynamics of neuronal populations: the equilibrium solution. *SIAM Journal on Applied Mathematics*, **60**(6):2009–2028, 2000.

[82] B. W. Knight. Dynamics of encoding in neuron populations: some general mathematical features. *Neural Computation*, **12**(3):473–518, 2000.

[83] F. Sharpe and A. J. Lotka. A problem in age-distribution. *Philosophical Magazine*, **6**:435–438, 1911.

[84] A. G. McKendrick. Applications of mathematics to medical problems. *Proceedings of the Edinburgh Mathematical Society*, **44**:98–130, 1926.

[85] W. Feller. On the integral equation of renewal theory. *The Annals of Mathematical Statistics*, **12**:243–267, 1941.

[86] R. Bellman and K. L. Cooke. *Differential-Difference Equations*. Academic Press, New York, 1963.

[87] M. Y. Kim and Y. Kwon. A Collocation Method for the Gurtin–MacCamy Equation with Finite Life-Span. *SIAM Journal on Numerical Analysis*, 39(6):1914–1937, 2002.

[88] L. M. Abia, O. Angulo, J. C. López-Marcos, and M. López-Marcos. Numerical schemes for a size-structured cell population model with equal fission. *Mathematical and Computer Modelling*, 50(5-6):653–664, 2009.

[89] V. K. Baranwal, R. K. Pandey, M. P. Tripathi, and O. P. Singh. Analytic algorithms for some models of nonlinear Age-Structured population dynamics and epidemiology. *Journal of Modern Physics*, 2:236–247, 2011.

[90] S. C. S. Rao and S. Kumar. Robust high order convergence of an overlapping Schwarz method for singularly perturbed semilinear reaction-diffusion problems. *Journal of Computational Mathematics*, **31**(1):509–521, 2013.

[91] S. C. S. Rao and M. Kumar. Exponential B-spline collocation method for self-adjoint singularly perturbed boundary value problems. *Applied Numerical Mathematics*, **58**(1):1572–1581, 2008.

[92] L. M. Abia, O. Angulo, and J. C. López-Marcos. Age-structured population dynamics models and their numerical solutions. *Ecological Modelling*, **188**(1):112–136, 2005.

[93] V. Kanwar. A family of third-order multipoint methods for solving nonlinear equations. *Applied Mathematics and Computation*, **176**(2):409–413, 2006.

[94] M. Y. Kim and T. Selenge. Discontinuous-continuous Galerkin methods for population diffusion with finite life span. *Mathematical Population Studies*, **23**(1):17–36, 2016.

[95] H. Ramos, G. Singh, V. Kanwar, and S. Bhatia. An efficient variable step-size rational Falkner-type method for solving the special second-order IVP. *Applied Mathematics and Computation*, **291**(1):39–51, 2016.

[96] V. M. Magagula, S. S. Motsa, and P. Sibanda. Multidomain bivariate pseudo-spectral quasilinearization method for systems of nonlinear partial differential equations. *Computational and Mathematical Methods*, 2(4):e1096, 2020.

[97] H. Ramos and M. A. Rufai. Numerical solution of boundary value problems by using an optimized two-step block method. *Numerical Algorithms*, 84(1):229–251, 2020.

[98] P. Singh and K. K. Sharma. Numerical approximations to the transport equation arising in neuronal variability. *International Journal of Pure and Applied Mathematics*, 69(3):341–356, 2011.

[99] S. Gowrisankar and S. Natesan. An efficient robust numerical method for singularly perturbed Burgers' equation. *Applied Mathematics and Computation*, 346:385–394, 2019.

[100] S. Dhawan, S. K. Bhowmik, and S. Kumar. Galerkin-least square B-spline approach toward advection-diffusion equation. *Applied Mathematics and Computation*, 261:128–140, 2015.

[101] J. C. Strikwerda. *Finite Difference Schemes and Partial Differential Equations*. SIAM, Philadelphia, second edition, 2004.

[102] M. Dehghan and A. Taleei. A compact split-step finite difference method for solving the nonlinear schrödinger equations with constant and variable coefficients. *Computer Physics Communications*, 181(1):43–51, 2010.

[103] K. W. Morton and D. F. Mayers. *Numerical Solution of Partial Differential Equations*.

Cambridge University Press, Cambridge, second edition, 2005.

[104] G. D. Smith. *Numerical Solution of Partial Differential Equations (Finite Difference Methods)*. Oxford University Press, Oxford, third edition, 1985.

[105] D. Gottlieb and S. A. Orszag. *Numerical Analysis of Spectral Methods: Theory and Applications*. SIAM, 1977.

[106] C. Canuto, M. Y. Hussaini, A. Quarteroni, and T. A. Zang. *Spectral Methods in Fluid Dynamics*. Springer-Verlag, Berlin, 1998.

[107] B. Fornberg. *A Practical Guide to Pseudospectral Methods*. Cambridge University Press, Cambridge UK, 1996.

[108] L. N. Trefethen. *Spectral Methods in MATLAB*. SIAM, Philadelphia, PA, 2000.

[109] J. Shen and T. Tang. *Spectral and high-order methods with applications*. Science Press, Beijing, 2007.

[110] J. S. Hesthaven, S. Gottlieb, and D. Gottlieb. *Spectral Methods for Time-Dependent Problems*. Cambridge University Press, Cambridge, 2007.

[111] G.-Q. Chen and C. Christoforou. Solutions for a nonlocal conservation law with fading memory. *Proc. Amer. Math. Soc.*, **135**(12):3905–3915, 2007.

[112] D. Colton and R. Kress. *Integral Equation Methods in Scattering Theory*. John Wiley and Sons, New York, 1983.

[113] S. Brenner and R. Scott. *The Mathematical Theory of Finite Element Methods*, volume 15. Springer Science & Business Media, Berlin/Heidelberg, Germany, 2007.

[114] J. N. Reddy. *An Introduction to the Finite Element Method*. McGraw-Hill New York, 3 edition, 2005.

[115] J. Hesthaven and T. Warburton. *Nodal Discontinuous Galerkin Methods: Algorithms, Analysis, and Applications*. Springer-Verlag New York, 2008.

[116] B. Cockburn, G. E. Karniadakis, and C.-W. Shu. *Discontinuous Galerkin Methods: Theory, Computation and Applications*, volume 11. Springer Science & Business Media, Berlin/Heidelberg, Germany, 2012.

[117] D. Sharma, P. Singh, R. P. Agarwal, and M. E. Koksal. Numerical approximation for nonlinear noisy leaky integrate-and-fire neuronal model. *Mathematics*, 7(4):363, 2019.

[118] D. Sharma and P. Singh. Discontinuous Galerkin approximation for excitatory-inhibitory networks with delay and refractory periods. *International Journal of Modern Physics C*, 31(03):1–25, 2020.

[119] D. Sharma and P. Singh. Discontinuous galerkin method for a nonlinear age-structured tumor cell population model with proliferating and quiescent phases. *International Journal of Modern Physics C*, 32(03):1–18, 2021.

[120] L. Sirovich, A. Omurtag, and K. Lubliner. Dynamics of neural populations: Stability and Synchrony. *Network: Computation in neural systems*, 17(1):3–29, 2006.

[121] H. C. Tuckwell. *Stochastic Processes in the Neurosciences*. SIAM, 1989.

[122] M. J. Cáceres, J. A. Carrillo, and B. Perthame. Analysis of nonlinear noisy integrate-and-fire neuron models : blow-up and steady states. *The Journal of Mathematical Neu-*

roscience, 1:1–7, 2011.

[123] M. J. Cáceres, P. Roux, D. Salort, and R. Schneider. Global-in-time solutions and qualitative properties for the NNLIF neuron model with synaptic delay. *Communications in Partial Differential Equations*, 44(12):1358–1386, 2019.

[124] M. J. Cáceres and R. Schneider. Analysis and numerical solver for excitatory-inhibitory networks with delay and refractory periods. *ESAIM: Mathematical Modelling and Numerical Analysis*, 52(5):1733–1761, 2018.

[125] M. J. Cáceres and R. Schneider. Blow-up, steady states and long time behaviour of excitatory-inhibitory nonlinear neuron models. *Kinetic and Related Models*, **10**:587–612, 2017.

[126] J. A. Carrillo, M. d. M. González, M. P. Gualdani, and M. E. Schonbek. Classical solutions for a nonlinear Fokker-Planck equation arising in computational neuroscience. *Communications in Partial Differential Equations*, 38(3):385–409, 2013.

[127] J. A. Carrillo, B. Perthame, D. Salort, and D. Smets. Qualitative properties of solutions for the noisy integrate and fire model in computational neuroscience. *Nonlinearity*, 28(9):3365, 2015.

[128] L. C. Evans. *Partial Differential Equations*. American Mathematical Society, Providence, 2010.

[129] M. de Kamps. A simple and stable numerical solution for the population density equation. *Neural Computation*, 15(9):2129–2146, 2003.

[130] N. H. Tuan, T. B. Ngoc, and S. Tatar. Recovery of the solute concentration and dispersion flux in an inhomogeneous time fractional diffusion equation. *Journal of Computational and Applied Mathematics*, 342:96–118, 2018.

[131] S. C. S. Rao and S. Chawla. Numerical solution of singularly perturbed linear parabolic system with discontinuous source term. *Applied Numerical Mathematics*, 127:249–265, 2018.

[132] S. K. Kenettinkara and G. D. V. Gowda. On the convergence of a second order approximation of conservation laws with discontinuous flux. *Bulletin of the Brazilian Mathematical Society, New Series*, 47(1):21–35, 2016.

[133] P. K. Kameswaran, P. Sibanda, and S. S. Motsa. A spectral relaxation method for thermal dispersion and radiation effects in a nanofluid flow. *Boundary Value Problems*, 2013(1):242, 2013.

[134] H. Ramos and M. F. Patricio. Some new implicit two-step multiderivative methods for solving special second-order ivp's. *Applied Mathematics and Computation*, 239:227–241, 2014.

[135] M. K. Kadalbajoo, L. P. Tripathi, and A. Kumar. An error analysis of a finite element method with IMEX-time semidiscretizations for some partial integro-differential inequalities arising in the pricing of American options. *SIAM Journal on Numerical Analysis*, 55(2):869–891, 2017.

[136] S. Bajpai, N. Nataraj, A. K. Pani, P. Damazio, and J. Y. Yuan. Semidiscrete galerkin

method for equations of motion arising in kelvin-voigt model of viscoelastic fluid flow. *Numerical Methods For Partial Differential Equations*, 29(3):857–883, 2013.

[137] T. Zhang, X. Feng, and J. Yuan. Implicit–Explicit schemes of finite element method for the non-stationary thermal convection problems with temperature-dependent coefficients. *International Communications in Heat and Mass Transfer*, 76:325–336, 2016.

[138] A. K. Pani, A. K. Pany, P. Damazio, and J. Y. Yuan. A modified nonlinear spectral Galerkin method for the equations of motion arising in the Kelvin-Voigt fluids. *Applicable Analysis*, 93(8):1587–1610, 2014.

[139] A. Öchsner and M. Merkel. *One-dimensional Finite Elements: An Introduction to the FE Method*. Springer, 2012.

[140] O. P. Yadav and R. Jiwari. Finite element analysis and approximation of Burgers-Fisher equation. *Numerical Methods for Partial Differential Equations*, 33(5):1652–1677, 2017.

[141] P. Kumar and S. Narayanan. Solution of Fokker-Planck equation by finite element and finite difference methods for nonlinear systems. *Sadhana*, 31(4):445–461, 2006.

[142] M. K. Kadalbajoo and P. Arora. Taylor-Galerkin B-spline finite element method for the one-dimensional advection-diffusion equation. *Numerical Methods for Partial Differential Equations*, 26(5):1206–1223, 2010.

[143] C. H. Huang, C. C. K. Lin, and M. S. Ju. Finite element method for population density approach for large-scale neuronal networks. *Journal of Medical and Biological Engineering*, 33(6):552–563, 2013.

[144] O. P. Yadav and R. Jiwari. A finite element approach for analysis and computational modelling of coupled reaction diffusion models. *Numerical Methods For Partial Differential Equations*, 35(2):830–850, 2019.

[145] David S Burnett. *Finite Element Analysis: From Concepts to Applications*. Prentice Hall, 1987.

[146] O. Lakkis and T. Pryer. A finite element method for nonlinear elliptic problems. *SIAM Journal on Scientific Computing*, 35(4):A2025–A2045, 2013.

[147] R. F. Galán, G. B. Ermentrout, and N. N. Urban. Stochastic dynamics of uncoupled neural oscillators: Fokker-Planck studies with the finite element method. *Physical Review E*, 76(5):056110, 2007.

[148] G. W. Harrison. Numerical solution of the Fokker-Planck equation using moving finite elements. *Numerical Methods for Partial Differential Equations*, 4(3):219–232, 1988.

[149] S. B. Gazi Karakoc, S. K. Bhowmik, and F. Gao. A numerical study using finite element method for generalized Rosenau-Kawahara-RLW equation. *Computational Methods for Differential Equations*, 7(3):319–333, 2019.

[150] V. Thomée. *Galerkin Finite Element Methods for Parabolic Problems*, volume 1054. Springer, 1984.

[151] K. Eriksson and C. Johnson. Adaptive finite element methods for parabolic problems IV: Nonlinear problems. *SIAM Journal on Numerical Analysis*, 32(6):1729–1749, 1995.

[152] K. Burrage, P. Burrage, A. Leier, and T. Marquez-Lago. A review of stochastic and delay

simulation approaches in both time and space in computational cell biology. In *Stochastic Processes, Multiscale Modeling, and Numerical Methods for Computational Cellular Biology*, pages 241–261. Springer, 2017.

[153] R. Mittal and R. Jiwari. A higher order numerical scheme for some nonlinear differential equations: models in biology. *International Journal for Computational Methods in Engineering Science and Mechanics*, 12(3):134–140, 2011.

[154] M. Mattia and P. Del Giudice. Population dynamics of interacting spiking neurons. *Physical Review E*, 66(5):051917, 2002.

[155] Z. Liu, S. Tatar, S. Ulusoy, and M. Zeki. Structural stability for the Morris-Lecar neuron model. *Applied Mathematics and Computation*, 270:261–268, 2015.

[156] Jocirei D Ferreira and V Sree Hari Rao. Current trends in the bifurcation methods of solutions of real world dynamical systems. In *International workshop of Mathematical Analysis and Applications in Modeling*, pages 459–497. Springer, 2018.

[157] K. S. Kumar and G. D. V. Gowda. Second order scheme for scalar conservation laws with discontinuous flux. *Applied Numerical Mathematics*, 80:46–64, 2014.

[158] M. J. Cáceres, J. A. Carrillo, and L. Tao. A numerical solver for a nonlinear Fokker-Planck equation representation of neuronal network dynamics. *Journal of Computational Physics*, **230**(4):1084–1099, 2011.

[159] M. Koksal and M. E. Koksal. Commutativity of linear time-varying differential systems with nonzero initial conditions: A Review and some new extensions. *Mathematical Problems in Engineering*, 2011:25, 2011.

[160] H. Ramos, Z. Kalogiratou, T. Monovasilis, and T. E. Simos. An optimized two-step hybrid block method for solving general second order initial-value problems. *Numerical Algorithms*, 72(4):1089–1102, 2016.

[161] A. Bellen and M. Zennaro. *Numerical Methods for Delay Differential Equations*. Oxford university press, 2013.

[162] P. Singh and K. K. Sharma. Numerical solution of first-order hyperbolic partial differential-difference equation with shift. *Numerical Methods for Partial Differential Equations*, 26(1):107–116, 2010.

[163] P. Singh and K. K. Sharma. Finite difference approximations for the first-order hyperbolic partial differential equation with point-wise delay. *International Journal of Pure and Applied Mathematics*, **67**(1):49–67, 2011.

[164] S. S. Motsa, P. Sibanda, and S. Shateyi. A new spectral-homotopy analysis method for solving a nonlinear second order bvp. *Communications in Nonlinear Science and Numerical Simulation*, 15(9):2293–2302, 2010.

[165] J. Mohapatra and S. Natesan. Uniformly convergent numerical method for singularly perturbed differential-difference equation using grid equidistribution. *International Journal for Numerical Methods in Biomedical Engineering*, 27(9):1427–1445, 2011.

[166] S. Wang, W. Deng, J. Yuan, and Y. Wu. Characteristic local discontinuous Galerkin methods for incompressible Navier-Stokes equations. *Communications in Computational*

Physics, 22(1):202–227, 2017.

[167] S. K. Bhowmik. Error estimates for discontinuous Galerkin finite element methods for a neuron network model. *Applicable Analysis*, **94**(10):2011–2022, 2015.

[168] S. Tatar and S. Ulusoy. An inverse coefficient problem for a nonlinear reaction diffusion equation with a nonlinear source. *Electronic Journal Of Differential Equations (EJDE)*, 245:2015, 2015.

[169] S. E. Hamamci and M. Koksal. Calculation of all stabilizing fractional-order PD controllers for integrating time delay systems. *Computers and Mathematics with Applications*, 59(5):1621–1629, 2010.

[170] S. Sedaghat, Y. Ordokhani, and Mehdi Dehghan. Numerical solution of the delay differential equations of pantograph type via chebyshev polynomials. *Communications in Nonlinear Science and Numerical Simulation*, 17(12):4815–4830, 2012.

[171] M. K. Kadalbajoo, L. P. Tripathi, and A. Kumar. Second order accurate IMEX methods for option pricing under Merton and Kou jump-diffusion models. *Journal of Scientific Computing*, 65(3):979–1024, 2015.

[172] A. Ashyralyev, M. E. Koksal, and R. P. Agarwal. An operator-difference scheme for abstract Cauchy problems. *Computers and Mathematics with Applications*, **61**(1):1855–1872, 2011.

[173] M. Dehghan and R. Salehi. The numerical solution of the non-linear integro-differential equations based on the meshless method. *Journal of Computational and Applied Mathematics*, 236(9):2367–2377, 2012.

[174] R. Jiwari, S. Pandit, and M. E. Koksal. A class of numerical algorithms based on cubic trigonometric B-spline functions for numerical simulation of nonlinear parabolic problems. *Computational and Applied Mathematics*, 38(3):140, 2019.

[175] M. Dehghan and A. Nikpour. Numerical solution of the system of second-order boundary value problems using the local radial basis functions based differential quadrature collocation method. *Applied Mathematical Modelling*, 37(18-19):8578–8599, 2013.

[176] B. Cockburn and C.-W. Shu. The Runge-Kutta local projection-discontinuous-Galerkin finite element method for scalar conservation laws. *ESAIM: Mathematical Modelling and Numerical Analysis*, 25(3):337–361, 1991.

[177] W. H. Reed and T. Hill. Triangular mesh methods for the neutron transport equation. Technical report, Los Alamos Scientific Lab., N. Mex.(USA), 1973.

[178] B. Cockburn and C.-W. Shu. The local discontinuous Galerkin method for time-dependent convection-diffusion systems. *SIAM Journal on Numerical Analysis*, 35(6):2440–2463, 1998.

[179] B. Cockburn and C.-W. Shu. Runge-Kutta discontinuous Galerkin methods for convection-dominated problems. *Journal of Scientific Computing*, 16(3):173–261, 2001.

[180] F. Bassi and S. Rebay. A high-order accurate discontinuous finite element method for the numerical solution of the compressible Navier-Stokes equations. *Journal of Computational Physics*, 131(2):267–279, 1997.

[181] G. Dumont and P. Gabriel. The mean-field equation of a leaky integrate-and-fire neural network: measure solutions and steady states. *arXiv preprint arXiv:1710.05596*, 2017.

[182] G. M. Phillips. *Interpolation and Approximation by Polynomials*, volume 14. Springer Science & Business Media, 2003.

[183] C.-W. Shu and S. Osher. Efficient implementation of essentially non-oscillatory shock-capturing schemes. *Journal of Computational Physics*, 77(2):439–471, 1988.

[184] R. J. Spiteri and S. J. Ruuth. A new class of optimal high-order strong-stability-preserving time discretization methods. *SIAM Journal on Numerical Analysis*, 40(2):469–491, 2002.

[185] Y. Dong, G. Huang, R. Miyazaki, and Y. Takeuchi. Dynamics in a tumor immune system with time delays. *Applied Mathematics and Computation*, 252:99–113, 2015.

[186] K. O. Okosun and O. D. Makinde. A co-infection model of malaria and cholera diseases with optimal control. *Mathematical Biosciences*, 258:19–32, 2014.

[187] Y. Dong, R. Miyazaki, and Y. Takeuchi. Mathematical modeling on helper t cells in a tumor immune system. *Discrete and Continuous Dynamical Systems-B*, 19(1):55, 2014.

[188] A. J. Lotka. Elements of physical biology. *Science Progress in the Twentieth Century (1919-1933)*, 21(82):341–343, 1926.

[189] T. Arbogast and F. A. Milner. A finite difference method for a two-sex model of population dynamics. *SIAM Journal on Numerical Analysis*, 26(6):1474–1486, 1989.

[190] M. Iannelli, M.-Y. Kim, and E.-J. Park. Splitting methods for the numerical approximation of some models of age-structured population dynamics and epidemiology. *Applied Mathematics and Computation*, 87(1):69–93, 1997.

[191] P. Das and S. Natesan. Numerical solution of a system of singularly perturbed convection diffusion boundary value problems using mesh equidistribution technique. *Australian Journal of Mathematical Analysis and Applications*, 10(1):1–17, 2013.

[192] L. Von Bertalanffy. Quantitative laws in metabolism and growth. *The quarterly review of biology*, 32(3):217–231, 1957.

[193] J. A. Florian, J. L. Eiseman, and R. S. Parker. Accounting for quiescent cells in tumour growth and cancer treatment. *IEE Proceedings-Systems Biology*, 152(4):185–192, 2005.

[194] B. P. Ayati, G. F. Webb, and A. R. Anderson. Computational methods and results for structured multiscale models of tumor invasion. *Multiscale Modeling & Simulation*, 5(1):1–20, 2006.

[195] D. Liu, S. Ruan, and D. Zhu. Stable periodic oscillations in a two-stage cancer model of tumor and immune system interactions. *Mathematical Biosciences and Engineering*, 9(2):347–368, 2012.

[196] S. Ruan P. Bi and X. Zhang. Periodic and chaotic oscillations in a tumor and immune system interaction model with three delays. *Chaos: An Interdisciplinary Journal of Nonlinear Science*, 24(2):023101, 2014.

[197] J. Dyson, R. Villella-Bressan, and G. Webb. Asynchronous exponential growth in an age structured population of proliferating and quiescent cells. *Mathematical Biosciences*, 177:73–83, 2002.

[198] P. Gabriel, S. P. Garbett, V. Quaranta, D. R. Tyson, and G. F. Webb. The contribution of age structure to cell population responses to targeted therapeutics. *Journal of Theoretical Biology*, 311:19–27, 2012.

[199] D. R. Tyson, S. P. Garbett, P. L. Frick, and V. Quaranta. Fractional proliferation: a method to deconvolve cell population dynamics from single-cell data. *Nature Methods*, 9(9):923, 2012.

[200] G. D. V. Gowda. Numerical methods for nonlinear system of hyperbolic equations arising in oil reservoir simulation. In *Industrial Mathematics and Complex Systems*, pages 187–191. Springer, 2017.

[201] S. M. Hosseini and S. Shahmorad. Tau numerical solution of Fredholm integro-differential equations with arbitrary polynomial bases. *Applied Mathematical Modelling*, 27:145–154, 2003.

[202] S. K. Bhowmik. Fast and efficient numerical methods for an extended black–scholes model. *Computers & Mathematics with Applications*, 67(3):636–654, 2014.

[203] M. K. Singh and S. Natesanan. A parameter-uniform hybrid finite difference scheme for singularly perturbed system of parabolic convection-diffusion problems. *International Journal of Computer Mathematics*, 97(4):875–905, 2020.

[204] T. Ak, S. Dhawan, S. B. G. Karakoc, S. K. Bhowmik, and K. R. Raslan. Numerical study of Rosenau-KdV equation using finite element method based on collocation approach. *Mathematical Modelling and Analysis*, 22(3):373–388, 2017.

[205] L. M. Abia, O. Angulo, and J. C. López-Marcos. Size-structured population dynamics models and their numerical solutions. *Discrete and Continuous Dynamical Systems Series B*, 4:1203–1222, 2004.

[206] T. Kostova. An explicit third-order numerical method for size-structured population equations. *Numerical Methods for Partial Differential Equations: An International Journal*, 19(1):1–21, 2003.

[207] S. Adjerid and A. Klauser. Superconvergence of discontinuous finite element solutions for transient convection–diffusion problems. *Journal of Scientific Computing*, 22(1-3):5–24, 2005.

[208] M.-Y. Kim. Discontinuous Galerkin methods for the Lotka-Mckendrick equation with finite life-span. *Mathematical Models and Methods in Applied Sciences*, 16(02):161–176, 2006.

List of Publications

International Journal

1. Dipty Sharma, Paramjeet Singh, Ravi P. Agarwal, Mehmet Emir Koksal. *"Numerical Approximation for Nonlinear Noisy Leaky Integrate-and-Fire Neuronal Model"*, Mathematics, **7 (4)**, 363, 2019.

2. Dipty Sharma, Paramjeet Singh. *"Discontinuous Galerkin Approximation for an Excitatory-Inhibitory Networks with Delay and Refractory Periods"*, International Journal of Modern Physics C, **31(03)**, 2050041, 2020.

3. Dipty Sharma, Paramjeet Singh. *"Discontinuous Galerkin method for a nonlinear age-structured tumor cell population model with proliferating and quiescent phases"*, International Journal of Modern Physics C, **32(03)**, 1-18, 2021.